NEW GENUS AND SPECIES OF DJADOCHTATHERIID MULTITUBERCULATE (ALLOTHERIA, MAMMALIA) FROM THE UPPER CRETACEOUS BAYAN MANDAHU FORMATION OF INNER MONGOLIA

Article *in* Annals of Carnegie Museum · December 2019

CITATIONS
0

READS
256

3 authors:

John R. Wible
Carnegie Museum Of Natural History
109 PUBLICATIONS **5,686** CITATIONS
SEE PROFILE

Sarah L Shelley
Carnegie Museum Of Natural History
18 PUBLICATIONS **20** CITATIONS
SEE PROFILE

Shundong Bi
Indiana University of Pennsylvania
33 PUBLICATIONS **545** CITATIONS
SEE PROFILE

ANNALS OF CARNEGIE MUSEUM

VOL. 85, NUMBER 4, PP. 285–327 31 DECEMBER 2019

NEW GENUS AND SPECIES OF DJADOCHTATHERIID MULTITUBERCULATE (ALLOTHERIA, MAMMALIA) FROM THE UPPER CRETACEOUS BAYAN MANDAHU FORMATION OF INNER MONGOLIA

JOHN R. WIBLE
Curator, Section of Mammals, Carnegie Museum of Natural History
5800 Baum Boulevard, Pittsburgh, Pennsylvania 15206
wiblej@carnegiemnh.org
Centre for Vertebrate Evolutionary Biology, Yunnan University
2 Green Lake North Road, Kunming, China, 650091

SARAH L. SHELLEY
Postdoctoral Fellow, Section of Mammals, Carnegie Museum of Natural History
5800 Baum Boulevard, Pittsburgh, Pennsylvania 15206
shelleys@carnegiemnh.org

SHUNDONG BI
Centre for Vertebrate Evolutionary Biology, Yunnan University
2 Green Lake North Road, Kunming, China, 650091
Department of Biology, Indiana University of Pennsylvania,
975 Oakland Avenue, Indiana, Pennsylvania, 15705
shundong.bi@iup.edu

Address correspondence to John Wible or Shundong Bi.

ABSTRACT

The superfamily Djadochtatherioidea is a distinctive clade of multituberculates from Upper Cretaceous beds of Mongolia and Inner Mongolia, China. Because many of the 11 included genera are known from skulls, more is known about the cranial anatomy of djadochtatherioids than any other clade of multituberculates. Within Djadochtatherioidea, the most diverse and widely accepted group is the family Djadochtatheriidae. Within the family, the basal genus, *Kryptobaatar* Kielan-Jaworowska, 1970, is small with a skull length of about 30 mm, whereas the other four genera, *Djadochtatherium* Simpson, 1925, *Catopsbaatar* Kielan-Jaworowska, 1994, *Tombaatar* Rougier et al., 1997, and *Mangasbaatar* Rougier et al., 2016, have skulls approximately twice as long. Here, we describe a **new genus and species, *Guibaatar castellanus***, based on a single specimen from the Upper Cretaceous Bayan Mandahu Formation, Inner Mongolia that we refer to Djadochtatheriidae. *Guibaatar* is represented by a relatively complete rostrum, a partial right braincase, and partial lower jaws. As revealed by CT scanning, the specimen is a juvenile, with deciduous enlarged upper and lower incisors with permanent replacements forming, m2 erupting, and M2 forming. Based on the preserved cranial parts, we estimate the skull length to be approximately 50 mm, but as an adult, *Guibaatar* would have been in the size range of the larger djadochtatheriids.

Phylogenetic analysis including *Guibaatar*, known djadochtatherioids, and outgroups places *Guibaatar* within Djadochtatheriidae, as sister to a clade of *Mangasbaatar* and *Catopsbaatar*. We suspect the relationships of djadochtatherioids are likely to be refined given the announcements by other researchers that skulls are known for the djadochtatheriids *Tombaatar* and *Djadochtatherium*, which were previously represented by incomplete material.

KEY WORDS: Bayan Mandahu Formation, Djadochtatheriidae, Djadochtatherioidea, *Guibaatar castellanus*, multituberculate

INTRODUCTION

The first cranial remains of a Late Cretaceous multituberculate from Mongolia were discovered in 1922 by the Third Asiatic Expedition of the American Museum of Natural History at Shabarakh Usu or Bayn Dzak (Bayan Zag of Benton 2000), better known as the Flaming Cliffs. The specimen, a rostrum and lower jaws, was described by G.G. Simpson as *Djadochtatherium matthewi* Simpson, 1925. It was more than 50 years before the next Late Cretaceous multituberculate was found in Mongolia. In 1968, an upper postcanine dentition was discovered at Khaichin Uul in Bugin Cav (Bügiin Tsav of Benton 2000) by the Soviet-Mongolian Geological Expedition and named *Buginbaatar transaltaiensis* Kielan-Jaworowska and Sochava, 1969. Zofia Kielan-Jaworowska, the renown leader of the Polish-Mongolian Palaeontological Expeditions (1963–1971), went on to describe 11 additional monotypic multituberculate genera from the Late Cretaceous of Mongolia. The others include, from Bayn Dzak, *Gobibaatar parvus* Kielan-Jaworowska, 1970, *Sloanbaatar mirabilis* Kielan-Jaworowska, 1970, *Kryptobaatar dashzevegi* Kielan-Jaworowska, 1970, *Kamptobaatar kuczynskii* Kielan-Jaworowska, 1970, and *Bulganbaatar nemegtbaataroides* Kielan-Jaworowska, 1974; from the Nemegt Basin, *Nemegtbaatar gobiensis* Kielan-Jaworowska, 1974, *Chulsanbaatar vulgaris* Kielan-Jaworowska, 1974, *Catopsbaatar catopsaloides* (Kielan-Jaworowska, 1974),

and *Nessovbaatar multicostatus* Kielan-Jaworowska and Hurum, 1997; and from Tugrigeen Shiree (Toogreek Shire of Benton 2000), *Tugrigbaatar saichanensis* Kielan-Jaworowska and Dashzeveg, 1978. The last was recognized as *Kryptobaatar saichanensis* by Kielan-Jaworowska and Hurum (1997) (see also Rougier et al. 1997), and *Gobibaatar parvus* was regarded as a junior synonym of *Krytpobaatar dashzevegi* by Kielan-Jaworowska (1980). Two additional monotypic multituberculate genera from the Late Cretaceous of Mongolia were reported by Rougier and co-workers: from Ukhaa Tolgod, *Tombaatar sabuli* Rougier et al., 1997, and from Udan Sayr (Üüden Sair of Benton 2000), *Mangasbaatar udanii* Rougier et al., 2016.

In 1997, two studies (Rougier et al. 1997; Kielan-Jaworowska and Hurum 1997) were published supporting the monophyly of most Late Cretaceous Mongolian multituberculates, although there were differences in the results of their cladistic analyses. Kielan-Jaworowska and Hurum (1997) formerly named the suborder Djadochtatheria to include all then known Late Cretaceous Mongolian multituberculates except for *Buginbaatar* Kielan-Jaworowska and Sochava, 1969, and tentatively assigned two North American taxa, Late Cretaceous *Paracimexomys* Archibald, 1982, and Paleocene *Pentacosmodon* Jepsen, 1940. They also erected a new family Djadochtatheriidae to include *Djadochtatherium* Simpson, 1925, *Kryptobaatar* Kielan-Jaworowska, 1970, *Catopsbaatar* Kielan-Jaworowska, 1994, and *Tombaatar* Rougier et al., 1997, to which Rougier et al. (2016) added *Mangasbaatar*. In 2001, Kielan-Jaworowska and Hurum replaced the suborder Djadochtatheria with the superfamily Djadochtatherioidea to only include Mongolian taxa (see also Kielan-Jaworowska et al. 2004).

In 1988, the Sino-Canadian Dinosaur Project discovered multituberculates at Bayan Mandahu, Inner Mongolia, in sediments lithologically and faunally similar to those of the Djadochta Formation, the type section of which is Bayn Dzak (Dong 1993; Jerzykiewicz et al. 1993). The latter authors (p. 2189) reported that "about 50 skulls, three or four with partial skeletons, have been collected," all but one being multituberculates. These specimens have not yet been described. During 1995, 1996, and 1999, the Sino-Belgian expedition found seven skulls and postcranial remains of multituberculates at Bayan Mandahu (Smith et al. 2001). To date, two publications of this material have appeared. Smith et al. (2001) named a new species of *Kryptobaatar*, *K. mandahuensis*, based on two skulls, and Ladevèze et al. (2010) described the petrosal of a skull provisionally referred to cf. *Tombaatar*, new species. Here, we report a new genus and species of djadochtatheriid multituberculate, based on a partial skull with lower jaws collected in 2013 at Bayan Mandahu.

Late Cretaceous multituberculates from Mongolia and China are from the Djadochta (Djadokhta of Benton 2000), Barun Goyot (Baruungoyot of Benton 2000), and Bayan Mandahu formations or equivalents. The Djadochta Formation most recently has been tentatively assigned a Campanian age based on biochronologic and magnetostratigraphic analyses (Dashzeveg et al. 2005; Dingus et al. 2008). As noted above, the Bayan Mandahu Formation is considered a Djadochta equivalent (Jerzykiewicz et al. 1993) whereas the Barun Goyot Formation is considered to be slightly younger (Gradzínski et al. 1977). Makovicky (2008) used a cladogram-based method (cladistic biochronologic analysis) to age these formations; Bayan Mandahu was the oldest, followed successively by the Djadochta localities of Bayn Dzak and Ukhaa Tolgod, and the Barun Goyot localities were the youngest.

MATERIALS AND METHODS

The basis for the new genus and species is material from a block with a single specimen prepared into four pieces: a relatively complete rostrum from the mid-orbit forwards, partial left and right dentaries, and part of the right braincase and zygoma including partial petrosal, squamosal, and jugal (Fig. 1). Our comparative sample is based entirely on the literature. Fortunately, two djadochtatheriids have been the subjects of monographic treatment providing a strong basis for comparison: *Kryptobaatar* (Wible and Rougier 2000; see also, Kielan-Jaworowska 1970; Rougier et al. 1996b; Kielan-Jaworowska and Hurum 1997; Smith et al. 2001; Kik 2002) and *Mangasbaatar* (Rougier et al. 2016). Of the remaining three djadochtatheriid genera, *Catopsbaatar* has been described from multiple specimens but its meso- and basicranium are poorly known (Kielan-Jaworowska et al. 2002, 2005); *Djadochtatherium* is based on a poorly preserved rostrum and dentaries collected in 1922 housed at the American Museum of Natural History (Simpson 1925; Rougier et al. 1997) [a well-preserved skull attributed to *Djadochtatherium* has been commented on and tentatively included in a reconstruction of that taxon by Kielan-Jaworowska et al. 2005: fig. 11B, but never fully described and, as pointed out by Rougier et al. 2016 may not be *Djadochtatherium*]; and *Tombaatar* is described from a rostrum less complete than that of the new genus and species (Rougier et al. 1997), although an additional more complete skull is known (Rougier et al. 2016) but not yet described [Ladevèze et al. 2010 reported on the petrosal from the skull of a multituberculate from Bayan Mandahu that they referred to cf. *Tombaatar*, new species]. Of the remaining djadochtatherioids, the skulls of *Nemegtbaatar*, *Chulsanbaatar*, and *Kamptobaatar* have received the most study (Kielan-Jaworowska 1970, 1974; Kielan-Jaworowska et al. 1986; Hurum 1994, 1998; Hurum et al. 1996; Kielan-Jaworowska and Hurum 1997); *Sloanbaatar* is known from a single skull that does not preserve as much detail as the prior named taxa (Kielan-Jaworowska 1970; Kielan-Jaworowska and Hurum 1997); *Nessovbaatar* is known from only two dentaries (Kielan-Jaworowska and Hurum 1997); and *Bulganbaatar* is known from a single incomplete and badly damaged rostrum (Kielan-Jaworowska 1974). Sereno and McKenna

(1995) tentatively referred an articulated skeleton to *Bulganbaatar*, but subsequently Sereno (2006) identified it as *Kryptobaatar dashzevegi*.

Our anatomical terminology follows that employed for *Kryptobaatar* by Wible and Rougier (2000), which in turn was based on that of Kielan-Jaworowska and co-authors (e.g., Kielan-Jaworowska 1970, 1974; Kielan-Jaworowska et al. 1986; Gambaryan and Kielan-Jaworowska 1995) except for the auditory region and cranial vasculature, which followed Wible (1987, 1990), Rougier et al. (1992, 1996a, b), and Wible and Hopson (1993, 1995). For cusp formulae on premolars and molars, cusp numbers are in rows from labial to lingual separated by a colon (Kielan-Jaworowska et al. 2004).

Measurements were taken using digital calipers to two decimal places. For the comparative sample, measurements were taken from the literature in Adobe Photoshop.

The four pieces of *Guibaatar* (i.e., rostrum, right petrosal and squamosal, and right and left dentaries) were scanned at the Center for Quantitative Imaging at the Pennsylvania State University on their General Electric v|tome|x L300 nano/microCT. The scanning had the following parameters: voltage of 220kV, current of 100 µA, and voxel size of 0.02500002. The dentition was segmented in Avizo® 9.5.0 software (Visualization and Sciences Group, 1995–2018).

Institutional Abbreviations

CEVB—Centre for Vertebrate Evolutionary Biology, Yunnan University, Kunming, China.

YPM VPPU—Princeton University Collection, Department of Vertebrate Paleontology, Yale Peabody Museum of Natural History, New Haven, Connecticut, U.S.A.

ZPAL—Institute of Paleobiology, Polish Academy of Sciences, Warsaw, Poland.

Other Abbreviation

LCMM—Late Cretaceous Mongolian multituberculates (including those from Outer and Inner Mongolia).

SYSTEMATIC PALEONTOLOGY

Class Mammalia Linnaeus, 1758

Subclass Allotheria Marsh, 1880

Order Multituberculata Cope, 1884

Superfamily Djadochtatherioidea Kielan-Jawowroska and Hurum, 2001

Family Djadochtatheriidae Kielan-Jaworowska and Hurum, 1997

Guibaatar, new genus
Guibaatar castellanus, new species

(Figs. 1–16)

TABLE 1. Skull measurements of *Guibaatar castellanus* in mm. R and L specify the side (right or left) on which the measurement was made.

Length of premaxilla along alveolar border	7.24R
Length of premaxilla in sutural contact with nasal	10.72R
Length of palate between premaxillary-maxillary suture and choanae	13.36L
Width of palate between P4	10.15
Depth of skull above I2	6.28R
Depth of skull above M2	11.46L
Length of nasals	19.88L
Depth of mandible below p3	6.95R, 6.82L
Depth of mandible below m1	7.31R, 7.20R

Holotype.—CEVB 11908, an incomplete cranium in two pieces (rostrum and right petrosal/squamosal/jugal) and incomplete lower jaws.

Locality and horizon.—The holotype and only specimen was collected in 2013 near the Gate, on the lower slopes of Castle Butte, 15 km north of Bayan Mandahu village, Urad Houqi Banner, Bayan Nor League, Inner Mongolia Province, P.R. China (see Smith et al. 2001: fig. 2).

Etymology.—*Gui*, for Guillermo W. Rougier, in recognition of his contributions to Late Cretaceous Mongolian multituberculates; *baatar*, transliteration from the Mongolian for hero, a common suffix for Mongolian multituberculates, first used by Kielan-Jaworowska and Sochava (1969) in allusion to the capital of Mongolia, Ulaanbaatar; *castellanus*, Latin, associated with a castle, after the type locality, Castle Butte.

Diagnosis for genus and species.—Juvenile djadochtatherioid multituberculate with skull length approximately 50 mm. Cusp formulae of P2 (3:3), P4 (2:5:1), M1 (5:5:2), and m2 (1:2) unique among known djadochtatherioids. Shares with known djadochtatherioids I3 in middle of palatine process of premaxilla and small incisive foramen (subequal to I2 length). Shares thickenings in palatine process of premaxilla with known djadochtatherioids except *Kamptobbatar*. Shares sub-trapezoidal rostrum with straight sides with djadochtatheriids *Kryptobaatar*, *Djadochtatherium*, *Catopsbaatar*, *Tombaatar*, and *Mangasbaatar*. Shares pronounced postpalatine torus projecting ventral to occlusal surface with *Kryptobaatar*, *Tombaatar*, and *Mangasbaatar*, but not *Catopsbaatar*. Differs from *Catopsbaatar*, *Mangasbaatar*, and *Tombaatar* in lacking first upper premolar. Shares secondary infraorbital

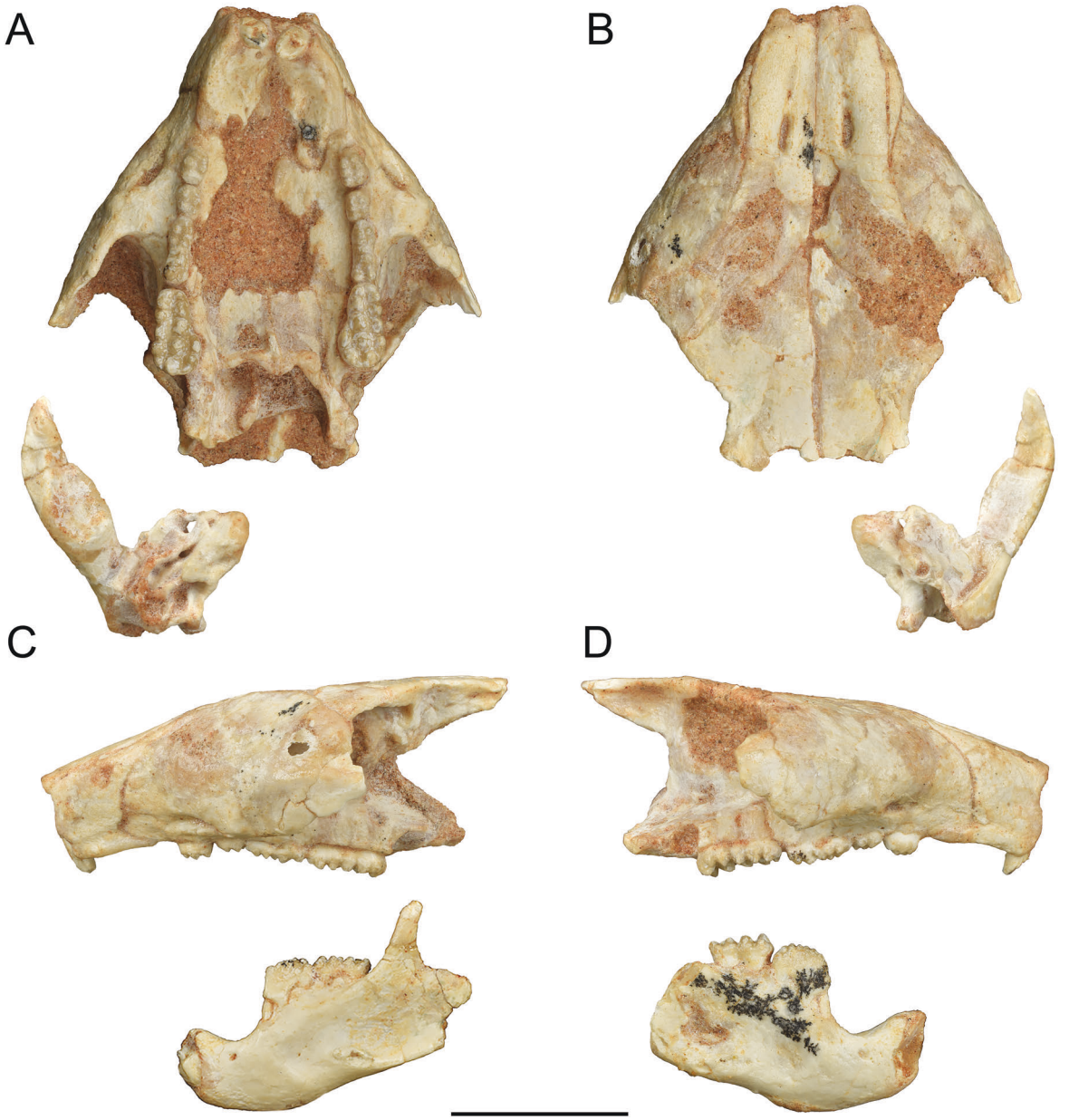

Fig. 1.—*Guibaatar castellanus*, CEVB 11908. **A, B,** rostrum and partial right braincase and zygoma in ventral and dorsal views, respectively; **C,** rostrum left side and left dentary in lateral view; **D,** rostrum right side and right dentary in lateral view. Scale = 10 mm.

foramen with *Mangasbaatar* and some *Catopsbaatar*, but differs in placement for foramen in premaxillary-maxillary suture rather than within maxilla. Shares narrow, digitiform coronoid process with *Catopsbaatar* and *Mangasbaatar*. Shares five cusps in the buccal row of M1 with *Mangasbaatar* and some *Catopsbaatar*. Resembles cf. *Tombaatar*, n. sp., in having hiatus Fallopii within petrosal visible in ventral view; hiatus not visible within petrosal in ventral view in *Mangasbaatar* and *Kryptobaatar*. Resembles *Mangasbaatar* in absence of midline crest of vomer posterior to choanae; crest is present in *Kryptobaatar*.

DESCRIPTION

Skull

The specimen is represented by a relatively complete rostrum with partial lower jaws found in close association with an incomplete right petrosal, squamosal, and jugal; the lower jaws subsequently were mechanically separated from the rostrum (Fig. 1). In general, the right side of the specimen's rostrum has suffered little in the way of deformation except near the dorsal midline, which is sunken (Fig. 2); the left side has been slightly displaced

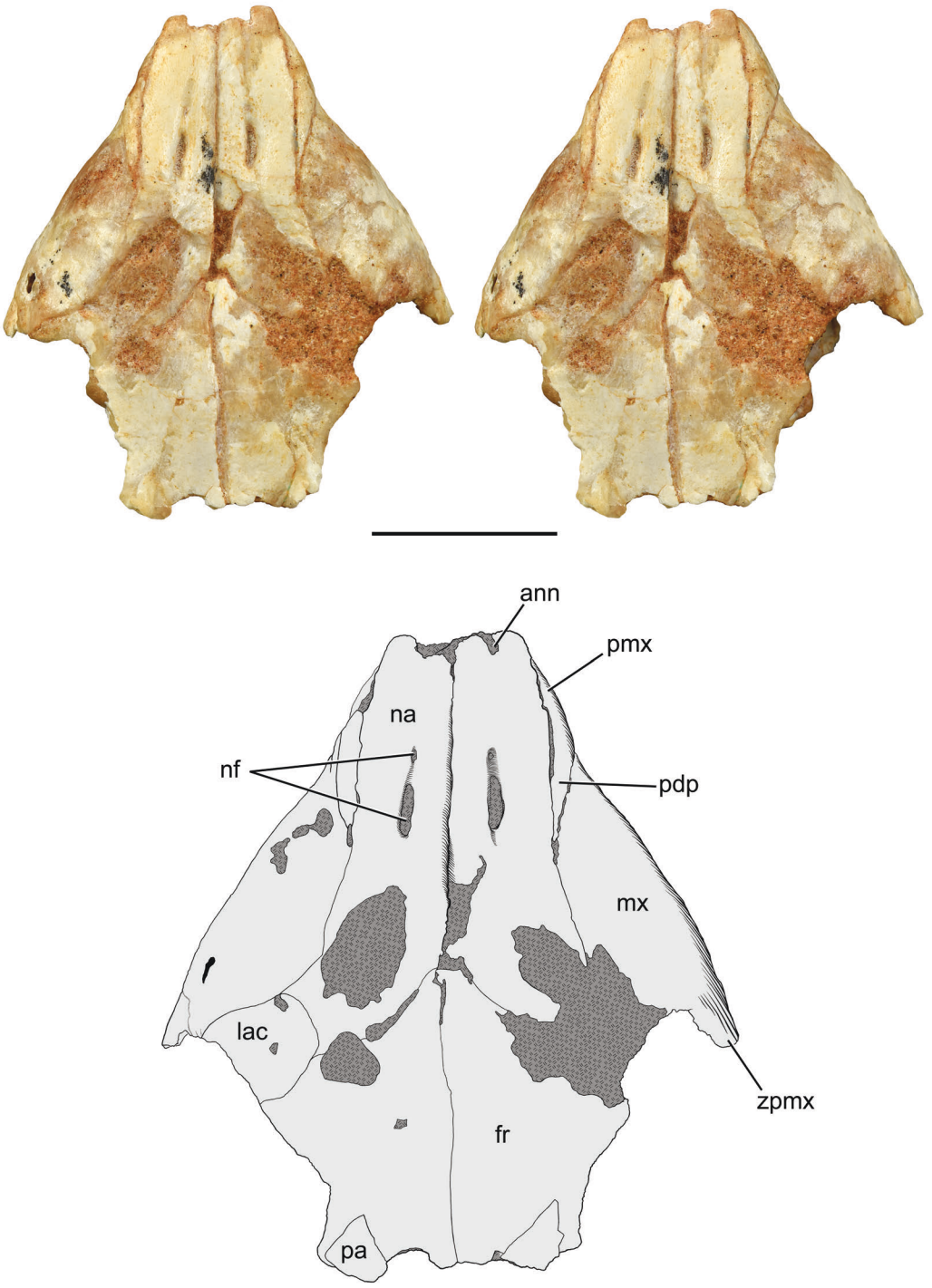

Fig. 2.—*Guibaatar castellanus*, CEVB 11908, rostrum in dorsal view. Stereophotographs and line drawing: light grey is bone and dark grey is matrix. Line drawing shows extent of lacrimal before damage (see text). Abbreviations: **ann,** anterior nasal notch; **fr,** frontal; **lac,** lacrimal; **mx,** maxilla; **na,** nasal; **nf,** nasal foramina; **pa,** parietal; **pdp,** posterodorsal process of premaxilla; **pmx,** premaxilla; **zpmx,** zygomatic process of maxilla. Scale = 10 mm.

such that the anterior left palate is dorsal to the right at the midline (Fig. 3). The specimen does not have a complete adult dentition and, as became apparent from the CT scans, includes some deciduous teeth (described with the Dentition below). In describing dental ontogeny in the lower jaw of the Paleogene taeniolabidoid *Lambdopsalis*, Miao (1986) identified four stages: juvenile, young, adult, and old. Greenwald (1988) proposed a six stage sequence in Late Cretaceous-Tertiary multituberculates. Following the dental parameters used by these authors, *Guibaatar* falls between the juvenile and young stages of Miao (1986) and in stage 2 of Greenwald (1988). From the rostrum and partial braincase, we estimate the skull length of *Guibaatar* to be approximately 50 mm. Kielan-Jaworowska (1980) reported a juvenile *Kryptobaatar* with a stage of dental ontogeny comparable to *Guibaatar* and from measurements of that specimen in Kielan-Jaworowska (1970) compared to adults in Wible and Rougier (2000), the juvenile *Kryptobaatar* is about 10% smaller than the adult. Bone-by-bone descriptions of *Guibaatar* follow below.

Premaxilla ("pmx" in Figs. 2–5).—The paired premaxilla is a well-developed bone of the rostrum, with a body and facial and palatal processes. The premaxilla forms the walls and floor of the external nasal aperture and the anteriormost nasal cavity and houses the upper incisors, the dI2 and its forming replacement, and the I3 (see Dentition). The external nasal aperture, which is roofed by the nasals, is somewhat cordiform in anterior view, nearly twice as wide dorsally as ventrally; it is also taller than wide. The right premaxilla is in life position, but the left is shifted such that it is separated from its counterpart at the midline and its medial margin is positioned far dorsal to its lateral margin. The anterior aspect of the premaxillary body, the mesial alveolar wall, is missing, exposing the roots of the right and left dI2s, and there is some damage along the midline on the palate and on the posterior aspect of the right palatal process. Otherwise, the remainder of both bones is well preserved.

The facial process is primarily erect (straight) with only a slight convexity, with its posterodorsal process extending onto the roof of the rostrum ("pdp" in Fig. 2). The facial process contacts the nasal dorsally and the maxilla posteriorly. The suture with the former is straight but with the maxilla is concave (Figs. 4–5). The deep incursion of maxilla into this concavity is bordered dorsally by the thin, tapering posterodorsal process and ventrally by the posterior part of the premaxillary's alveolar process. The former extends posteriorly nearly to the level of the main infraorbital foramen and the latter reaches the level of the I3 alveolus (Fig, 3). In the ventral quarter of the suture between the premaxilla and maxilla is a small, oblique foramen ("siof" in Figs. 4–5), which has a shallow groove running anteriorly from it. Rougier et al. (2016) described a similar foramen more posteriorly placed entirely within the maxilla in *Mangasbaatar* and identified it as a secondary infraorbital foramen. *Catopsbaatar* varies between having a single infraorbital to having one or two additional ones (Kielan-Jaworowska et al. 2005). Following these authors, we identify the foramen in the premaxilla-maxilla suture in *Guibaatar* as a secondary infraorbital foramen. Regarding the anterior margin of the facial process, the undamaged dorsal half has a shallow concavity, but the bone that would have formed the ventral half is missing bilaterally.

Neither premaxilla preserves all the features on the palate (Fig. 3), but between the two sides a relatively complete reconstruction can be made. The palatal process contacts the maxilla posteriorly at a generally U-shaped suture with a tongue of premaxilla fitting into the maxilla. Just anterior to the position of the tongue of premaxilla is the circular alveolus for the I3, which is therefore entirely within the premaxilla. The I3 alveolus lies roughly near the mediolateral midpoint of the palatal process. Medial to the I3 is the incisive foramen ("inf" in Fig. 3), which is oval with an anteroposterior long axis. The anterior and lateral borders of the incisive foramen are formed by the premaxilla, and the maxilla completes the narrow posterior border; the medial border is not preserved but if present must have been formed by the premaxilla. The lateral margin of the palatal process curves anteromedially toward the dI2 and has a very distinct ventral ridge, the crista premaxillaris (Kielan-Jaworowska et al. 2005), best seen on the right premaxilla ("cpmx" in Fig. 3). Centrally positioned on the right and left premaxillae is a circular depression, which is demarcated laterally by a raised ridge, the thickening of the premaxilla (Kielan-Jaworowska et al. 1986; "tpmx" in Fig. 3). Between the thickening and crista premaxillaris is an oval depression, with an anteroposterior long axis. Two small foramina of unknown function are positioned anterior and posterior to the thickening; the latter, which is smaller, is present bilaterally, but the former can only be confirmed on the left side due to damage on the right. The anterior foramen lies posteromedial to the dI2.

Maxilla ("mx" in Figs. 2–5).—As is typical in multituberculates, the paired maxilla is a sizeable bone and the major component of the rostrum, palate, orbit, and zygoma, with facial, palatal, orbital, and zygomatic processes. Both the left and right maxillae are for the most part in their life positions; the distortion to the left premaxilla reported above has resulted in some similar but minor displacement to the left maxilla. The alveolar process of the maxilla houses three premolars and one molar (P2, P3, P4, and M1; see Dentition). There is a small crypt, filled with matrix, for a second molar, M2, that is more fully preserved on the left side than the right.

The facial process is nearly complete on both sides, with only small areas of bone missing (Figs. 4–5). As is typical for djadochtatherioids, the facial process in *Guibaatar* is bulged laterally to a considerable extent, imparting a trapezoidal shape to the rostrum in dorsal view and reflecting the large size of the maxillary sinus (Fig. 2; Kielan-Jaworowska et al. 1986; Hurum 1994; Kik 2002;

Macrini 2006). The facial process contacts the premaxilla anteriorly (see above), the nasal dorsally, and the lacrimal posterodorsally. Much of the rear of the right nasal is missing, but enough of the left nasal and maxilla are preserved to reconstruct the suture between them. At their contact, the dorsal margin of the maxilla is strongly convex and the lateral margin of the nasal similarly concave. Because of the shape of this suture and the lateral bulging of the maxilla, there is a considerable exposure of the facial process in dorsal view. The shape of the suture between the facial process and lacrimal is the reverse, that is, the maxilla is concave and the lacrimal convex. Ventral to the lacrimal, the posterior margin of the facial process forms the anterior rim of the orbit. The primary feature on the facial process is the infraorbital foramen ("iof" in Figs. 3–5), which is positioned under the lateral bulge and, therefore, is visible in ventral view, again as typical in djadochtatherioids (Fig. 3; Kielan-Jaworowska and Hurum 1997; Wible and Rougier 2000; Rougier et al. 2016). The infraorbital foramen is oval (1.5 x 0.9 mm) with the long axis horizontal. It is centered opposite the P2–P3 embrasure and has a broad groove extending rostrally from it (Figs. 4–5). As noted above, a smaller secondary infraorbital foramen is in the premaxillay-maxillary suture on both sides.

As seen in dorsal and ventral views (Figs. 2–3), the facial process uninterruptedly continues posterolaterally as the zygomatic process. Both the left and right zygomatic processes are broken posteriorly, with the right side preserving a bit more than the left (the distal end of the zygomatic process may be attached to the squamosal, described with that bone below). In lateral view (Fig. 4), the zygomatic process is dorsoventrally tall, without any tapering posteriorly in what is preserved. As usual in djadochtatherioids, an anterior zygomatic ridge ("azr" in Figs. 4–5) arises posterolateral to the infraorbital foramen and curves posterodorsally on the anterior root of the zygoma (Gambaryan and Kielan-Jaworowska 1995; Wible and Rougier 2000). The ridge reaches the preserved posterior edge of the zygomatic process and likely extended farther posteriorly before bending ventrally. The surface circumscribed by the anterior zygomatic ridge is flat anteriorly and gently convex posteriorly, and provided attachment for the pars anterior of the superficial masseter muscle (Gambaryan and Kielan-Jaworowska 1995). On the right side, immediately dorsal to the posterior limit of the anterior zygomatic ridge is a small piece of maxilla with a smooth dorsal edge that would have contributed to the infraorbital margin. This shows that the squamosal did not reach forward into the orbit in *Guibaatar*, a condition reported in *Catopsbaatar* (Kielan-Jaworowska et al. 2005) and *Mangasbaatar* (Rougier et al. 2016). In ventral view (Fig. 3), the posterior root of the zygomatic process is at the level of the mesial root of the P4; because of its continuity with the facial process, the anterior root of the zygomatic process cannot be similarly demarcated. On the ventral surface of the root of the zygomatic process opposite the P3 is a small, shallow, circular depression ("fbuc" in Fig. 3). We have not seen this reported in multituberculates previously. Rather than providing attachment for masticatory muscles, we suggest this may have housed the buccinator muscle, which arises in a similar location from the maxilla in the dog (Evans 1993) and common opossum, *Didelphis marsupialis* (Hiiemae and Jenkins 1969).

The position of the teeth in the alveolar process of the right maxilla appears to be undamaged; the left alveolar process and premolars have been twisted ventromedially. Based on the right side, the maxillary dentition diverges slightly posteriorly. The palatal processes are imperfectly preserved. On the right side, medial to the P2 and P3, there is a small horizontal shelf of bone. Medial to the right M1, the inclined medial wall of the alveolar process has a small posterior contact with the broken lateral margin of the horizontal process of the palatine. The left side preserves more of the palatal process, with a broader continuous shelf of bone medial to the premolars and anterior half of M1. However, it is only in the anterior part, opposite the P2, that this shelf reaches the midline and contacts the premaxilla anteriorly (see Premaxilla above). As preserved, this shelf at the midline is positioned far dorsal to the alveolar process. The disparity is real but has been exaggerated by the dorsal displacement as reported for the left premaxilla above. Posterior to this shelf at the midline is a sizeable gap in the palate opposite the P3 and P4, anterior to the left palatine bone. None of the medial edges of the palatal process in this gap appear natural (unbroken). Palatal vacuities are absent in other djadochtatheriids (*Kryptobaatar*, Wible and Rougier 2000; *Tombaatar*, Rougier et al. 1997; *Catopsbaatar*, Kielan-Jaworowska et al. 2005; *Mangasbaatar*, Rougier et al. 2016); Simpson (1925) reported a palatal vacuity in *Djadochtatherium*, but Rougier et al. (1997) revisited this specimen and were not able to confirm or deny Simpson's observation. Among other djadochtatherioids, palatal vacuities are present within the maxilla in *Sloanbaatar* (Kielan-Jaworowska 1971), *Bulganbaatar* and *Nemegtbaatar* (Kielan-Jaworowska 1974). For reasons enumerated in the Palatine below, we find it unlikely that palatal vacuities occur in *Guibaatar*.

Medial to the left M1 in *Guibaatar*, the narrow shelf of the palatal process contacts the horizontal process of the palatine. The suture between the two is parasagittal posteriorly but curves slightly medially at its anterior end. In the posterior suture, opposite the M1–M2 embrasure is a narrow gap that we interpret as the minor palatine foramen ("mpf" in Fig. 3). The choanae are at the level of the posterior margin of the M1. On the left side, the alveolar process preserves most of the triangular-shaped crypt for the M2. The oblique medial side of the crypt contacts an element wedged between the palatine and maxilla. Based on the condition reported for *Kryptobaatar* (Wible and Rougier 2000), *Catopsbaatar* (Kielan-Jaworowska et al. 2005), and *Mangasbaatar* (Rougier et al. 2016), this element is most likely the alisphenoid in *Guibaatar* ("as" in Fig. 3).

Both orbits preserve bone that can be identified as belonging to the orbital process of the maxilla, and the extent

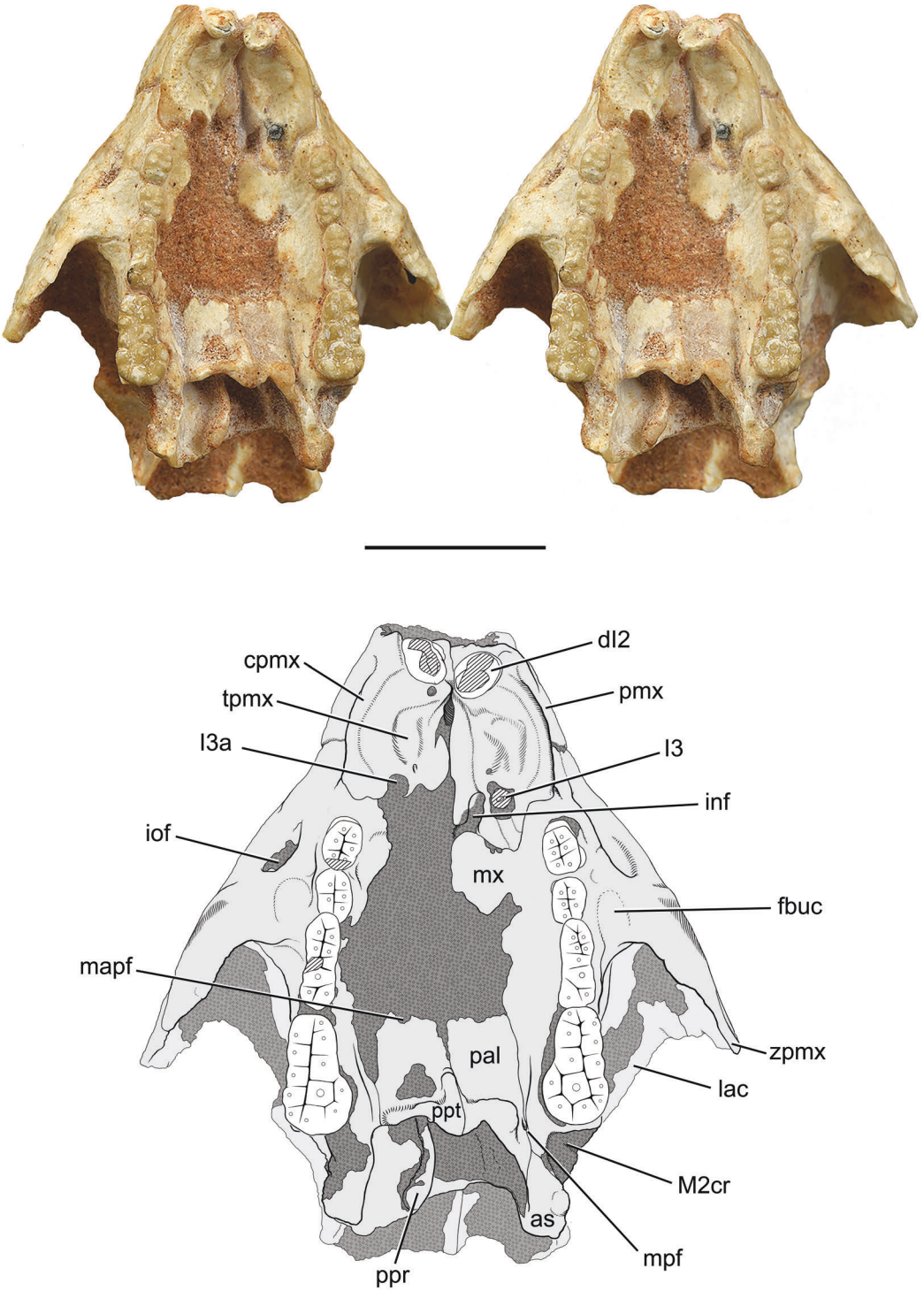

Fig. 3.—*Guibaatar castellanus*, CEVB 11908, rostrum in ventral view. Stereophotographs and line drawing: light grey is bone and dark grey is matrix. Only the posterior part of the major palatine foramen is preserved. Abbreviations: **as,** alisphenoid; **cpmx,** crista premaxillaris; **dI2,** deciduous second upper incisor; **fbuc,** facet for buccinator muscle; **I3,** third upper incisor; **I3a,** third upper incisor alveolus; **inf,** incisive foramen; **iof,** infraorbital foramen; **lac,** lacrimal; **M2cr,** second upper molar crypt; **mapf,** major palatine foramen; **mpf,** minor palatine foramen; **mx,** maxilla; **pal,** palatine; **pmx,** premaxilla; **ppr,** pterygopalatine ridge; **ppt,** postpalatine torus; **tpmx,** thickenings of premaxilla; **zpmx,** zygomatic process of maxilla. Scale = 10 mm.

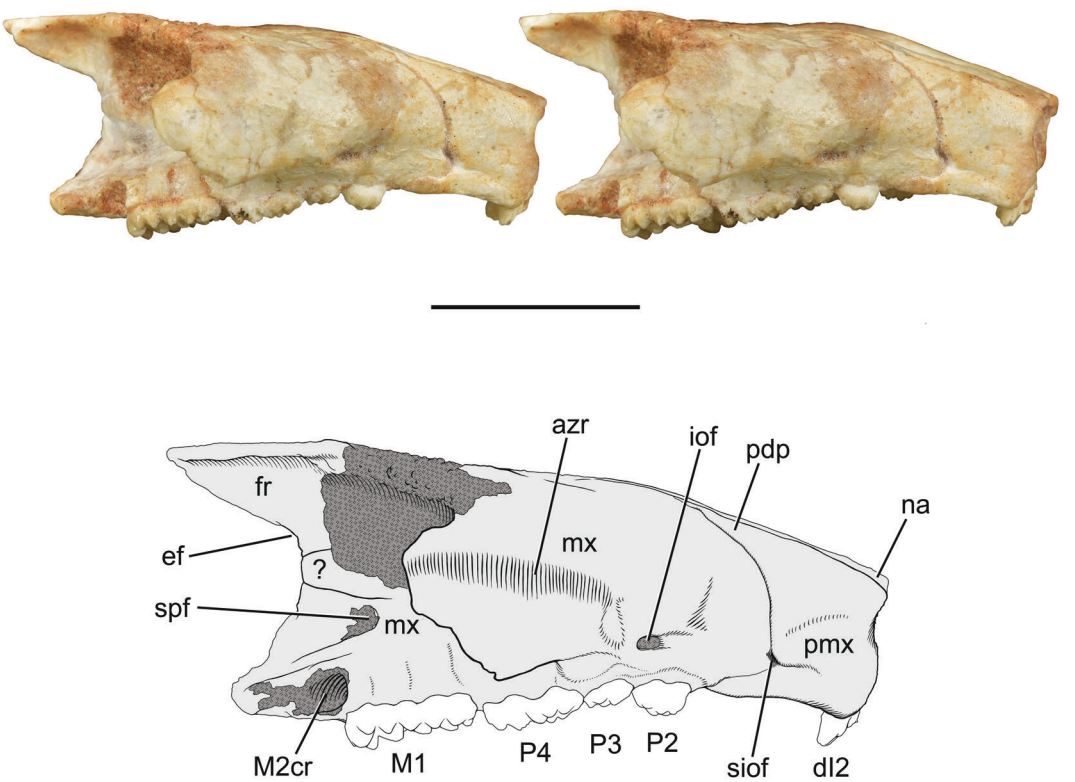

Fig. 4.—*Guibaatar castellanus*, CEVB 11908, rostrum in right lateral view. Stereophotographs and line drawing: light grey is bone and dark grey is matrix. "?" may be frontal or orbitosphenoid. Only the anterior surface of the ethmoidal foramen is preserved. Abbreviations: **azr,** anterior zygomatic ridge; **ef,** ethmoidal foramen; **fr,** frontal; **dI2,** deciduous second upper incisor; **iof,** infraorbital foramen; **M1,** first upper molar; **M2cr,** second upper molar crypt; **mx,** maxilla; **na,** nasal; **P2,** second upper premolar; **P3,** third upper premolar; **P4,** fourth upper premolar; **pdp,** posterodorsal process of premaxilla; **pmx,** premaxilla; **siof,** secondary infraorbital foramen; **spf,** sphenopalatine foramen. Scale = 10 mm.

of bone preserved differs between the two sides. Sutures are not readily visible on much of the bone in the orbit. Nevertheless, it is apparent that the orbital process of the maxilla is the major element of the anterior orbit and a major component of the posterior orbit (Fig. 4). In djadochtatherioids, the orbit is roofed by maxilla, lacrimal, and frontal, creating a sizeable space, the orbital pocket (theca orbitalis of Gambaryan and Kielan-Jaworowska 1995; "op" in Fig. 5), for muscle attachment (the pars anterior of the medial masseter, Gambaryan and Kielan-Jaworowska 1995). Because the orbital pocket does not have a floor, much of its roof is visible in ventral view. The anterior limit of the orbital pocket in *Guibaatar* is slightly in advance of the position of the posterior edge of the anterior root of the zygoma, which is at the level of the mesial root of the P4. The left orbit preserves bone in the roof and medial and lateral walls of the orbital pocket; the right side differs in that only the medial wall has bone and in the ventral third of this space. We interpret the vast majority of the bone delimiting the orbital pocket to be maxilla because of its continuity with the alveolar, zygomatic, and facial processes. The lacrimal forms the posterior part of the preserved roof of the left orbital pocket; it underlies the facial process of the maxilla in the orbital margin and is clearly set off by a suture along its anterior edge.

In the anteroventromedial aspect of the left and right orbits is the maxillary foramen (not visible in the figures), the oval posterior opening of the infraorbital canal, with a broad groove leading into it from behind. The maxillary foramen lies entirely within the maxilla, dorsal to and hidden in ventral view by the anterior root of the zygoma. The infraorbital canal runs through the anterior zygomatic root and is 3.75 mm in length on the left side and 3.95 mm on the right. The orbital process of the maxilla extends into the posterior orbit, dorsal to M1 and the crypt for M2, where it forms the ventral half of the medial orbital wall. On the left side (Fig. 5), the dorsal margin of this posterior part of the orbital process is vertical anteriorly above the M1 and more horizontal posteriorly above the M2 crypt. A narrow, unnatural gap separates the dorsal margin of the vertical part from the ventralmost limit of another orbital element, the frontal. A much larger gap separates the dorsal margin of the horizontal part from the frontal. There is a notch between the vertical and horizontal parts that is nearly completely closed on the right side to form the sphenopalatine foramen ("spf" in Figs. 4–5). The identity of the

element approximating the dorsal margin of the sphenopalatine foramen on the right side is not certain ("?" in Fig. 4). It is most likely frontal, but there are two horizontal cracks in this element that might represent sutures for another element, perhaps orbitosphenoid. This part of the orbit is not well known in other djadochtatheriids, but in the few instances that it has been reported, the sphenopalatine foramen is between the maxilla and frontal (i.e., *Kryptobaatar*, Wible and Rougier 2000; *Mangasbaatar*, Rougier et al. 2016). As reported in *Chulsanbaatar* and *Nemegtbaatar* (Kielan-Jaworowska et al. 1986), a shallow sphenopalatine groove leads into the sphenopalatine foramen from behind on the right side of *Guibaatar*. This groove appears to be mainly on the maxilla.

Palatine ("pal" in Fig. 3).—The palatine has a horizontal process exposed on the palate and a perpendicular process exposed in the lateral wall of the choanae. Although the orbit wall is incomplete in *Guibaatar*, it seems likely that the palatine had no orbital exposure as in other djadochtatherioids (Wible and Rougier 2000; Rougier et al. 2016) with the exception of *Nemegtbaatar* (Hurum 1994, 1998), which has been questioned by Rougier et al. (1997).

The horizontal process is best preserved on the left side. On the right, the anterior and posterior corners of the lateral margin are damaged and there is a large irregular hole in the posterior third of the ventral surface. The preserved anterior margin of both horizontal processes is at the level of the P4–M1 embrasure. Although the shape of the anterior margin is slightly different between the two sides, we suggest that there has been a minimal amount of damage. Accepting that, the shape of the horizontal process is roughly rectangular, with a slight rounding at the anterolateral corner, based on the left side. Both sides preserve a small, rounded notch near the midpoint of the anterior margin (deeper on the right side) that we interpret as marking the position of the major palatine foramen ("mapf" in Fig. 3); we argue here that the maxilla closed this foramen anteriorly and that *Guibaatar* lacked palatal vacuities. The major palatine foramen lies in the palatomaxillary suture in the anterior margin of the palatine in other djadochtatherioids (i.e., *Kamptobaatar*, Kielan-Jaworwoska 1971; *Chulsanbaatar*, Kielan-Jaworwoska and Hurum 1997; *Kryptobaatar*, Wible and Rougier 2000; *Tombaatar*, Rougier et al. 1997; *Catopsbaatar*, Kielan-Jaworowska et al. 2005; *Mangasbaatar*, Rougier et al. 2016). The only exceptions are *Nemegtbaatar* (Kielan-Jaworowska et al. 1986) and *Sloanbaatar* (Kielan-Jaworowska 1971), in which a major palatine foramen in the palatomaxillary suture is lacking and the more anteriorly-positioned palatal vacuity within the maxilla served as the passageway for the major palatine nerve. Given that all djadochtatherioids with major palatine foramina lack palatal vacuities and vice versa, we interpret the presence of a major palatine foramen in *Guibaatar* as supporting the absence of palatal vacuities in the maxilla.

In the mediolateral plane, the ventral surface of the paired palatines is convex with the high point of the convexity being the interpalatine suture. In the anteroposterior plane, the palatine slopes dorsally in the anterior direction. Given that the palatomaxillary suture on the lateral side of the left palatine is preserved undamaged, this sloping appears to be natural and not the result of deformation. A pronounced midline rounded ridge occupies the posterior half of the interpalatine suture. The anterior margin of this ridge has a steep slope and it intersects with and is at the same plane as the prominent postpalatine torus posteriorly ("ppt" in Fig. 3). The postpalatine torus is complete on the left palatine but damaged on the right. The torus is not uniform in height; there is a rounded, oval prominence midway between the midline and lateral margin that is at the same height as the midline rounded ridge. Lateral to the oval prominence, the torus slopes dorsolaterally to abut the small wedge of alisphenoid medial to the crypt for the left M2 (see Maxilla above). Anterior to the contact with the alisphenoid is a small, oval minor palatine foramen in the left palatomaxillary suture ("mpf" in Fig. 3), a position also found in *Catopsbaatar* (Kielan-Jaworowska et al. 2005); the foramen's position on the right side is not preserved due to damage to the lateral margin of the palatine. Whereas most djadochtotherioids have a postpalatine torus (Rougier et al. 2016), the prominences on the postpalatine torus in *Guibaatar* are nearly at the occlusal plane of the M1; a similar extreme development of the postpalatine torus has been reported for *Tombaatar* (Rougier et al. 1997) and *Mangasbaatar* (Rougier et al. 2016). The rear margin of the torus across the two palatines in *Guibaatar* has the shape of a cursive M, with the posterior aspect of the midline rounded ridge forming the valley of the M and the oval prominence the outer arm of the M.

We are uncertain about the extent of the choanal exposure of the perpendicular process. The left palatine lies medial to the alisphenoid at the choanae and can be traced a short distance dorsally before matrix buttressing the thin bone is encountered. More of the lateral wall and roof of the choanae are visible on the right side, but we are unable to trace any sutures there. The choanae are more than twice as wide as tall and the choanal roof is relatively flat.

Nasal ("na" in Figs. 2, 4–5).—The paired nasal is the major component of the roof of the rostrum and nasal cavity (Fig. 2). The anterior two-thirds of each nasal are well preserved; much bone has flaked off the posterior one-third, yet the general morphology and relationships of the bone can be reconstructed. The nasals are slightly compressed at the midline due to preservation, more so on the right side.

The left and right nasals are separated by an internasal suture. The anterior two-thirds of the nasal are roughly rectangular, with the lateral border in contact with the premaxilla. The posterior one-third is angled posterolaterally, with its lateral border in contact with the maxilla. The posteromedial border of the two nasals contacts a broad, V-shaped incursion of the right and left frontal, and the posterolateral border has a narrow contact with the lacrimal, based on the left side of *Guibaatar*. The preserved

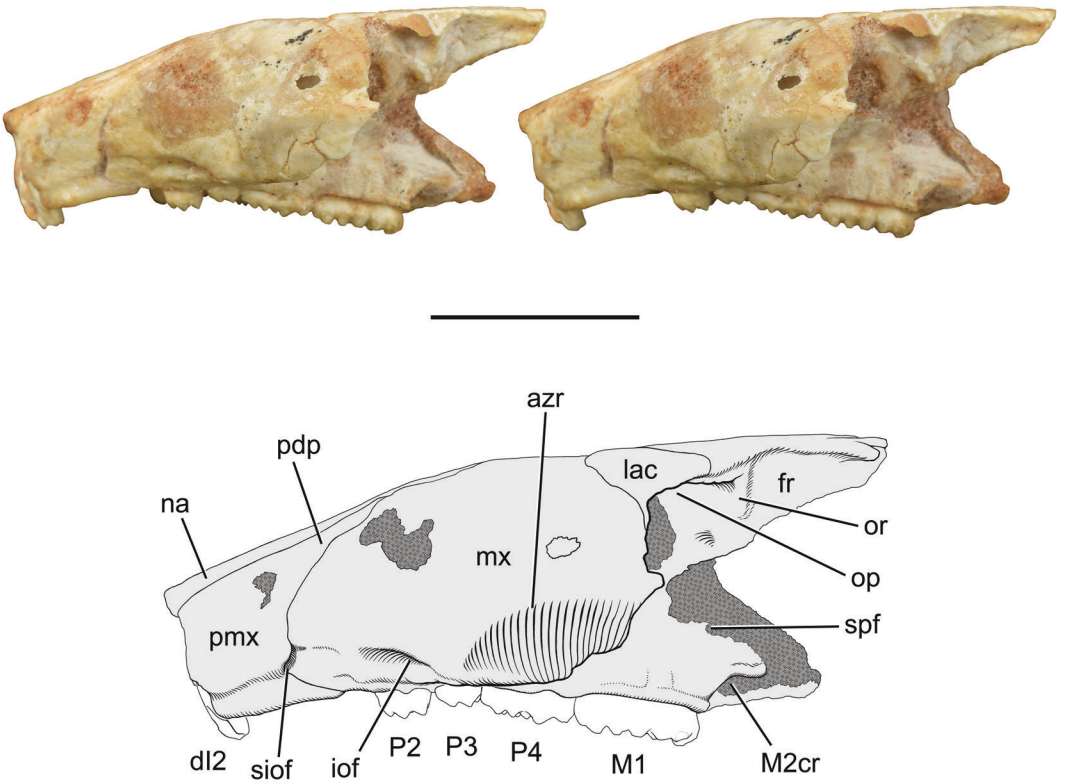

Fig. 5.—*Guibaatar castellanus*, CEVB 11908, rostrum in left lateral view. Stereophotographs and line drawing: light grey is bone and dark grey is matrix. Line drawing shows the extent of the lacrimal before damage. Only the anterior part of the sphenopalatine foramen is preserved. Abbreviations: **azr,** anterior zygomatic ridge; **dI2,** deciduous second upper incisor; **fr,** frontal; **iof,** infraorbital foramen; **lac,** lacrimal; **M1,** first upper molar; **M2cr,** second upper molar crypt; **mx,** maxilla; **na,** nasal; **op,** orbital pocket; **or,** orbital ridge; **P2,** second upper premolar; **P3,** third upper premolar; **P4,** fourth upper premolar; **pdp,** posterodorsal process of premaxilla; **pmx,** premaxilla; **siof,** secondary infraorbital foramen; **spf,** sphenopalatine foramen. Scale = 10 mm.

external surface of the nasals is gently convex.

The anteriormost margin of both nasals is damaged and it is not known how much bone is missing. This margin is poorly known in most djdachtatherioids; the best known taxon, *Kryptobaatar*, has a substantial nasal overhang of the external nasal aperture (Wible and Rougier 2000). Enough of the anterior margin of the nasal is preserved in *Guibaatar*, more so on the right side, to confirm the presence of an anterior nasal notch (Lilligraven and Krusat 1991; "ann" in Fig. 2), as in *Kryptobaatar* (Wible and Rougier 2000). A pair of nasal foramina ("nf" in Fig. 2) is present in each nasal in *Guibaatar* at the level of the posterodorsal process of the premaxilla. The much larger posterior nasal foramen is oval, with an anteroposterior long axis, and the small anterior foramen is circular. There is a minor difference between the two sides: the nasal foramina are within a common depression of the right side but not on the left. The CT scans show that both nasal foramina communicate with the nasal cavity.

Lacrimal ("lac" in Figs. 2–3, 5).—The lacrimal is only preserved on the left side, which is the basis for the descriptions that follow. The lacrimal had a pristine posterior border in the supraorbital margin, but this was damaged during preparation, fortunately after line drawings were made. The facial process of the lacrimal is substantial, arcuate, and gently convex. It is wedged between the maxilla anterolaterally, the nasal anteromedially, and the frontal posteromedially; its free posteromedial margin forms the supraorbital margin between the maxilla and frontal.

The lacrimal has an orbital process with an anteroposterior footprint greater than the facial process and is the major component of the orbital pocket roof. As noted with the Maxilla above, a small area of lacrimal anterior to the level of its facial process underlies the maxilla, demarcated by a suture, and contributes to the roof of the orbital pocket (Fig. 3). Posterior to the level of the facial process, there is a similar extension of the lacrimal orbital process in the orbital pocket roof reaching nearly to the orbital ridge ("or" in Fig. 5), the crest on the frontal marking the posterior limit of the orbital pocket in, for example, *Chulsanbaatar* and *Nemegtbaatar* (Kielan-Jaworowska et al. 1986), and

Tombaatar (Rougier et al. 1997). Breakage to the lacrimal in the orbital rim in *Guibaatar* revealed a double layer of bone anterior to the orbital ridge, with the orbital process of the lacrimal overlain by the frontal squama. Despite our attempts to locate a lacrimal foramen, we were not successful even in the CT scans. In *Nemegtbaatar* (Hurum 1994) and *Kryptobaatar* (Wible and Rougier 2000), the lacrimal foramen is immediately ventral to the supraorbital rim within the lacrimal. The corresponding area in *Guibaatar* does not preserve bone. Although the lacrimal's contribution to the orbital pocket roof is assured, we are uncertain how far ventrally the lacrimal extended into the medial wall of the orbit as sutures are not well preserved. There is an oblique line running from anterodorsal to posteroventral below the level of the lacrimal facial process that may represent the suture between the lacrimal and maxilla (not shown in the figures). If so, the lacrimal in *Guibaatar* has an orbital exposure resembling that in *Kryptobaatar* (Wible and Rougier 2000).

Frontal ("fr" in Figs. 2, 4–5).—The paired frontal has a squama in the skull roof and an orbital process in the medial wall. Between the two sides of *Guibaatar* most of the squama can be reconstructed, except the posteriormost extent between the parietals. The left orbital process preserves most of the anterodorsal aspect; the right side is missing the anterior part exposed on the left, but reaches farther ventrally, completing the medial orbital wall in the vicinity of the sphenopalatine foramen.

The left and right squamae are separated by an interfrontal or metoptic suture (Fig. 2). The left squama retains most of the oblique anterior margin, which contacts the nasals anteromedially and the lacrimal posterolaterally. As noted with the Nasal above, the left and right frontals together make a V-shaped incursion between the left and right nasals, as typical in djadochtatherioids (Kielan-Jaworowska and Hurum 1997; Wible and Rougier 2000; Rougier et al. 2016) and most Mesozoic mammaliaforms (e.g., *Morganucodon*, Kermack et al. 1981; *Haldanodon*, Lillegraven and Krusat 1991; *Vintana*, Krause et al. 2014). The squama's contribution to the supraorbital margin is most intact on the right side, which bends posteromedially. The squama immediately posterior to the facial process of the lacrimal in the supraorbital rim contributes to the orbital pocket roof, but as noted above is underlain by the lacrimal. The surface contour of the squama is generally flat, although the anteriormost part is slightly sunken, more so on the right side, likely the result of postmortem deformation. In the posterolateral aspect of each squama, recessed medially from the supraorbital margin is the overlying anterior process of the parietal, which is V-shaped with the apex directed anteriorly. As the frontal is incomplete posterior to this level, the shape of the frontoparietal (coronal) suture between the anterior processes of the parietal is unknown. This is typically a U-shaped suture in djadochtatherioids (Kielan-Jaworowska and Hurum 1997; Wible and Rougier 2000; Rougier et al. 2016), although the U is not very deep in *Guibaatar* given the orientation of the medial aspect of the anterior processes of the parietal.

On the left side (Fig. 5), the orbital ridge on the frontal is close to the anteroposterior middle of the orbital process. Anterior to the orbital ridge, the frontal forms the posteromedial wall of the orbital pocket. Although a suture is not preserved as bone is missing, the dorsal margin of the frontal here likely contacted the lacrimal, which lies in the orbital pocket roof. Anteriorly, the frontal likely contacted the maxilla, although a sizeable gap currently separates the two bones. We interpret this gap as artefactual, but given that the specimen's right side lacks any bone in this area (Fig. 4), we are uncertain how the frontal and/or maxilla closed this gap. Posterior to the orbital ridge and ventral to the broken supraorbital margin is a concavity in the frontal orbital process that is shallower than the orbital pocket (Fig. 5). This concavity likely did not house musculature (Gambaryan and Kielan-Jaworowka 1995) but may have marked externally the tapering anterior end of the cerebrum (see Kielan-Jaworowska and Lancaster 2004). Most of the ventral contacts of the left orbital process are not preserved, except for a narrow one with the maxilla anterodorsal to the sphenopalatine foramen.

On the right side (Fig. 4), only the part of the orbital process posterior to the orbital ridge is preserved. Here, bone extends from the supraorbital margin to the area dorsal and posterior to the sphenopalatine foramen. This column of bone is anteroposteriorly broad dorsally and ventrally and narrow in the middle. As noted with the Maxilla above, it is uncertain if this entire column is frontal or if one or two roughly horizontal cracks mark the incursion of another bone, such as the orbitosphenoid. Either the frontal contacts the maxilla to complete the sphenopalatine foramen (as reported in *Kryptobaatar*, Wible and Rougier 2000, and *Mangasbaatar*, Rougier et al. 2016) or the orbitosphenoid (see "?" in Fig. 4) may separate the two bones posterior to the sphenopalatine foramen (as reported in *Nemegtbaatar*, Hurum 1994). In the posterior margin of the narrowest part of this column of bone is a smooth-edged notch present bilaterally in *Guibaatar*. We interpret this as the anterior border of the ethmoidal foramen ("ef" in Fig. 4), which occupies a similar position in other djadochtatheriids (Wible and Rougier 2000; Rougier et al. 2016).

Parietal ("pa" in Fig. 2).—In djadochtatherioids, the paired parietal is a major component of the posterior braincase roof and also forms the postorbital process, which is particularly prominent in djadochtatheriids (Kielan-Jaworowska and Hurum 1997; Wible and Rougier 2000; Rougier et al. 2016). Each parietal has a laterally placed anterior process overlying the frontal squama, and the frontoparietal suture between the anterior processes is U-shaped. The anterior process forms the supraorbital margin and the base for the postorbital process. In *Guibaatar*, the only part of the parietal that is preserved is the pointed tip of the anterior process overlying the frontal squama

(Fig. 2). There is shape disparity between the preserved tip of the anterior process on the two sides: the left side has straight medial and lateral sides but the lateral side on the right is irregular. Given that the underlying frontal squamae do not show facets accommodating more parietal on either side, we interpret this shape disparity as real. The anterior process of *Guibaatar* differs slightly from that in other djadochtatherioids in that its lateral margin is not entirely in the supraorbital rim, but has a narrow strip of frontal squama between it and the rim. As noted with the Frontal above, the frontoparietal suture was likely U-shaped in *Guibaatar*, but given the shape of the anterior processes of the parietals the U was not very deep.

Alisphenoid ("as" in Fig. 3).—The lateral walls of the space housing the nasopharynx posterior to the choanae, the basipharyngeal canal (Evans 1993), are formed primarily by the anterior process of the alisphenoid in djadochtatherioids (Wible and Rougier 2000; Rougier et al. 2016). The anterior process has a pointed anterior tip that is wedged between the palatine and maxilla medial to the M2. This pointed anterior tip on the left side (Fig. 3) is the only part of the alisphenoid that we can confidently identify in *Guibaatar*, suggesting that it follows the usual djadochtatherioid pattern. As noted with the Palatine above, the right side exposes the roof and lateral wall of the basipharyngeal canal immediately posterior to the choanae, where some contribution from the anterior process of the alisphenoid is anticipated but we cannot confirm.

Pterygoid.—As noted by Wible and Rougier (2000), following Barghusen (1986), the mesocranium in many multituberculates has a pair of pterygopalatine ridges that subdivide the basipharyngeal canal into a pair of medial and lateral pterygopalatine troughs. In some (e.g., *Kryptobaatar*, Wible and Rougier 2000), there is also a midline crest on the vomer that further subdivides the space. Despite the name pterygopalatine, this structure is generally held to be composed of pterygoid (Wible and Rougier 2000; Rougier et al. 2016). *Guibaatar* preserves most of the right pterygopalatine ridge ("ppr" in Fig. 3) and part of the base of the left one (not visible in Fig. 3). The ridge extends posteriorly 4 mm from the choanae and is a little over 1 mm high. It can be traced anteriorly into the nasal cavity only a short distance before it disappears into matrix, including in the CT scans. The anterior half of the ridge is narrow and lies in a parasagittal plane. The posterior half bends laterally and enlarges into a digitiform end, resembling the therian pterygoid hamulus. The knobby posterior end of the pterygopalatine ridge in *Guibaatar* is not freestanding but is connected to the mesocranial roof by the base running the length of the ridge.

Vomer.—As noted with the Pterygoid above, some multituberculates (e.g., *Kryptobaatar*, Wible and Rougier 2000) have a midline crest formed by the vomer between the pterygopalatine ridges in the basipharyngeal canal. Enough of the midline roof between the pterygopalatine ridges is preserved in *Guibaatar* to confirm the absence of a midline crest. This condition has also been reported in *Mangasbaatar* by Rougier et al. (2016).

Squamosal ("sq" in Figs. 6–7).—The paired squamosal is only represented by the partial right element in articulation with the partial right petrosal and jugal in *Guibaatar*. The squamosal has a dorsal flange ("df" in Fig. 7A) appressed on the petrosal and a zygomatic process ("zpsq" in Figs. 6A, 7A) bearing the glenoid fossa.

Most of the dorsal flange is preserved (Fig. 7); it is a tall and narrow element entirely excluded from the endocranium by the petrosal. Its dorsal margin is broken and a segment that likely extended to meet the parietal is missing. Distinct sutures on its anterior and posterior borders separate the dorsal flange from the underlying petrosal. Regarding the former (see Fig. 7), the anterior suture ends ventrolaterally in a crack in an area covered by thick glue and cannot be traced onto the zygomatic process. Running parallel to and behind the anterior suture is a rounded ridge on the dorsal flange that represents the continuation of the nuchal crest onto the squamosal ("nc" in Fig. 7B). The ventral part of the posterior suture is visible in Figure 6.

Extending laterally and then curving anteriorly from the dorsal flange is the zygomatic process. The ventral extension of the nuchal crest described on the dorsal flange continues onto the dorsolateral aspect of the zygomatic process. In ventral view, the main feature on the zygomatic process is the glenoid fossa ("gf" in Fig. 6A), which is oval, mediolaterally wider than anteroposteriorly long. The articular surface is relatively flat, although a weak prominence on the posterolateral border creates a slight degree of concavity. The weak prominence marks the posterior end of the intermediate zygomatic ridge, which is visible in lateral view (not shown). The intermediate zygomatic ridge provides attachment for the pars posterior of the superficial masseter (Gambaryan and Kielan-Jaworowska 1995). A posterior zygomatic ridge as reported in other djadochtatherioids (Gambaryan and Kielan-Jaworowska 1995) is not in evidence. Posteromedial to the glenoid fossa, the zygomatic process has a long, narrow neck, which has a crack across it that goes completely through the squamosal; the parts have been rearticulated and glued together. The suture delimiting the squamosal and the petrosal follows the anterior border of the neck medially and disappears into matrix left to buttress the crista parotica ("cp" in Fig. 6B). It likely ran posteriorly, parallel to the posterior part of the crista parotica as, for example, in *Mangasbaatar* (Rougier et al. 2016: fig. 21).

Anterior to the glenoid fossa, the zygomatic process tapers, is mediolaterally constricted, and ultimately broken at its anterior end (Fig. 6A). Interpreting the morphology distal to the glenoid is hampered by calcite matrix infill and several breaks repaired with glue. There is a separate thin bone on the inner aspect of the zygomatic process that we interpret as a partial jugal (see below). However, it is

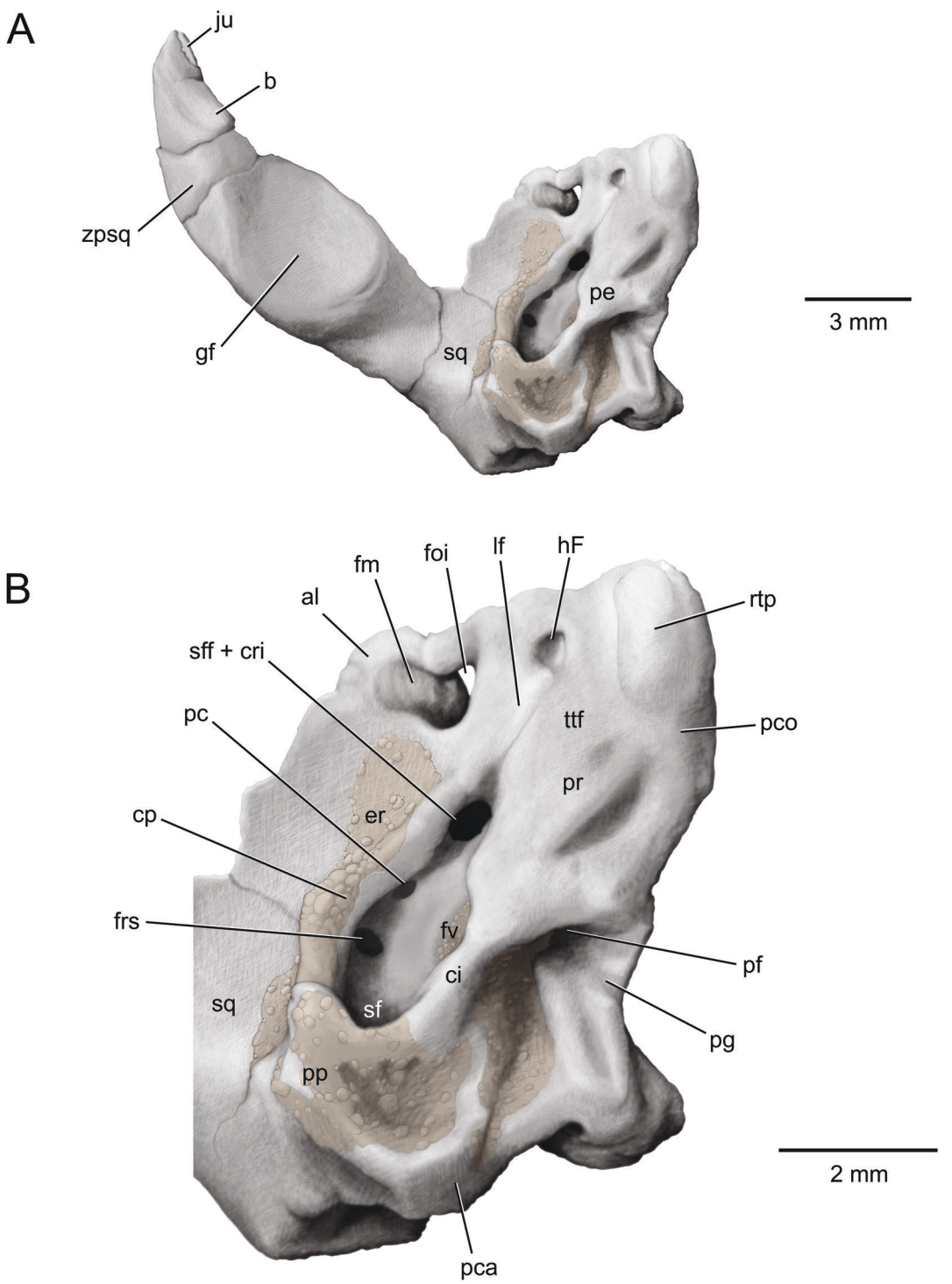

Fig. 6.—*Guibaatar castellanus*, CEVB 11908. **A,** left petrosal and squamosal in ventral view; **B,** close up of left petrosal in ventral view. Reddish-brown is matrix. Abbreviations: **al,** anterior lamina; **b,** boss on zygoma possibly marking anterior limit of squamosal; **ci,** crista interfenestralis; **cp,** crista parotica; **er,** epitympanic recess; **fm,** foramen masticatorum; **foi,** foramen ovale inferium; **frs,** foramen for ramus superior; **fv,** fenestra vestibuli; **gf,** glenoid fossa; **hF,** hiatus Fallopii; **ju,** jugal; **lf,** lateral flange; **pc,** prootic canal; **pca,** pars canalicularis; **pco,** pars cochlearis; **pe,** petrosal; **pf,** perilymphatic foramen; **pg,** perilymphatic groove; **pp,** paroccipital process of petrosal; **pr,** promontorium of petrosal; **rtp,** rostral tympanic process of petrosal; **sf,** stapedius fossa; **sff + cri,** secondary facial foramen and canal for ramus inferior of stapedial artery; **sq,** squamosal; **ttf,** tensor tympani fossa; **zpsq,** zygomatic process of squamosal.

possible that a third bone, the distal end of the zygomatic process of the maxilla is also included. In ventral view, there is a prominent boss on the lateral margin ("b" in Fig. 6A), which marks the anterior end of the intermediate zygomatic ridge in lateral view. A seam of matrix runs along the medial side of this boss, separating it from the jugal, which lies medial to the squamosal. Although a suture is not apparent on the lateral surface because of calcite obscuring matrix, this boss may mark the posterior limit of the zygomatic process of the maxilla, resembling the condition in *Catopsbaatar* (Kielan-Jaworowska et al. 2005).

Jugal ("ju" in Figs. 6A, 7A).—The paired jugal is represented by a partial right element applied to the inner aspect of the zygoma preserved with the partial squamosal and petrosal. The thin jugal is incomplete anteriorly. What is preserved is oval and not as dorsoventrally tall as the bones it abuts. If our interpretation that the distal part of the zygomatic process of the maxilla is preserved with zygomatic process of the squamosal is correct, the jugal straddled the oblique suture between the two bones. The partial jugal closely resembles that described for *Kryptobaatar* (Wible and Rougier 2000).

Petrosal ("pe" in Figs. 6A, 7A).—The paired petrosal is represented by the partial right element preserved with the partial right squamosal and jugal. The petrosal in therians, for descriptive purpose, is generally divided into the pars cochlearis (for the cochlear duct and saccule) and the pars canalicularis (for the utricle and semicircular canals). As in most extinct non-therian mammaliforms (Kermack and Kielan-Jaworowska 1971; Hopson and Rougier 1993; Rougier and Wible 2006), the petrosal of *Guibaatar* has a third part, the anterior lamina. Among extant mammals, monotremes have an ossification resembling the anterior lamina in fossils; however, it forms as a separate intramembranous ossification, the lamina obturans, that fuses with the endochondral petrosal during development (Griffiths 1978; Presley 1981; Kuhn and Zeller 1987; Zeller 1989). Sutures have not been found delimiting the anterior lamina from the petrosal in fossils, yet an origin as a separate intramembranous ossification as in monotremes seems likely as they represent the only model for reconstructing this morphology. Nevertheless, we describe the anterior lamina with the petrosal here. In the following, we report the surficial features of the petrosal; unless noted the CT scans confirm our superficial identifications.

In ventral (tympanic) view, the pars cochlearis is represented by the elongate promontorium ("pco" and "pr" in Fig. 6B) housing the cochlear duct. In the other djadochtatherioids for which the cochlear duct is known (i.e., *Nemegtbaatar*, *Chulsanbaatar*, Hurum 1998; cf. *Tombaatar*, n. sp., Ladevèze et al. 2010), it is reported to be slightly curved laterally. As revealed in the CT scans, the cochlear duct in *Guibaatar* has a similar shape, but is subtly more curved laterally, reminiscent of the condition in the Late Cretaceous gondwanatherian *Vintana* (Hoffmann et al. 2014: fig. 8). As in these taxa, *Guibaatar* has a tubular promontorium; the anterior half lies in what we interpret as a parasagittal plane and the posterior half is oblique to that. The anteromedial aspect of the promontorium has a well-developed, rounded prominence with an oval outline, longer than wide ("rtp" in Fig. 6B); the anterior half of this structure is filled with calcite matrix. This prominence is roughly in the same place as the rostral tympanic process in *Kryptobaatar* (Wible and Rougier 2000) but is even larger in girth and height, yet not to the extreme extent as the rostral tympanic process reported for *Mangasbaatar* (Rougier et al. 2016). Posterior to the rostral tympanic process in *Guibaatar* is a depression in the medial aspect of the promontorium, which produces an incurved outline as has been noted in other djadochtatheriids (e.g., *Kryptobaatar*, Wible and Rougier 2000; cf. *Tombaatar*, n. sp., Ladevèze et al. 2010; *Mangasbaatar*, Rougier et al. 2016). The surface of the promontorium does not have distinct vascular grooves for the internal carotid and stapedial arteries as has been described for other djadochtatheriids (e.g., *Kryptobaatar*, Wible and Rougier 2000; cf. *Tombaatar*, n. sp., Ladevèze et al. 2010; *Mangasbaatar*, Rougier et al. 2016). The space lateral to the rostral tympanic process in *Guibaatar* has a broad, shallow concavity that likely housed the tensor tympani muscle ("ttf" in Fig. 6B).

Two large openings are imperfectly preserved in the rear face of the promontorium: the fenestra vestibuli posterolaterally and the perilymphatic foramen posteriorly ("fv" and "pf," respectively in Fig. 6B). Due to preservation, the shape of neither foramen can be fully visualized. The preserved three sides of the fenestra vestibuli suggest a rmore circular opening, which is in line with the stapedial ratio (length to width; Segall 1970) in other djadochtatheriids (i.e., 1.39 in *Kryptobaatar*, Wible and Rougier 2000; 1.13 in cf. *Tombaatar*, n. sp., Ladevèze et al. 2010; and 1.3 in *Mangasbaatar*, Rougier et al. 2016). The ventral border of the fenestra vestibuli has a faint indentation that likely accommodated the stapedial artery. The preserved three sides of the perilymphatic foramen suggest an oval opening, wider than high, perhaps twice the size of the fenestra vestibuli. A groove for the perilymphatic duct ("pg" in Fig. 6B), marked by a low posterior wall, runs from the medial border to the perilymphatic foramen. Separating the fenestra vestibuli and perilymphatic foramen is a horizontal crista interfenestralis ("ci" in Fig. 6B), as tall as the promontorium, that extends posterolaterally onto the pars canalicularis ("pca" in Fig. 6B).

In ventral view, the pars canalicularis lies posterior and lateral to the pars cochlearis. Delimiting medial and lateral spaces on the pars canalicularis is the crista interfenestralis. The medial space includes a relatively flat, triangular shelf posterior to the perilymphatic foramen that contains the subtle groove for the perilymphatic duct described above; the bone lateral to this shelf is broken. The posterior margin of the medial space is also imperfectly preserved and it is unclear how much bone is missing. Given the morphology of the rear of the promontorium, the crista interfenestralis,

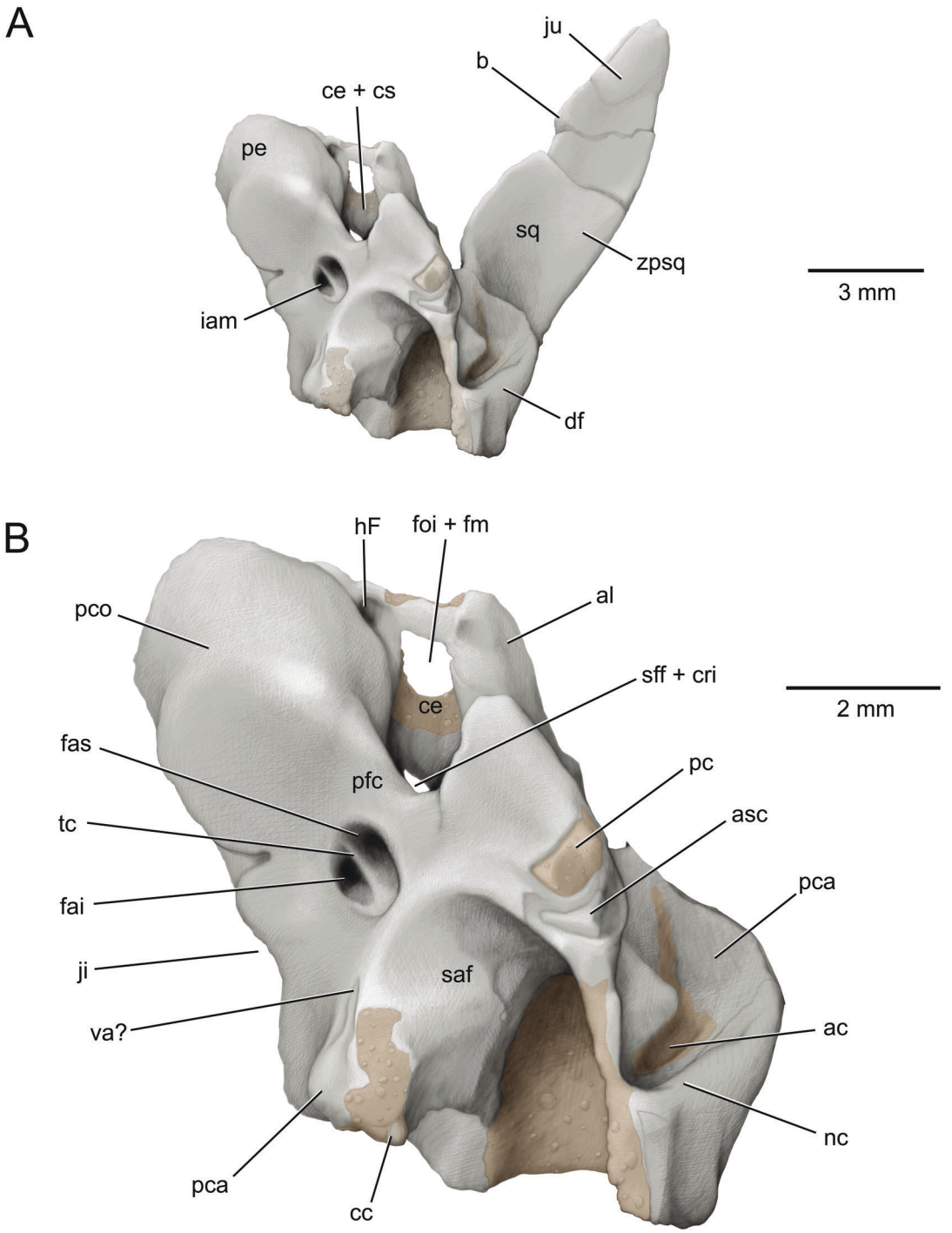

Fig. 7.—*Guibaatar castellanus*, CEVB 11908. **A,** left petrosal and squamosal in oblique dorsal view; **B,** close up of left petrosal in oblique dorsal view. Reddish-brown is matrix. Petrosal is tilted laterally to show the internal acoustic meatus, which exposes the medial aspect of the zygoma in A. Abbreviations: **ac,** ascending canal; **al,** anterior lamina; **asc,** anterior semicircular canal; **b,** boss on zygoma possibly marking anterior limit of squamosal; **cc,** crus commune; **ce + cs,** cavum epiptericum and cavum supracochleare; **df,** dorsal flange of squamosal; **fai,** foramen acusticum inferius; **fas,** foramen acusticum superius; **foi + fm,** foramen ovale inferium and foramen masticatorium; **hF,** hiatus Fallopii; **iam,** internal acoustic meatus; **ji,** jugular incisure; **ju,** jugal; **nc,** nuchal crest; **pc,** prootic canal; **pca,** pars canalicularis; **pco,** pars cochlearis; **pe,** petrosal; **pfc,** prefacial commissure; **saf,** subarcuate fossa; **sff + cri,** secondary facial foramen and canal for ramus inferior; **sq,** squamosal; **tc,** transverse crest; **va?,** vestibular aqueduct?; **zpsq,** zygomatic process of squamosal.

and this triangular shelf, *Guibaatar* likely had a well-developed jugular fossa, a portion of the tympanic cavity around the jugular foramen, as in other djadochtatheriids (e.g., *Kryptobaatar*, Wible and Rougier 2000; *Mangasbaatar*, Rougier et al. 2016).

The lateral space extends farther anteriorly than the medial space and is delimited medially by the posterior third of the promontorium as well as the crista interfenestralis. Defining the lateral space laterally is another high crest, the crista parotica ("cp" in Fig. 6B). This crest is thin and shows some broken surfaces along its ventral edge, in particular anteriorly. There is no indication of a tympanohyal on the crista parotica posteriorly, but this may be due to preservation rather than absence. In the rear of the lateral space is a shelf largely hidden in ventral view with a subtle round depression, the stapedius fossa ("sf" in Fig. 6B), which we were unable to fully expose. The stapedius fossa is in the same position as in *Kryptobaatar*, and based on the CT scans of *Guibaatar* we report that the fossa extends onto the lateral face of the crista interfenestralis as in *Kryptobaatar* (Wible and Rougier 2000). The posterior wall of the lateral space is formed by the broad base of the paroccipital process ("pp" in Fig. 6B), which projects ventral to the abutting squamosal and the promontorium. How much farther the paroccipital process projected is not known as its tip is missing. The two cristae defining the lateral space, the cristae interfenestralis and parotica, likely contacted the paroccipital process as in other djadochtatheriids (e.g., *Kryptobaatar*, Wible and Rougier 2000; *Mangasbaatar*, Rougier et al. 2016), but this is not preserved in *Guibaatar*.

Under cover of the crista parotica in the roof of the lateral space are three foramina. The middle foramen, the smallest of the three, is oval and opposite the fenestra vestibuli; the posterior one is round; and the anterior foramen, the largest, is oval and opens into the rear of the endocranial space housing the cavum supracochleare and cavum epiptericum (see below). The middle foramen is the tympanic aperture of the prootic canal, the posterior is the foramen for the ramus superior of the stapedial artery, and the anterior is the most complex, including the secondary facial foramen and the canal for the ramus inferior of the stapedial artery ("pc," "frs," and "sff + cri," respectively in Fig. 6B); the rationale for our interpretation is included with the nervous and vascular reconstructions below. Whereas the canal for the ramus inferior (canal for ?maxillary artery of Kielan-Jaworowska et al. 1986; post-trigeminal canal of Rougier et al. 1996a) is a stand-alone structure in most multituberculates (Kielan-Jaworowska et al. 1986; Wible and Hopson 1995; Wible and Rougier 2000), the other three foramina exhibit three different patterns in djadochtatherioids: the prootic canal and ramus superior foramen confluent (e.g., *Kryptobaatar*, Wible and Rougier 2000), the prootic canal and secondary facial foramen confluent (i.e., cf. *Tombaatar*, n. sp., Ladevèze et al. 2010; *Mangasbaatar*, Rougier et al. 2016), and as in *Guibaatar* all three separated (i.e., *Chulsanbaatar*, Wible and Rougier 2000). The crista parotica continues anteromedially passed the combined secondary facial foramen and canal for the ramus inferior as a low lateral flange ("lf" in Fig. 6B). In turn, the lateral flange ends anteriorly at an anteromedially directed foramen ("hF" in Fig. 6B) that opens endocranially within the cavum epiptericum (Fig. 7B). We interpret this foramen as the hiatus Fallopii for the greater petrosal nerve; Ladevèze et al. (2010) reported a similarly situated hiatus Fallopii in cf. *Tombaatar*, n. sp.

On the ventral surface, lateral to the crista parotica and paroccipital process is an elongate concavity that is deepest next to the crista parotica ("er" in Fig. 6B). Slightly more than half of this concavity is on the petrosal, extending anteriorly to the level of the secondary facial foramen + canal for the ramus inferior, and the posterior remainder is on the squamosal. Part of the roof of this concavity is obscured by matrix left on both bones to support the lateral aspect of the delicate crista parotica. The bulk of this space represents the epitympanic recess, the roof of the mallear-incudal articulation (Klaauw 1931). In other multituberculates, the posterior part of the epitympanic recess usually narrows and has an identifiable fossa incudis for the crus breve of the incus (*Kryptobaatar*, Wible and Rougier 2000: cf. *Tombaatar*, n. sp., Ladevèze et al. 2010; *Mangasbaatar*, Rougier et al. 2016). *Guibaatar* does not have such a constriction. Anterior to the epitympanic recess in what is interpreted as the anterior lamina ("al" in Fig. 6B) is a large dumbbell-shaped foramen that opens endocranially in the cavum epiptericum. In other multituberculates, two foramina are situated here, which following Simpson (1937; see Wible and Rougier 2000) are identified as the foramen ovale inferium medially and the foramen masticatorium laterally ("foi" and "fm," respectively in Fig. 6B), both transmitting branches of the mandibular division of the trigeminal nerve. The bone at the slight constriction between the two openings in *Guibaatar* appears smooth, but we cannot exclude the possible presence of a thin bony septum fully separating the foramina.

In dorsal (endocranial) view (Fig. 7), the pars cochlearis is elongate and tubular, as in ventral view. The anterior third of the pars cochlearis is calcite and the posterior two-thirds bone. The calcite portion has a rounded prominence on its lateral aspect that resembles a similar structure on the petrosal in *Kryptobaatar* that buttresses the pila antotica on the basisphenoid (Wible and Rougier 2000: fig. 25). The bony portion of the pars cochlearis in *Guibaatar* is flat with no distinct crista petrosa. At the posterior end of the pars cochlearis is the round, deep internal acoustic meatus ("iam" in Fig. 7A). Recessed in the meatus is the transverse crest ("tc" in Fig. 7B), which delimits the smaller foramen acusticum inferius medially and the foramen acusticum superius laterally ("fai" and "fas," respectively in Fig. 7B). The former appears to have only a single oval opening, which would include passage for the cochlear nerve and ventral branch of the vestibular nerve; the latter has a facial canal anteriorly and the larger dorsal vestibular area posteriorly. Anterolateral to the internal acoustic meatus

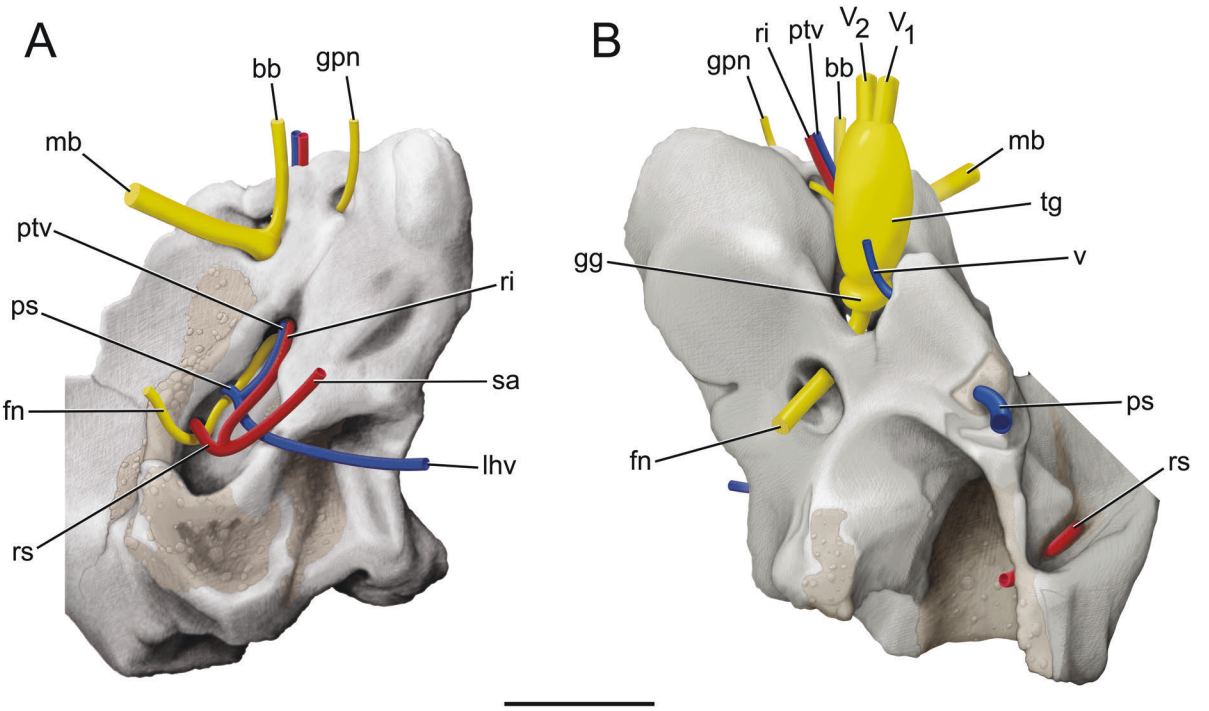

Fig. 8.—*Guibaatar castellanus*, CEVB 11908, nervous and vascular reconstruction on left petrosal. **A,** ventral view; **B,** dorsal view. Trigeminal ganglion and maxillary and ophthalmic divisions would be visible in A, but are not included in order to reduce clutter. Abbreviations: **bb,** buccinator branch; **fn,** facial nerve; **gg,** geniculate ganglion; **gpn,** greater petrosal nerve; **lhv,** lateral head vein; **mb,** masticatory branch; **ps,** prootic sinus; **ptv,** post-trigeminal vein; **ri,** ramus inferior; **rs,** ramus superior; **sa,** stapedial artery; **tg,** trigeminal ganglion; **v,** unnamed vein; **V_1,** ophthalmic division of trigeminal nerve; **V_2,** maxillary division of trigeminal nerve. Scale = 3 mm.

is a thin bar of bone, the prefacial commissure ("pfc" in Fig. 7B), and medial to the internal acoustic meatus is a shallow concavity in the medial margin of the petrosal, the jugular incisure ("ji" in Fig. 7B) indicating the position of the jugular foramen.

Most of the pars canalicularis is missing in dorsal view; the portion preserved forms much of the floor of and part of the opening to the subarcuate fossa ("saf" in Fig. 7B). The preserved part of the subarcuate fossa opening is about three times the width of the internal acoustic meatus. The preserved floor of the fossa is as deep as the width of the opening and also shows that the opening is constricted compared to the fossa. The full depth of the fossa is uncertain as the posterior wall is not preserved. Exposed on the broken dorsal edge of the subarcuate fossa opening are calcite matrix infills for the crus commune medially and the anterior semicircular canal laterally ("cc" and "asc," respectively in Fig. 7B). An open seam of matrix on the anteroventral surface where the crus commune is located may represent the vestibular aqueduct for the endolymphatic duct ("va?" in Fig. 7B). Anterodorsal to the infill for the anterior semicircular canal is a larger matrix infill in what we interpret as the endocranial aperture of the prootic canal ("pc" in Fig. 7B). Continuity between the endocranial and tympanic apertures is not fully assured in the CT scans but represents the most likely channel. In *Ornithorhynchus*, the prootic canal forms between the pars canalicularis and the independent intramembranous lamina obturans (which ossifies to form the anterior lamina), whereas in *Tachyglossus* it is preformed in cartilage considered as pars canalicularis (Wible and Hopson 1995). No matter what the ontogenetic pattern may have been in *Guibaatar*, its prootic canal is close to the probable boundary between the pars canalicularis and the anterior lamina.

Following this criterion, the braincase wall anterior to the squamosal is formed by the pars canalicularis posteriorly, lateral to the subarcuate fossa, and the anterior lamina anteriorly. The anterior lamina is thinner than the pars canalicularis and is broken along its dorsal and anterior edges. The posterolateral surface of the pars canalicularis has an open seam of matrix running parallel to the anterior margin of the dorsal flange of the squamosal ("ac" in Fig. 7B). This seam is in the same position as the ascending canal for the ramus superior of the stapedial artery, a closed vascular channel in other LCMM (e.g., *Nemegtbaatar*, Kielan-Jaworowska et al. 1986; *Kryptobaatar*, Wible and Rougier 2000). It seems likely that the ascending canal was similarly closed in *Guibaatar*. There is no indication

of any foramina for rami temporales in *Guibaatar* as usually occurs on the ascending canal (Wible and Rougier 2000), but this may be a preservation issue.

Between the anterior lamina laterally and the pars cochlearis medially is a deep, oval space, which has several openings in its floor. This space houses the cavum epiptericum anteriorly and cavum supracochleare posteriorly ("ce + cs" in Fig. 7A), for the trigeminal (semilunar) and facial (geniculate) ganglia, respectively, with no identifiable osseous border separating them. The foramen in the floor of the cavum supracochleare is the secondary facial foramen + canal for the ramus inferior already described in the ventral view. In the cavum epiptericum laterally is the foramen for the mandibular nerve that was dumbbell-shaped in ventral view and anteromedially the endocranial aperture of the hiatus Fallopii. Hidden in endocranial view is another foramen posterodorsal to the cavum supracochleare. This foramen runs posteriorly and appears to join the prootic canal based on the CT scans.

In occipital (posterior) view (not illustrated), a ventral portion of the mastoid exposure is present. This exposure is the shape of an inverted triangle with the ventrally directed apex the broken base of the paroccipital process. As preserved, the mastoid exposure is half the height of the incomplete dorsal flange of the squamosal and shows no sign of a posttemporal opening or canal. Nevertheless, it is highly likely that *Guibaatar* had a posttemporal opening and canal, given the broad distribution of this channel in multituberculates where the foramen is generally entirely within the petrosal (Miao 1988; Wible and Rougier 2000; Rougier et al. 2016). Following the terminology of Rougier et al. (1992), the position of the posttemporal canal was used by Wible and Rougier (2000) as the marker to divide the ascending canal for the ramus superior into ventral and dorsal parts in *Kryptobaatar*. Applying the same criteria to *Guibaatar*, much of the ascending canal open between the pars canalicularis and dorsal flange of the squamosal is ventral to the level of the preserved mastoid exposure, which in turn would be ventral to the posttemporal canal. Therefore, much of the open ascending canal in *Guibaatar* is a ventral ascending canal. The composition of the ventral ascending canal of *Guibaatar* may differ from that of *Kryptobaatar*. In *Guibaatar*, the ventral ascending canal is entirely within the pars cancalicularis given its position lateral to the subarcuate fossa; in *Kryptobaatar*, Wible and Rougier (2000: 120) stated that the ventral ascending canal was "presumably entirely within the anterior lamina." The few CT sections of *Kryptobaatar* published in Kik (2002) do not confirm or deny the composition suggested by Wible and Rougier (2000).

Our reconstruction of nerves and vessels on the petrosal of *Guibaatar* are shown in Figure 8. In dorsal view, the facial nerve ("fn" in Fig. 8B) ran through the internal acoustic meatus to the facial canal in the anterolateral aspect of the foramen acusticum superius. After passing ventral to the prefacial commissure, the facial canal opens in the posterolateral aspect of the cavum supracochleare (which is confluent anteriorly with the cavum epiptericum) where the facial nerve joined the geniculate ganglion ("gg" in Fig. 8B). In ventral view (Fig. 8A), the main trunk of the facial nerve ("fn" in Fig. 8A) exited the cavum supracochleare for the middle ear via the secondary facial foramen + canal for the ramus inferior. As this opening is more than three times the area of the facial canal, we are confident that it is more than just a secondary facial foramen, also playing a role in the vascular system as the canal for the ramus inferior (see below). Within the middle ear, the facial nerve ran posteriorly medial to the crista parotica and exited via the stylomastoid notch, the location of which is uncertain as the tympanohyal, which marks the location of the notch, is not preserved but presumably anterior to the paroccipital process. The other major branch of the facial nerve, the greater petrosal ("gpn" in Fig. 8), ran anteriorly along the lateral aspect of the pars cochlearis within the cavum epiptericum and exited that space via the hiatus Fallopii. Anterior to the geniculate ganglion in the cavum epiptericum was the large trigeminal or semilunar ganglion ("tg" in Fig. 8B). The first and second divisions of the trigeminal nerve, the ophthalmic and maxillary ("V_1" and "V_2" in Fig. 8B, respectively), ran forward in the cavum, whereas the third division, the mandibular (V_3), exited the cavum ventrally through the large dumbbell-shaped foramen described above. It divided into masticatory and buccinator branches ("mb" and "bb" in Fig. 8A, respectively), in a manner observed in extant rodents (Hill 1935; Wahlert 1974).

Regarding the arteries, there is no well-developed bony indication for the course of the internal carotid artery in *Guibaatar*, in contrast to the transpromontorial groove present in other djadochtatheriids (e.g., *Kryptobaatar*, Wible and Rougier 2000; cf. *Tombaatar*, n. sp., Ladevèze et al. 2010; *Mangasbaatar*, Rougier et al. 2016). It seems likely that this artery was present as in other multituberculates, and a possible conduit for the internal carotid is across the rear of the rostral tympanic process and then along the lateral side of that structure (Fig. 6). A slight indentation on the ventral margin of the fenestra vestibuli (Fig. 6) is the only indication for the stapedial artery ("sa" in Fig. 8A), which has an extensive groove in other djadochtatheriids (e.g., *Kryptobaatar*, Wible and Rougier 2000; cf. *Tombaatar*, n. sp., Ladevèze et al. 2010; *Mangasbaatar*, Rougier et al. 2016). The presence of the ramus superior of the stapedial artery in *Guibaatar* ("rs" in Fig. 8A) is indicated by a foramen medial to the crista parotica and anterior to the stapedius fossa. Based on the CT scans, this foramen for the ramus superior transmitted the artery to the ventral ascending canal on the lateral surface of the petrosal (Fig. 8B) via an initial posterior and then dorsal course. Following Rougier et al. (1992) and Wible and Rougier (2000), the ventral ascending canal would then lead to the dorsal ascending canal and the posttemporal canal, but these are not preserved in *Guibaatar*. The final artery to consider is the ramus inferior of the stapedial artery ("ri" in Fig. 8A). The details of the course of this artery

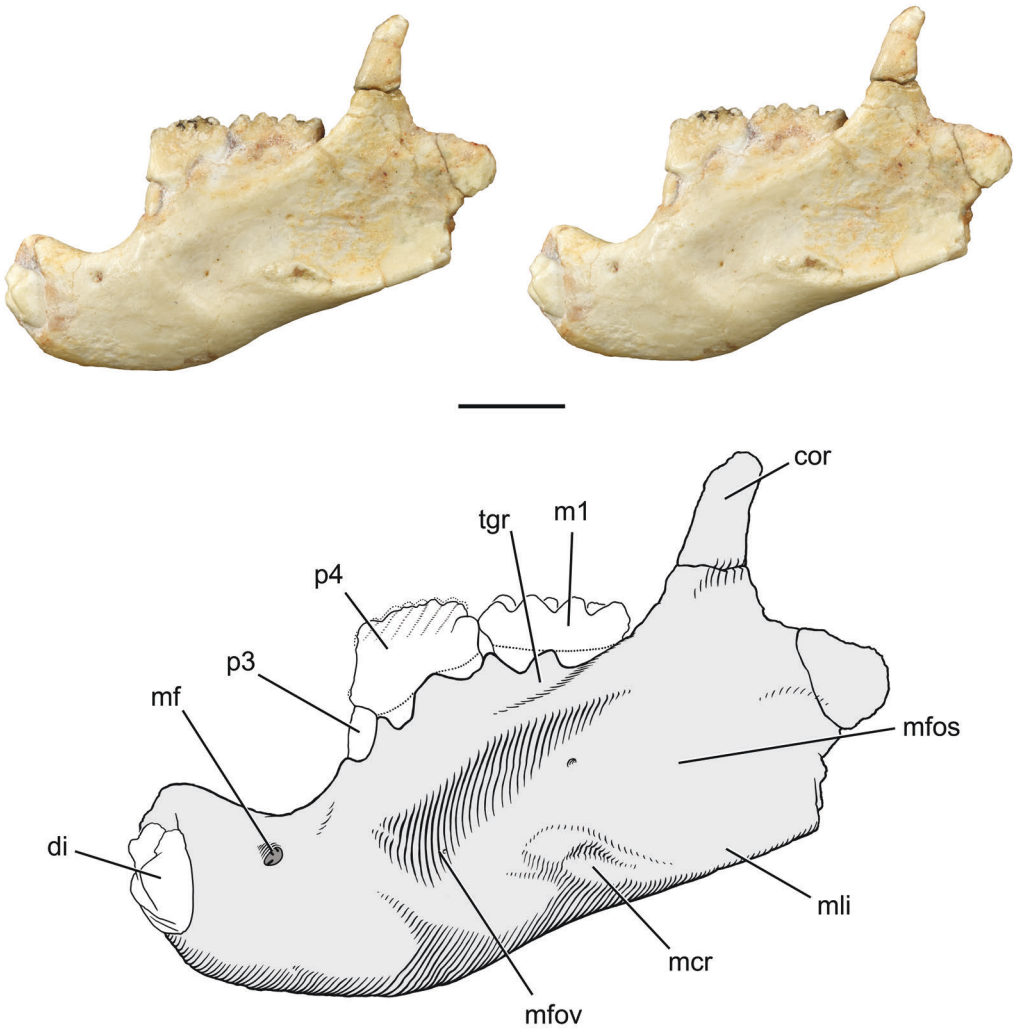

Fig. 9.—*Guibaatar castellanus*, CEVB 11908, left mandible in lateral view. Stereophotographs and line drawing: light grey is bone and dark grey is matrix. Abbreviations: **cor,** coronoid process; **di,** deciduous lower incisor; **m1,** first lower molar; **mcr,** masseteric crest; **mf,** mental foramen; **mfos,** masseteric fossa; **mfov,** masseteric fovea; **mli,** masseteric line; **p3,** third lower premolar; **p4,** fourth lower premolar; **tgr,** temporal groove. Scale = 5 mm.

are known for only a handful of multituberculates. A canal for the ramus inferior has been reported in isolated petrosals assigned to the taeniolabidoid cf. "*Catopsalis*" *joyneri* (= "*Valenopsalis*" *joyneri*, Williamson et al. 2016), the ptilodontoid cf. *Mesodma thompsoni*, and the cimolomyid ?*Meniscoessus* (Kielan-Jaworowska et al. 1986; Luo 1989; Wible and Hopson 1995); this canal opens posteriorly adjacent to the secondary facial foramen and anteriorly at the anterior aspect of the bone. A similar course for the ramus inferior was interpreted for *Kryptobaatar* by Wible and Rougier (2000), although only the posterior entry into the canal was observed, confluent with the prootic canal. Ladevèze et al. (2010) reconstructed a different pathway for the ramus inferior in cf. *Tombaatar*, n. sp., with the artery exposed on the ventral surface of the petrosal. In *Guibaatar*, a separate canal for the ramus inferior is lacking and, as noted above, the foramen transmitting the facial nerve from the cavum supracochleare to the middle ear is too large just to hold the nerve. We suggest that it also transmitted the ramus inferior and perhaps the post-trigeminal vein. These vessels would then run anteriorly in the medial floor of the cavum epiptericum in company with the greater petrosal nerve. As the greater petrosal nerve left the cavum via the hiatus Fallopii, the ramus inferior and post-trigeminal vein continued anteriorly within the cavum. This course is reminiscent of that in the isolated petrosals noted above, just not fully enclosed in a separate canal.

Regarding the veins, the prootic sinus in *Guibaatar* ("ps" in Fig. 8B) left the endocranium via the prootic canal, the broken dorsal end of which is visible anterior to the anterior semicircular canal. We identify two possible foramina of exit for the prootic sinus. One is the tympanic

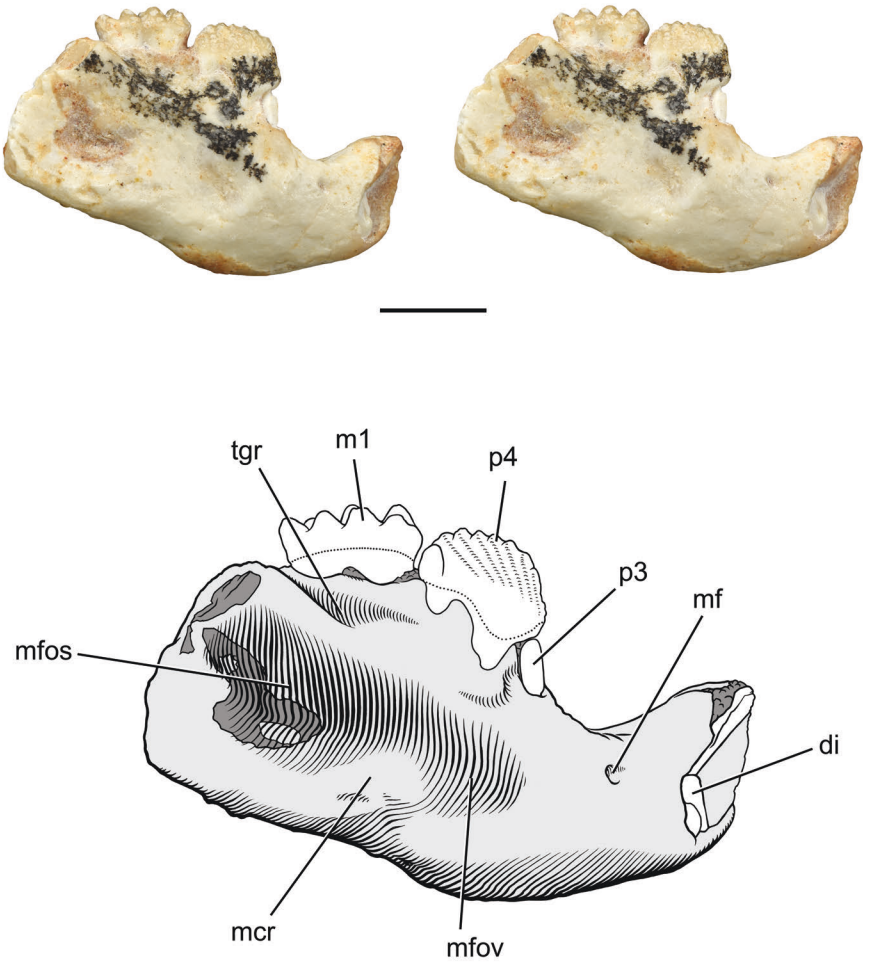

Fig. 10.—*Guibaatar castellanus*, CEVB 11908, right mandible in lateral view. Stereophotographs and line drawing: light grey is bone and dark grey is matrix. Abbreviations: **di,** deciduous lower incisor; **m1,** first lower molar; **mcr,** masseteric crest; **mf,** mental foramen; **mfos,** masseteric fossa; **mfov,** masseteric fovea; **p3,** third lower premolar; **p4,** fourth lower premolar; **tgr,** temporal groove. Scale = 5 mm.

aperture of the prootic canal on the ventral surface between the secondary facial foramen + canal for the ramus inferior anteriorly and the foramen for the ramus superior posteriorly (Fig. 8A). The other is the unnamed opening in the posterodorsal wall of the cavum supracochleare mentioned above ("v" in Fig. 8B). To our knowledge, this latter opening has not been described for any multituberculate. However, it lies in proximity to the course for the prootic sinus in an open sulcus through the cavum supracochleare reconstructed for cf. *Tombaatar*, n. sp., by Ladevèze et al. (2010). The prootic sinus likely joined the post-trigeminal vein mentioned above and left the middle ear in proximity to the jugular foramen as the lateral head vein ("lhv" in Fig. 8A). The petrosal shows no evidence for an inferior petrosal sinus, but this may have been lost due to damage along the medial side of the bone.

Mandible.—Incomplete left and right dentaries are present (Figs. 9–13); the body (horizontal ramus) is well preserved in both but the left one retains more of the ramus (ascending ramus). Missing entirely is the posterior part of the ramus, from the level posterior to the coronoid process. The mandible has a large deciduous incisor, with a permanent replacement forming beneath it, separated by a U-shaped diastema from four cheek teeth, p3–4, m1–2 (see Dentition below). The erupting m2 is preserved only on the right mandible (Fig. 12).The alveolus for the large deciduous incisor occupies the rostral aspect (Figs. 9–10). It is oval with a dorsoventral long axis. The medial margin of the alveolus appears unbroken on both dentaries, whereas the lateral margin shows some damage. A single mental foramen ("mf" in Figs. 9–10) is situated in the deepest part of the diastema, close to the dorsal margin; it is directed

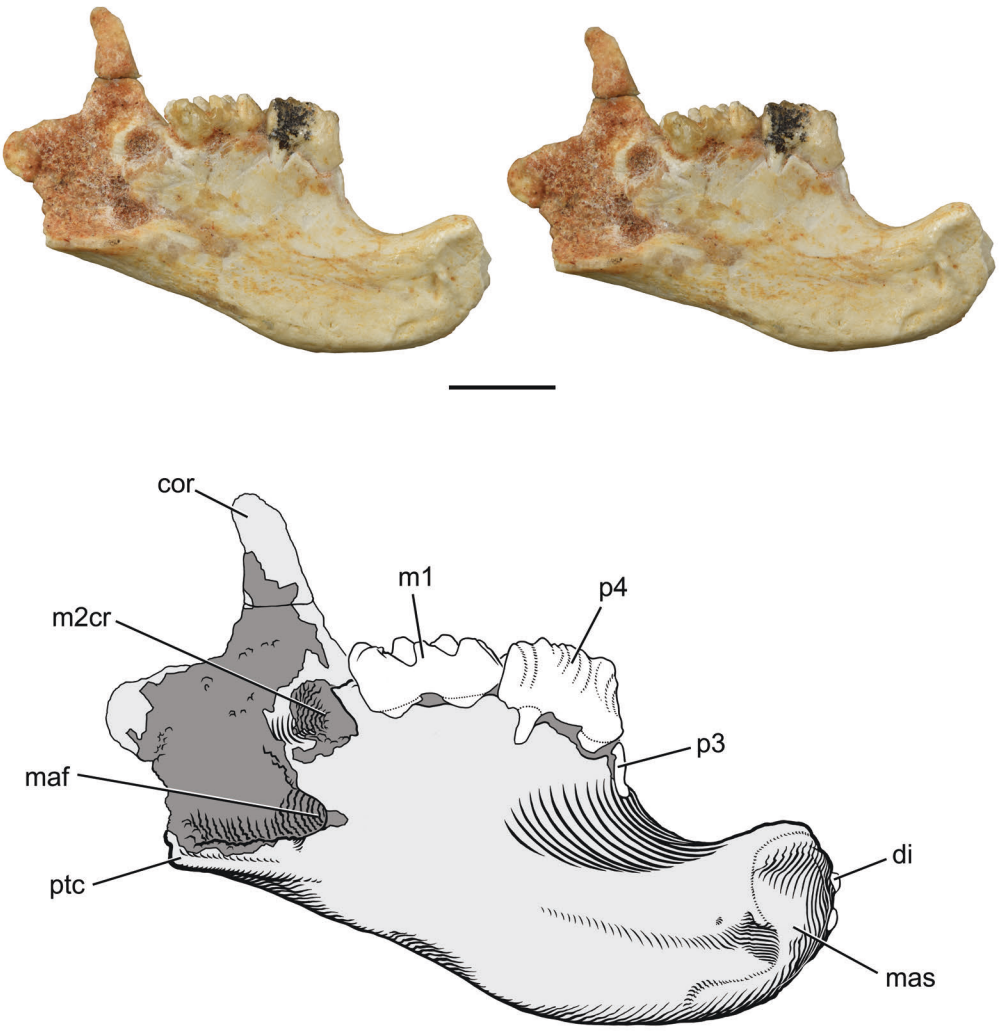

Fig. 11.—*Guibaatar castellanus*, CEVB 11908, left mandible in medial view. Stereophotographs and line drawing: light grey is bone and dark grey is matrix. Abbreviations: **cor,** coronoid process; **di,** deciduous lower incisor; **m1,** first lower molar; **m2cr,** second lower molar crypt; **maf,** mandibular foramen; **mas,** mandibular symphysis; **p3,** third lower premolar; **p4,** fourth lower premolar; **ptc,** pterygoid crest. Scale = 5 mm.

anteriorly and has a short, subtle groove extending from it. The ventral margin of the mandible from anterior to posterior is convex below the incisor and diastema in a horizontal plane, and straight posterior to that but angled posterodorsally. The mandible is deepest at the level of the mesial root of the p4.

Much of the lateral surface of the body ventral to the cheek teeth and the preserved ramus have features marking the attachment of different parts of the masseter muscle, following Gambaryan and Kielan-Jaworowska (1995). Ventral to the p4 is a distinct concavity delimited anteriorly by a rounded prominence; this concavity is the masseteric fovea ("mfov" in Figs. 9–10), which is interpreted as housing the pars anterior of the medial masseter. Posteroventral to the masseteric fovea at the level of the m1 is a thick, raised ridge, the masseteric crest for the pars anterior of the superficial masseter ("mcr" in Figs. 9–10). The masseteric crest is directed obliquely from anterodorsal to posteroventral and continues posteriorly as the weak masseteric line ("mli" in Fig. 9) marking the ventral margin of the ramus and the attachment of the masseter lateralis profundus. Dorsal to the masseteric crest and line is a subtle concave surface ("mfos" in Figs. 9–10) reaching about halfway up the ramus and then flattening out anteriorly in the direction of the masseteric fovea, dorsally toward the coronoid process, and posteriorly toward the missing rear of the ramus; this concavity, the masseteric fossa, likely held the pars intermedia of the medial masseter.

The coronoid process ("cor" in Fig. 9) is preserved on the left dentary and it appears to be unbroken and undistorted. The process is digitiform, slightly convex anteriorly and slightly concave posteriorly. Although the apex of the

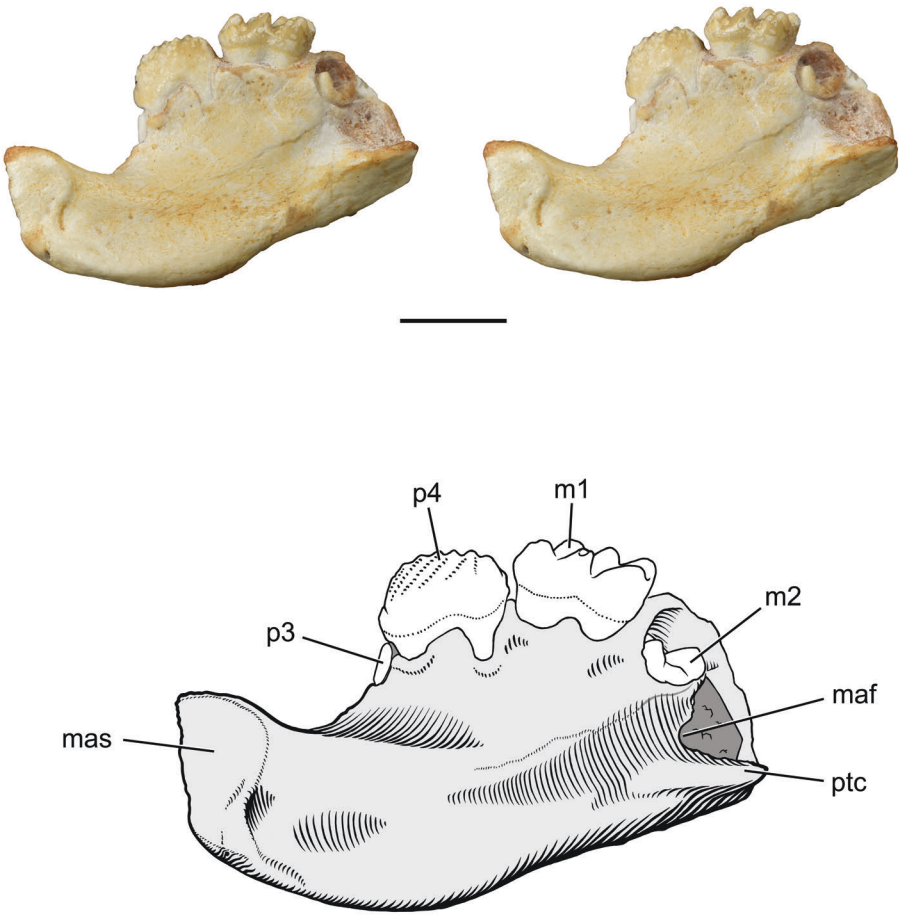

Fig. 12.—*Guibaatar castellanus*, CEVB 11908, right mandible in medial view. Stereophotographs and line drawing: light grey is bone and dark grey is matrix. Abbreviations: **m1,** first lower molar; **m2,** second lower molar; **maf,** mandibular foramen; **mas,** mandibular symphysis; **p3,** third lower premolar; **p4,** fourth lower premolar; **ptc,** pterygoid crest. Scale = 5 mm.

coronoid process is at a level posterior to the m2 crypt, the erupted m2 would have likely been hidden in lateral view by the coronoid; this relationship likely changed in the adult with additional growth. Extending anteriorly from the coronoid process is a crest that can be traced to the distal root of the p4 and marks the dorsal margin of the part of the masseteric fossa containing the pars intermedia of the medial masseter. Dorsolateral to this crest is a shallow temporal groove ("tgr" in Figs. 9–10). A lunule, the half-moon shaped convexity above the temporal groove and below the p4, m1, and anterior part of m2 described by Gambaryan and Kielan-Jaworowska (1995) in, for example, *Nemegtbaatar*, is not identifiable.

In medial view, the surface of the mandibular symphysis ("mas" in Figs. 11–12) is well preserved and demarcated on both mandibles. It has vertical and horizontal components. The larger vertical component spans the dorsoventral height of the mandible's anterior margin and its greatest anteroposterior dimension is dorsally; the contiguous smaller horizontal component hugs the ventral margin of the mandible and its anteroposterior dimension is subequal to the dorsoventral height of the vertical component. The medial aspect of the diastema has a near horizontal shelf extending posteromedially from it to the level of the distolingual root of the p4 (best seen in occlusal view in Fig. 13). Recessed slightly from the ventral margin at the level of the distal root of the m2 is the beginning of the pterygoid crest (Simpson 1926; pterygoideus shelf of Miao 1988) ("ptc" in Figs. 11–13). In djadochtatherioids, this prominent, horizontal ridge continues posteriorly on the ventral margin of the ramus and marks the lower limit of the pterygoid fossa for the attachment of the medial pterygoid muscle (Gambaryan and Kielan-Jaworowska 1997). The bone between the anterior root of the pterygoid crest and the crypt for the m2 is partially broken but includes a rounded edge on both dentaries that we interpret as the anterior margin of the mandibular foramen ("maf" in Figs. 11–12).

TABLE 2. Dental measurements of *Guibaatar castellanus* in mm.

	Right	Left
P2 length	1.98	2.10
P2 width	1.51	1.47
P3 length	1.67	1.72
P3 width	1.44	1.50
P4 length	4.10	3.83
P4 width	1.52	1.59
M1 length	4.99	5.01
M1 width	3.01	2.94
p4 length	3.99	4.14
p4 width	1.56	1.48
m1 length	4.07	4.08
m1 width	235	2.49
m2 length	2.18	-
m2 width	1.52	-

Dentition

Initial descriptions of the dentition were made through the usual study of the specimen under the microscope, from which we identified two incisors, three premolars, and one molar with a crypt for a second molar in the upper jaw, and one incisor, two premolars, and one molar with an erupting second molar in the left lower jaw. We were concerned that the first of the upper premolars might be a deciduous tooth because of the high number of cusps, unlike the similarly positioned adult teeth of other djadochtatherioids and like the deciduous premolars described for *Nemegtbaatar* and *Chulsanbaatar* (Kielan-Jaworowska 1974). Fortunately, the opportunity to CT scan the specimen arose, because through that we discovered our initial identifications of several tooth positions were in error. Most notedly and unexpectedly, the enlarged mesial upper incisor and single lower incisor were found to be deciduous teeth with permanent replacements forming. As noted above, the presence of these teeth and the forming m2 places *Guibaatar* between the juvenile and young stages of Miao (1986) and in stage 2 of Greenwald (1988). Table 2 contains measurements of the premolars and molars.

Upper dentition.—Adult djadochtatherioids have two upper incisors, which are designated as I2 and I3, because the earlier 'plagiaulacid' multituberculates have three upper incisors with the mesialmost one lost in later groups (Hahn 1969; Kielan-Jaworowska et al. 2004). CT scanning of *Guibaatar* reveals that the mesial incisor is a deciduous tooth with a permanent replacement forming behind it within the premaxilla (Fig. 14). The dI2 is a large tooth that curves sharply posteriorly and slightly laterally into the premaxilla (Fig. 15). It is broken (or worn) less than a millimeter ventral to its alveolus on both sides, chipped with more of the lingual surface preserved than the buccal. The enamel is uniformly distributed and not as densely mineralized as its replacement (Fig. 14). It is oval in cross section with slight buccolingual compression and its root tapers distally into the premaxilla (Figs. 14–15). The right dI2 appears to be preserved in life position, whereas the left dI2 along with the premaxilla have been displaced medially (Fig. 3). The right dI2 is fairly erect and would not have contacted the left dI2 ventral to their alveoli. The dI2 alveolus is closer to the lateral margin and is separated from the midline by more than a tooth width.

The forming replacement I2 is entirely contained within the premaxilla (Fig. 14). It is a larger tooth in girth than its deciduous predecessor, although anteroposteriorly shorter at this stage of its development, and more buccolingually compressed (Fig. 15). It tapers to a point anteriorly, follows a similar curvature to the dI2, and has a broadly open root. It is U-shaped in cross section with a flat distal surface. Whereas the enamel of the dI2 is uniform, that of the I2 is much thicker on the mesial surface and the mesial half of the buccal surface; it is also thicker than the enamel of the dI2 (Fig. 14). Given the evidence available to us at this time, we are uncertain if enamel surround the entire tooth or if it is restricted mesially and mesiobuccally as in other djadochtatherioids (Kielan-Jaworowska and Hurum 1997; Rougier et al. 2016).

Posteromedial to the left dI2 is an alveolus for a second incisor (the I3 position) that contains a small, round tooth broken at the alveolus; the right alveolus is incomplete posteriorly due to missing bone (Fig. 3). The CT scans show that a replacement tooth is absent on the left side (Fig. 15) and that the right alveolus is completely empty. We are unsure how to identify the tooth in the left alveolus; it is either a deciduous tooth that is unreplaced or with the replacement yet to form, or a permanent tooth without deciduous predecessor or with the deciduous predecessor already shed. A search through the multituberculate literature reveals only one specimen showing replacement at the I3 position: *Kryptobaatar dashzevegi*, ZPAL MgM-I/10 (originally described as the type of *Gobibaatar parvus* by Kielan-Jaworowska 1970). According to Kielan-Jaworowska (1970), this specimen has both the dI3 and I3 along with the I2 and the full complement of adult cheek teeth. If *Guibaatar* shows a similar replacement pattern, then its small distal left incisor is a deciduous tooth, given that it does not have an erupted I2 and a full complement of adult cheek teeth. However, what is preserved of this tooth, essentially the root, has very thick walls that are highly mineralized, which is very different from the morphology of the dI2. Consequently, we tentatively designate this tooth as the I3. This incisor (Fig. 15) has a single straight root that tapers slightly dorsally into the premaxilla. Because of postmortem displacement of the left premaxilla, the I3 root is at an angle, canted dorsolaterally, but was likely more or less straight in life.

The maximum upper premolar count in djadochtatherioids is four (Kielan-Jaworowska and Hurum 1997; Rougier

Fig. 13.—*Guibaatar castellanus*, CEVB 11908, right mandible in occlusal view. Stereophotographs and line drawing: light grey is bone and dark grey is matrix. Abbreviations: **di,** deciduous incisor; **m1,** first lower molar; **m2,** second lower molar; **p3,** third lower premolar; **p4,** fourth lower premolar; **ptc,** pterygoid crest; **tgr,** temporal groove. Scale = 5 mm.

et al. 1997, 2016); of these, the first three are known to be diphyodont and the last apparently not in this clade (Kielan-Jaworowska 1974; Greenwald 1988). *Guibaatar* has three double-rooted upper premolars, which we initially identified as P2–4 (Fig. 15). The mesialmost premolar is unusual in having six cusps arranged in two rows of three (Figs. 16, 17A), whereas other djadochtatherioids have only three or four cusps altogether at this permanent tooth position. Deciduous premolars with an increased number of cusps over their replacement teeth have been noted for some djadochtatherioids: *Nemegtbaatar* was reported to have six cusps on the dP1 and *Chulsanbaatar* six on dP3 (Kielan-Jaworowska 1974); Szalay (1965) found the same phenomenon in the ptilodontoid *Cimolodon* sp. with a five-cusped dP2 replaced by a three-cusped P2. As noted above, the possibility that the high number of cusps on the mesialmost premolar might be indicative of a deciduous tooth led us to CT scan *Guibaatar*. However, in the scans, we were unable to find a replacement tooth for any upper premolars, which means the six-cusped tooth is either permanent, deciduous without replacement, or deciduous with the replacement yet to form. The last is doubtful as the CT scans show that the bone around the tooth lacks any indication of a crypt whatsoever. Because the extent of mineralization of this tooth resembles that of the other premolars, which we interpret as permanent teeth P3–4 (Fig. 14), we identify this tooth as the P2. Further supporting our interpretation is the similar root morphology between the three upper premolars (Fig. 15); in other extinct Mesozoic mammals (e.g., the "symmetrodont" *Zhangheotherium*, Luo and Ji 2005), the roots of deciduous upper premolars are very short compared to their replacements.

The pattern of upper premolar replacement is poorly known in djadochtatherioids and the taxon that is best known, *Catopsbaatar*, is perhaps the most unusual, judging from the report by Kielan-Jaworowska et al. (2005). *Catopsbaatar* has a maximum of three upper premolars, identified as P1, P3, and P4. In very young individuals, Kielan-Jaworowska et al. (2005) found single-rooted, simple-crowned dP1 and dP3, which were replaced by double-rooted, simple-crowned permanent teeth in juvenile individuals. These teeth were subsequently lost in older individuals with the alveoli disappearing.

In *Guibaatar*, the P2 is oval-shaped with two roots; the mesial root is larger and angled slightly anterodorsally (Figs. 14–15). The crown of the left P2 (Figs. 16, 17A) has six cusps arranged in buccal and lingual rows for a formula of 3:3; the distal two cusps are broken off on the right P2 (Fig. 3). The cusps in each row increase in size slightly from mesial to distal with the mesiobuccal cusp as the smallest (Figs. 16, 17A). Additionally, the cusps in the buccal row are situated slightly in advance of (mesial to) those in the lingual row.

The P3 is well preserved bilaterally (Fig. 3). It is slightly smaller than the P2 and with two roots (Figs. 14–15). The mesial root on the left P3 in Figure 15 is damaged; on the right P3, the roots are subequal and taper distally. The P3 crown has buccal and lingual rows that line up with those of the P2 (Figs. 16, 17A). There are two cusps in the buccal row and three in the lingual for a formula of 2:3. The cusps are subequal except for the smaller mesiolingual cusp. The cusps of the two rows occupy alternate positions, with the middle cusp in the lingual row at a level between the two cusps of the buccal row. The occlusal surface of the P3

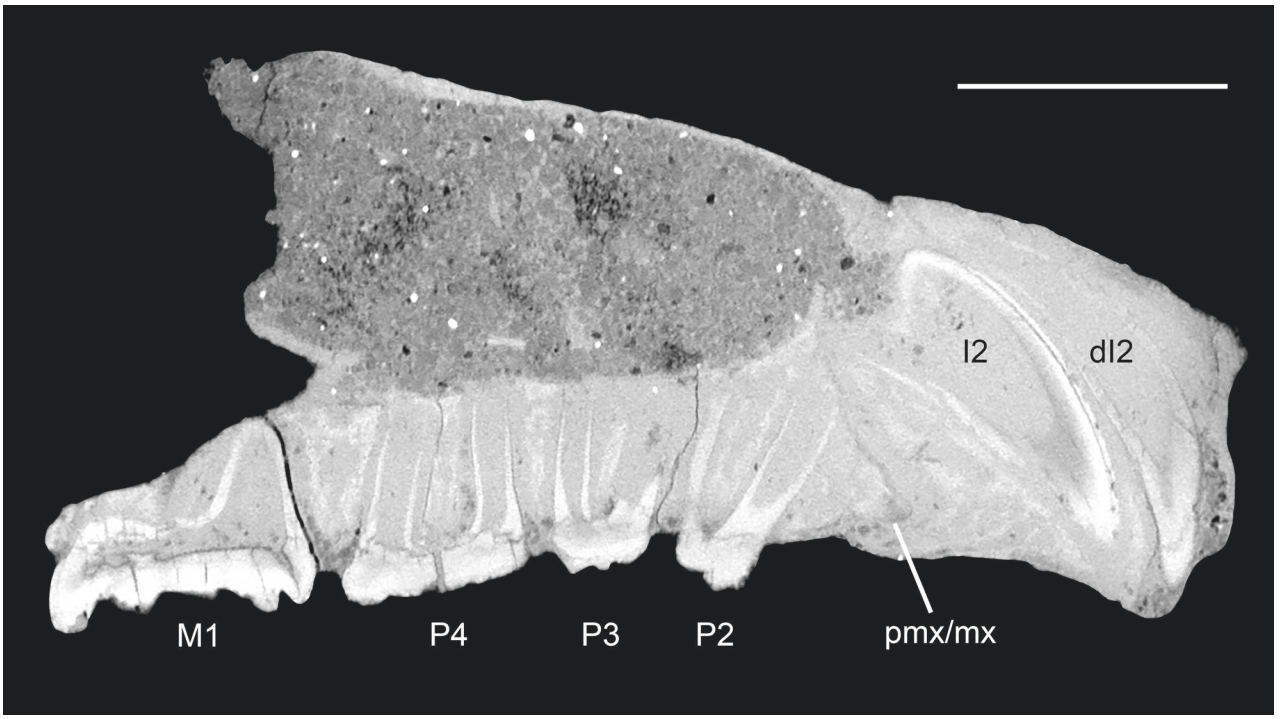

Fig. 14. —*Guibaatar castellanus*, CEVB 11908, parasagittal section through the right upper dentition lateral to the I3 (section 263 of 1110 in XZ plane in Avizo). I2 has an artefactual split in the mesial side enamel. Abbreviations: **dI2,** deciduous second upper incisor; **I2,** second upper incisor; **M1,** first upper molar; **P2,** second upper premolar; **P3,** third upper premolar; **P4,** fourth upper premolar; **pmx/mx,** premaxillary/maxillary suture. Scale = 5 mm.

is higher than those of its neighbors (Figs. 4–5, 15) and, therefore, the P3 may not be fully erupted, although there are no wear differences between the premolars and M1.

The P4 is the largest premolar. It has two subequal roots that taper distally (Figs. 14–15). The right P4 is more fully preserved (Figs. 3, 16); the left has a chip missing from the buccal half. The P4 crown (Figs. 16, 17A) has three rows of cusps with a formula of 2:5:1; the buccal two rows line up with the two rows on the P2–P3. A short buccal row with two subequal cusps is situated ventral to the mesial root. A long middle row with five cusps extends the length of the tooth; the first four cusps increase in height posteriorly and the fifth cusp is lower than the others and separated from the fourth by a greater distance than between the more mesial cusps. The two cusps in the buccal row line up with the first two in the middle row. A short lingual row with a single cusp that is the lowest cusp on the tooth occupies the distolingual corner.

The M1, the largest tooth in the entire dentition, is well preserved bilaterally (Fig. 3). It is elongate with the mesial half narrower than the distal half. Djadochtatherioid M1s are usually reported as double rooted (e.g., *Mangasbaatar*, Rougier et al. 2016), but *Guibaatar* has a third small root arising from near the mesiodistal center of the tooth on the buccal aspect (Fig. 15). Of the other two roots, the distal one is the larger. The M1 crown has three rows of cusps with a formula of 5:5:2 (Figs. 16, 17A). The buccal row extends the length of the tooth and lines up with the middle row of the P4. The mesial four cusps in the buccal row are subequal in size and height; the distal fifth cusp is smaller and closer to its mesial neighbor than the other cusps in the row. The middle row also extends the length of the tooth, lines up with the single cusp of the lingual row of P4, and has five cusps that increase in height posteriorly; the mesialmost cusp is the smallest in girth on the tooth, the fourth is the largest on the tooth, and the remainder in the row are subequal but larger than the cusps in the buccal row. A short lingual row has two cusps in line with the last two in the middle row; the mesial cusp in the lingual is smaller and lower and the distal cusp is subequal in height and girth to its neighbor in the middle row.

There is a crypt for a second molar, M2, nearly complete on the left side and partial on the right (Fig. 3). The CT scans revealed the presence of three forming cusps (enamel caps) arranged in two rows deep within the crypt of the left side (Figs. 15, 17A). The buccal row includes the largest cusp, which lines up with the middle row of the M1. The lingual row, lining up with the lingual row of the M1, includes the remaining two cusps; the larger mesial one is slightly distal to the level of the single cusp in the buccal row.

Lower dentition.—The deciduous lower incisor (di) is a large tooth that curves sharply posteriorly and laterally into the dentary. It is broken at its alveolus on the right side and extends slightly beyond it on the left (Figs. 9–10).

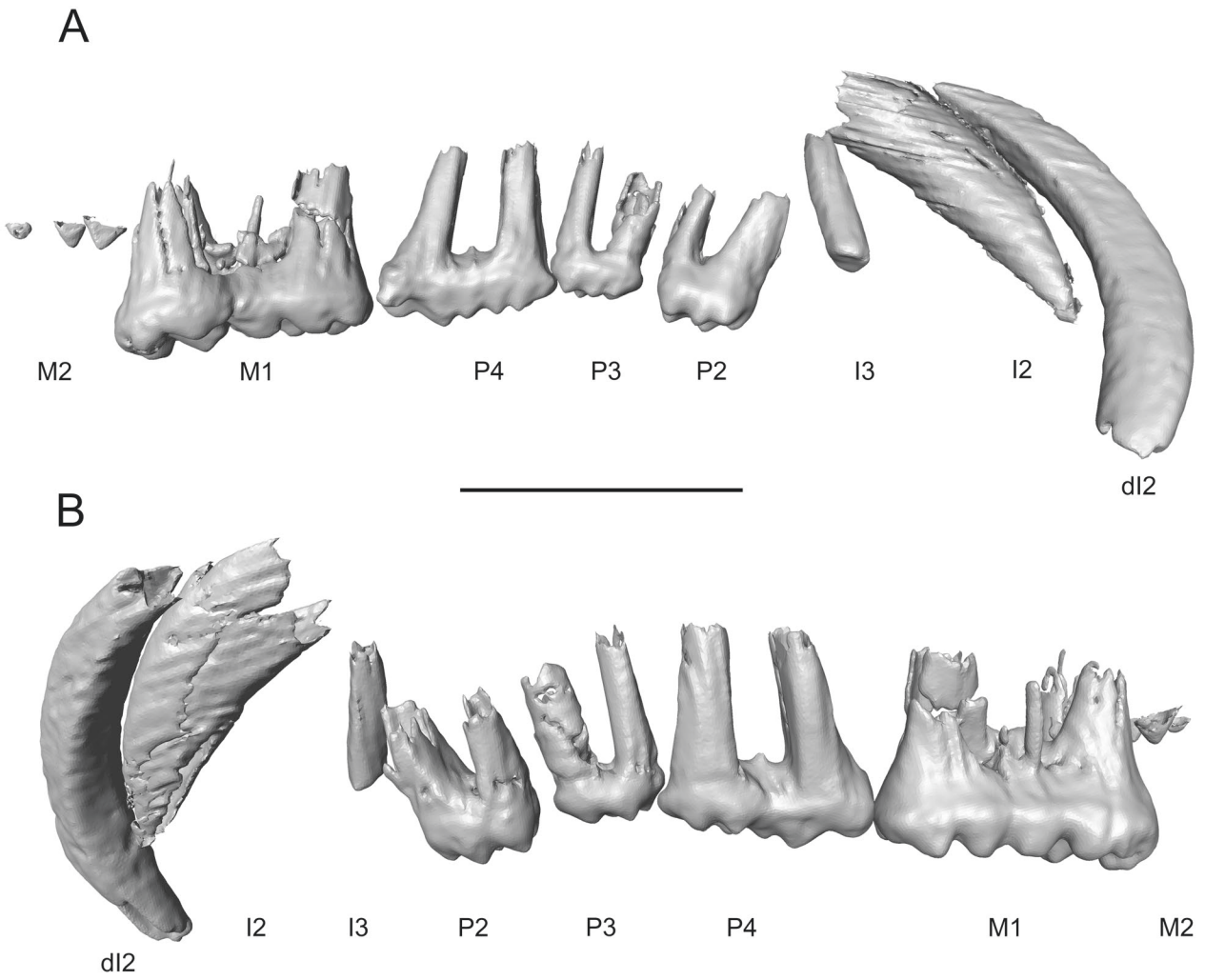

Fig. 15.—*Guibaatar castellanus*, CEVB 11908, isosurface renderings of upper left dentition from CT scan. **A,** buccal view; **B,** lingual view. Abbreviations: **dI2,** deciduous second upper incisor; **I2,** second upper incisor; **I3,** third upper incisor; **M1,** first upper molar; **M2,** enamel caps of second upper molar; **P2,** second upper premolar; **P3,** third upper premolar; **P4,** fourth upper premolar. Scale = 5 mm.

At its rostral end, the left di is 2.05 mm in height, whereas the corresponding dimension of the dentary is 4.10 mm; thus, the di at its alveolus occupies only half of the height of the dentary, primarily the ventral half. The right dentary preserves much of the roof of the incisor alveolus (Fig. 10) and it lies at an angle of 55° to the horizontal, suggesting that the tooth left its alveolus at a similar angle. This accords with what is preserved of the left incisor beyond its alveolus. The di root tapers distally and extends posteriorly below the p3 (Fig. 18). The tooth has uniform enamel and is not as densely mineralized as its replacement. It is buccolingually compressed with a flat dorsal surface and U-shaped in cross section.

The forming replacement incisor (Fig. 18) is larger in girth and length than its deciduous predecessor. It is more buccolingually compressed, oval in cross section, and tapers to a point anteriorly, following a similar curvature to the di. The permanent incisor has a broadly open root extending posteriorly below the posterior half of the m1 and the anterior half of the m2. Whereas the enamel of the di is uniform, that of the replacement incisor is much thicker on the ventral surface and ventral half of the buccal surface; it is also thicker than the enamel of the di. As we reported for the I2, it is uncertain if enamel surrounds the permanent lower incisor or is restricted mesially and mesiobuccally as in other djadochtatherioids (Kielan-Jaworowska and Hurum 1997; Rougier et al. 2016).

Two lower premolars are present, p3 and p4, following the convention for multituberculates (Kielan-Jaworowska et al. 2004). The p3 is well preserved bilaterally (Figs.

Fig. 16.—*Guibaatar castellanus*, CEVB 11908, stereophotographs of left upper premolars and molars in occlusal view; from top to bottom: P2, P3, P4, M1, and crypt for M2. Scale = 5 mm.

9–12). It is a small, single-rooted, peg-like tooth positioned ventral to the mesial aspect of the large p4 (Fig. 18). The p3 is not erect but is slanted somewhat posterodorsally. It is buccolingually compressed to a slight extent with a subtle constriction delimiting the crown from the root above its alveolus. The apex of the tooth is rounded and in contact with the ventromesial surface of the p4. The short root is angled in the same plane as the crown.

The p4 is a blade-like, serrated tooth best preserved in the right dentary (Figs. 10, 12–13); the left p4 has a chip missing from the mesial aspect (Fig. 11) and damage along the tooth apex. The p4 has an arcuate outline in buccal view, strongly arched along the mesial border and less so distally. The tooth is supported by three roots (Fig. 18), as reported for *Mangasbaatar* (Rougier et al. 2016). Stout, subequal mesial and distal roots support the entire tooth width. The mesial root is the longer of the two and both roots show little distal tapering. The mesial root is recessed distally from the mesial border of the tooth, leaving a lobe that overhangs the p3; the distal root is more in line with the rear of the tooth. A third root, the smallest in girth and length, is only visible in the CT scans. It is centrally positioned between the other two roots. The apex of the p4 has six distinct cusps forming a serrated edge (Figs. 9–13), reaching the height of the lingual row of the m1; the size of the cusps increases distally. Ridges slant anteroventrally from these cusps about halfway down the crown on both buccal and lingual sides. An additional distinct cusp is present on the buccal side of the sixth cusp in the serrated row (Figs. 9–10, 17B, 18A). This distobuccal cusp is more than half the height of those in the serrated row.

Two lower molars are present. The m1 is well preserved bilaterally (Figs. 9–12) whereas the m2 is only present on the right dentary and is in the process of forming (Figs. 12, 17A, 18). The m1 is the largest lower cheek tooth, is supported by two large roots, and is separated from the p4 by a narrow interdental space. The m1 (Figs. 13, 17A) has buccal and lingual rows of conical cusps, four in the former and three in the latter. The lingual cusps are higher than the buccal and increase in size posteriorly; in the buccal row, the mesialmost is the smallest with the remaining three subequal in size. The cusps of the two rows occupy alternate positions, with the lingual cusps positioned between two successive buccal cusps.

The right m2 is within a crypt and matrix was removed to reveal the cusp pattern (Figs. 12–13); CT data revealed

that only the enamel cap of the crown has formed (Figs. 16B, 17). The m2 is triangular with two primary cusps and a much smaller third cusp (Fig. 16B). As preserved in the crypt, the largest cusp is positioned distally, with the next largest positioned mesiolingually, and the small cusp mesiobuccally. The distance between the mesial and distal cusps is greater than the distance between the cusps in the rows on the m1. When erupted, the two large cusps of the m2 will likely occupy a lingual row in line with that on the m1, with the small cusp in a buccal row. An empty crypt for the m2 is present on the left dentary.

DISCUSSIONS

Phylogenetic Analysis

Phylogenetic analyses including all LCMM known at the time have been published by Simmons (1993), Kielan-Jaworowska and Hurum (1997), and Rougier et al. (1997, 2016). The latter two sets of authors recognized Djadochtatherioidea as a monophyletic group including all LCMM except *Buginbaatar*. We used the character list and taxon sampling from Kielan-Jaworowska and Hurum (1997) with modifications made by Rougier et al. (2016) as the starting point for our phylogenetic analysis, because these two studies focused on relationships within Djadochtatherioidea. Rougier et al. (2016) sampled 44 craniodental characters across 17 taxa. As chronicled in Appendix 1, we sampled 74 craniodental characters across the same 17 taxa plus *Guibaatar*; of the 44 characters in Rougier et al. (2016), we eliminated six (#20, 25, 31, 33, 36, 41), retained or modified the remainder, and added 26 new ones. For all taxa except *Guibaatar*, our scores came from the literature or on-line resources (Appendix 2).

Our taxon-character matrix (Appendix 3) was analyzed using equally weighted parsimony in TNT version 1.5 (Goloboff and Catalano 2016). *Ptildous* was designated as the outgroup following Kielan-Jaworowska and Hurum (1997). The dataset was first analyzed under the 'New Technology' search option using sectorial search, ratchet (perturbation phase stopped after 17 substitutions), drift (perturbation phase stopped after 17 substitutions), and tree fusing (three rounds) options, which identified three most parsimonious trees of 178 steps via a driven search. A subsequent Traditional TBR search of trees recovered from the 'New Tech' search found no additional trees. The three trees had a consistency index of 0.652 and retention index of 0.656. The strict consensus of the three trees (Fig. 19) shows a monophyletic Djadochtatherioidea including all LCMM minus *Buginbaatar* and a monophyletic Djadochtatheriidae including the same taxa as in Rougier et al. (2016) plus *Guibaatar*. Whereas the single most parsimonious tree in Rougier et al. (2016) is fully resolved, our consensus tree has a polytomy in Djadochtatherioidea.

Djadochtatheriidae (*Djadochtatherium*, *Kryptobaatar*, *Catopsbaatar*, *Tombaatar*, *Mangasbaatar*, and *Guibaatar*) is distinguished from other djadochtatherioids by seven

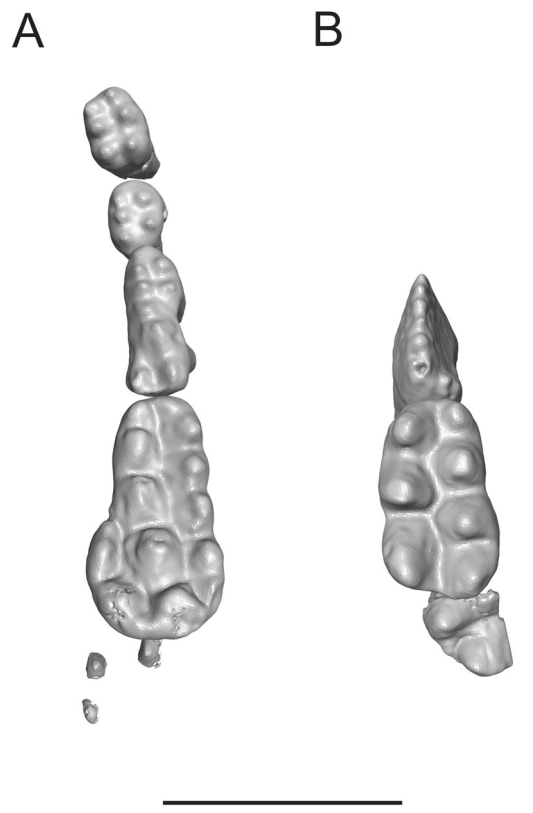

Fig. 17.—*Guibaatar castellanus*, CEVB 11908, isosurface renderings of left premolars and molars from CT scan. **A,** upper premolars and molars (P2-4, M1-2); **B,** lower premolars and molars (p4, m1-2; p3 is completely hidden by p4). Scale = 5 mm.

synapomorphies: absence of a lingual row on P4, width of snout to skull length greater than or equal to 0.4, strongly developed postpalatine torus, postorbital process equal to or greater than half orbit width, supraorbital notch present, irregular outline to anterior promontorium with incurvatures, and mandibular condyle opposite or below the level of the molars. Within Djadochtatheriidae, *Mangasbaatar* and *Tombaatar* are sister taxa in Rougier et al. (2016), but in our analysis *Mangasbaatar* is allied with *Catopsbaatar*, by the absence of P2, the trapezoidal shape and serration count of five or fewer of the p4, and the width ratio of P4–M1 less than or equal to 0.45. *Guibaatar* is sister to *Mangasbaatar* + *Catopsbaatar* by a single synapomorphy, the presence of a secondary infraorbital foramen.

In Rougier et al. (2016) and our analysis, *Kryptobaatar* is the earliest diverging djadochtatheriid, which fits with the former authors' characterization of *Kryptobaatar* as a more generalized LCMM. *Kryptobaatar* is also the smallest of the djadochtatheriids, roughly half the skull length of *Catopsbaatar*, *Djadochtatherium*, *Mangasbaatar*, and *Tombaatar* (Wible and Rougier 2000; Kielan-Jaworowska

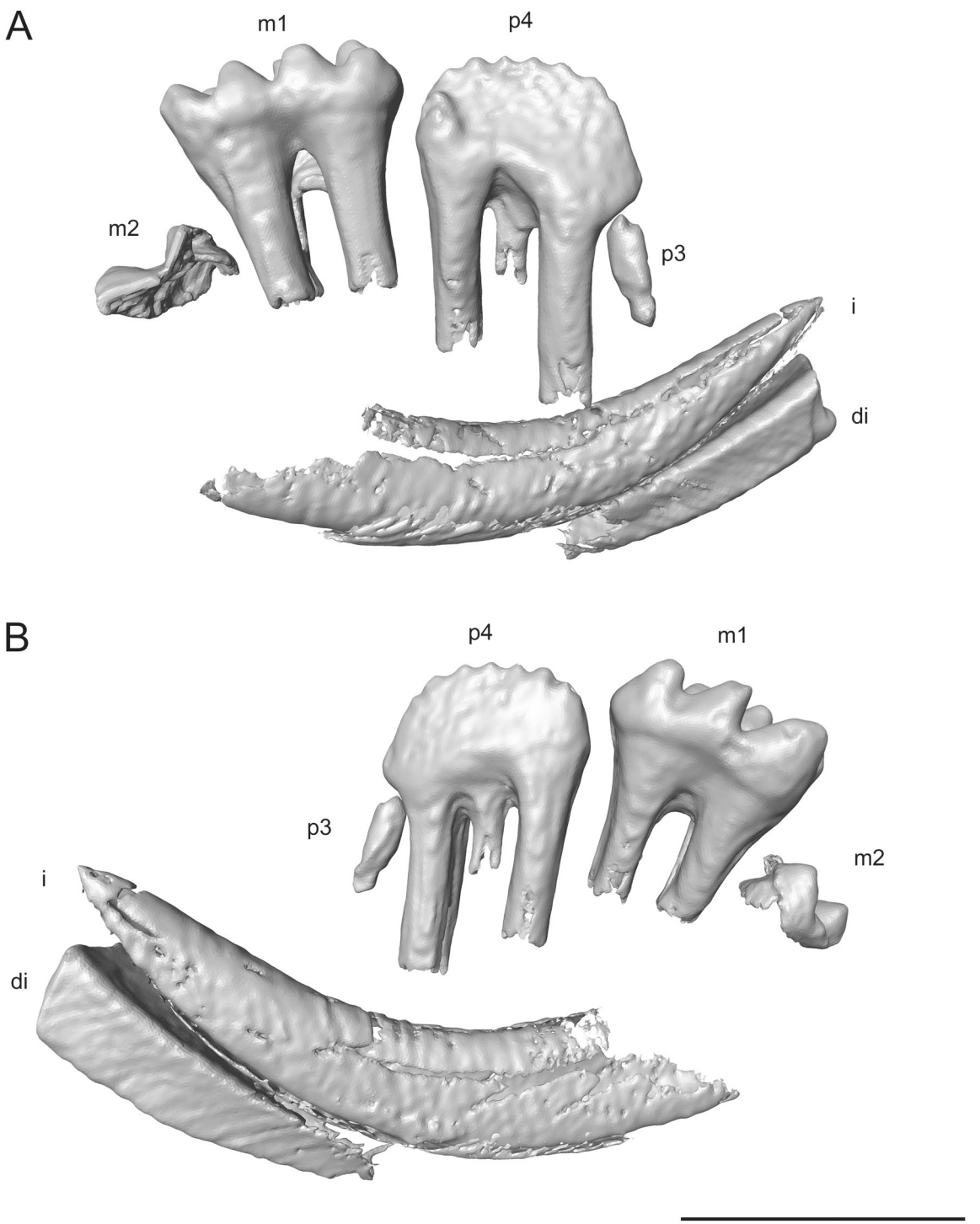

Fig. 18.—*Guibaatar castellanus*, CEVB 11908, isosurface renderings of lower right dentition from CT scan. **A,** buccal view; **B,** lingual view. Abbreviations: **di,** deciduous lower incisor; **i,** lower incisor; **m1,** first lower molar; **m2,** enamel cap of second lower molar; **p3,** third lower premolar; **p4,** fourth lower premolar. Scale = 5 mm.

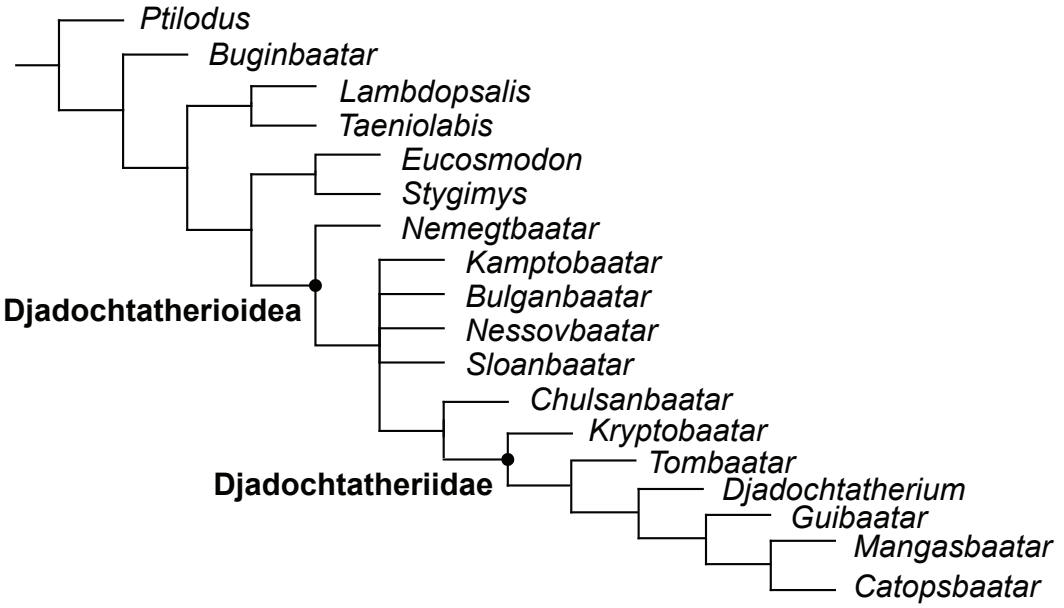

Fig. 19.—Strict consensus tree of three most parsimonious trees resulting from TNT analysis of taxon-character matrix in Appendix 2.

et al. 2005; Rougier et al. 2016). Skull length for *Guibaatar* is unknown, but articulating the right partial braincase with the snout, we estimate the skull length to be approximately 50 mm. However, as an adult, *Guibaatar* would have been in the size range of the larger djadochtatheriids.

Differences between the results of our phylogenetic analysis and that of Rougier et al. (2016) are not surprising, given that we included *Guibaatar* and used different characters. However, at this point, we do not impart much significance to the differences in trees, as we anticipate that relationships within Djadochtatheriidae will change upon description of the unpublished specimens of *Djadochtatherium* mentioned by Kielan-Jaworowska et al. (2005) and of *Tombaatar* mentioned by Rougier et al. (2016) as well as the rest of the skull of cf. *Tombaatar*, n. sp., in Ladevèze et al. (2010). Moreover, the djadochtatheriids and the remaining LCMM would benefit from restudy in the context of a more comprehensive character list and broader phylogenetic analysis.

Comparisons

Our comparisons follow the order used in the Descriptions above. Primary considerations are given to those multituberculates that have been more thoroughly preserved and described, which includes, for example, the djadochtatheriids *Kryptobaatar* (Wible and Rougier 2000; Smith et al. 2001; Kik 2002), *Catopsbaatar* (Kielan-Jaworowska et al. 2002, 2005), and *Mangasbaatar* (Rougier et al. 2016), and the taeniolabidoid *Lambdopsalis* (Miao 1988). Our reconstructions of *Guibaatar* in dorsal, ventral, and lateral views are shown in Figure 20.

Premaxilla.—All djadochtatheriids have a distinct posterodorsal process of the premaxilla that tapers posteriorly (Figs. 21G–J). This is the case in *Guibaatar* (Fig. 20C), *Mangasbaatar* (Fig. 21I; Rougier et al. 2016: fig. 18A), *Djadochtatherium* (Simpson 1925: fig. 2), *Catopsbaatar* (Fig. 21H; Kielan-Jaworowska et al. 2005: fig. 2B), *Tombaatar* (Rougier et al. 1997: fig. 2), and *Kryptobaatar* (Fig. 21G; Wible and Rougier 2000: figs. 10, 12). The last is distinguished from the others in that its posterodorsal process does not extend to the level of the anterior cheek teeth. In the other multituberculates considered here, the suture between the premaxilla and maxilla on the face is straighter and does not produce a distinct posterodorsal process (Figs. 21A–E), except for *Chulsanbaatar* (Fig. 21F; Hurum 1994: fig. 11).

On the palate, as in all djadochtatherioids, *Guibaatar* has a small incisive foramen, subequal to the length of the I2 (Figs. 3, 20B, 22D–K); this is in contrast to the other multituberculates considered where the incisive foramen is more in the range of the length of the I2 + I3 (Figs. 22A–C). As in most djadochtatherioids, *Guibaatar* has a central depression on the palatal surface of the premaxilla demarcated laterally by a curved ridge, the thickenings of the premaxilla (Kielan-Jaworowska et al. 1986; Figs. 3, 22G–H, J–K); the exception among djadochtatherioids is *Kamptobaatar* (Kielan-Jaworowska et al. 1986; Rougier et al. 1997, 2016; Wible and Rougier 2000). Regarding *Catopsbaatar*, Kielan-Jaworowska et al. (2005: 494) stated that the thickenings "are not recognizable" (see Fig. 22J), which may be a preservation issue. This feature has not been reported outside of Djadochtatherioidea. The majority of the multituberculates considered here, including *Guibaatar* (Fig. 3), have a distinct

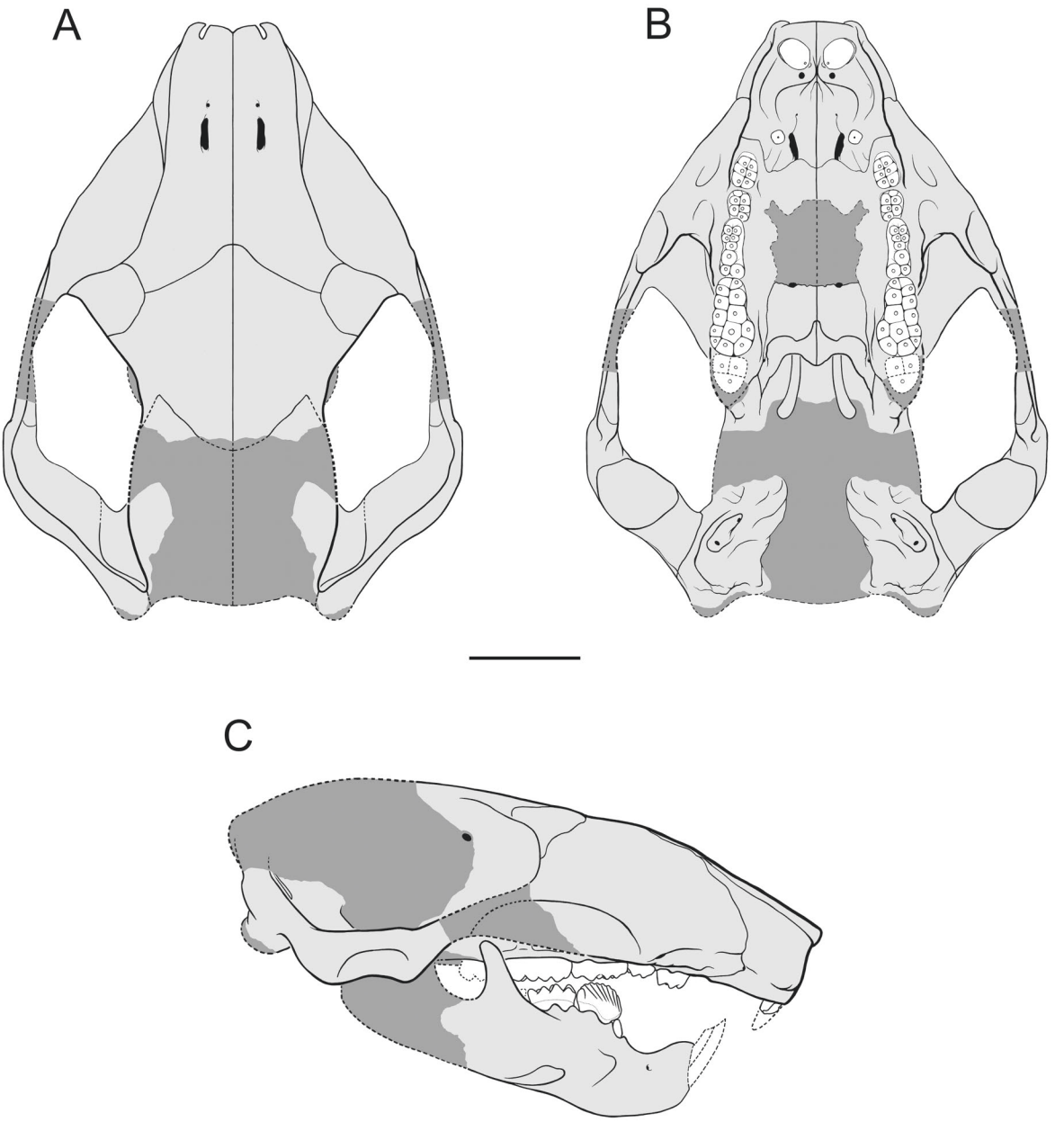

Fig. 20.—*Guibaatar castellanus*, CEVB 11908, reconstructions. Dark grey is matrix. As discussed in the text, we interpret the palate as without vacuities; additionally, postorbital processes were likely present on the parietal as in all other djadochtatherioids but are not included as their size varies across members of the group. **A,** skull in dorsal view; **B,** skull in ventral view; **C,** skull and lower jaw in right lateral view. Scale = 10 mm.

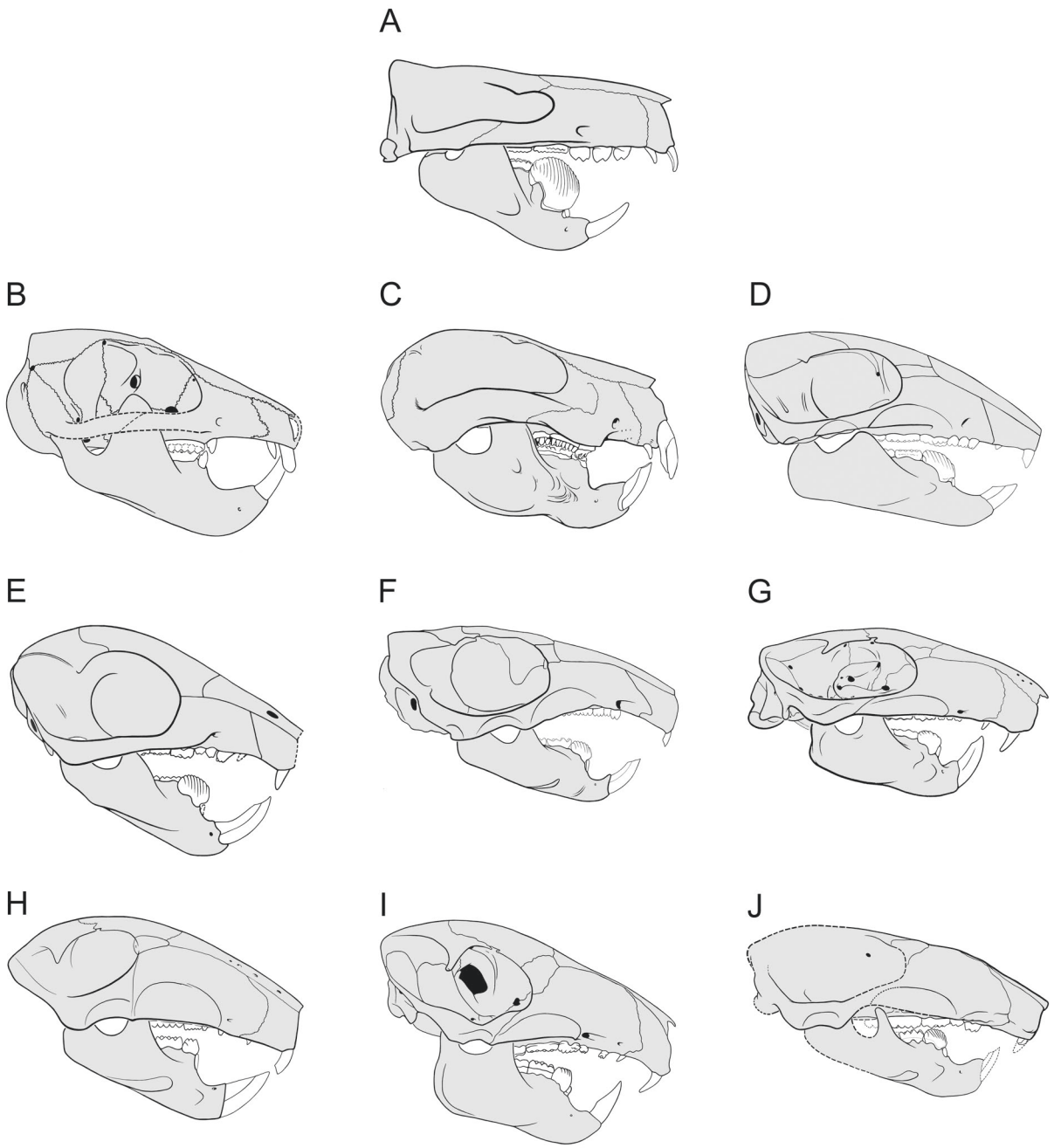

Fig. 21.—Multituberculate skull and lower jaw reconstructions in lateral view, rendered to approximately the same length. **A,** *Ptilodus* (redrawn from Krause 1982: figs. 1, 7B); **B,** *Lambdopsalis bulla* (redrawn from Miao 1988: fig. 4); **C,** *Taeniolabis taoensis* (redrawn from Sloan 1981: fig. 6.14); **D,** *Nemegtbaatar gobiensis* (modified from Keilan-Jaworowska et al. 2004: fig. 8.4C); **E,** *Sloanbaatar mirabilis* (modified from Kielan-Jaworowska 1970: fig. 1); **F,** *Chulsanbaatar vulgaris* (modified from Hurum 1994: fig. 11; Kielan-Jaworowska and Hurum 1998: fig. 12H); **G,** *Kryptobaatar dashzevegi* (redrawn from Wible and Rougier 2000: fig. 33); **H,** *Catopsbaatar catopsaloides* (redrawn from Kielan-Jaworowska et al. 2005: fig. 7); **I,** *Mangasbaatar udanii* (redrawn from Rougier et al. 2016: fig. 22); **J,** *Guibaatar castellanus*.

crista premaxillaris along the lateral edge of the palatal margin, the exceptions being *Ptilodus* and *Taeniolabis*.

Maxilla.—The shape of the snout has been used as a character to distinguish among multituberculates; djadochtatheriids are described as trapezoidal, not incurved anterior to the zygomatic arch, whereas other djadochtatherioids are said to be incurved with the anterior part directed posterolaterally (Kielan-Jaworowska and Hurum 1997; Rougier et al. 2016). However, we find these differences to be subtle (Figs. 23D–K) and have excluded this character in our analysis; for example, *Nemegtbaatar* (Fig. 23D) and *Chulsanbaatar* (Fig. 23G) were scored as incurved by Kielan-Jaworowska and Hurum (1997) and Rougier et al. (2016) but are not much different than djadochtatheriids (Figs. 23H–K). Outside of djadochtatherioids, the incurved state is much clearer and widespread, including among cimolodontans, for example, the kogianoids *Barbatodon* (Smith and Codrea 2015: fig. 2B) and *Litovoi* (Csiki-Sava et al. 2018: figs. 1A–B, E), *Ptilodus* (Fig. 23A), *Lambdopsalis* (Fig. 23B), and *Taeniolabis* (Fig. 23C).

Three djadochtatheriids have been reported to have more than one infraorbital foramen, a primitive mammaliaform feature present in basal multituberculates (Hahn 1985). These are *Guibaatar* (Figs. 4–5), *Mangasbaatar* (Fig. 21I; Rougier et al. 2016), and *Catopsbaatar* (Kielan-Jaworowska et al. 2005) with the last having different specimens with one (Fig. 21H), two, and three openings. *Guibaatar* differs from the other two in having the secondary infraorbital foramen between the premaxilla and maxilla. In most djadochtatheriids, including *Guibaatar*, the (primary) infraorbital foramen is positioned at the level of the P2 or the P2–P3 (Figs. 21I–J); the exceptions are *Kryptobaatar* (Fig. 21G), which is more anterior (Wible and Rougier 2000) and *Catopsbaatar*, which is both more anterior (Fig. 21H) and more posterior (Kielan-Jaworowska et al. 2005).

On the palate, one or two pairs of palatal vacuities are found within the maxilla in several djadochtatherioids (Kielan-Jaworowska 1970, 1974), that is, *Sloanbaatar* (Fig. 22F), *Bulganbaatar*, and *Nemegtbaatar* (Fig. 22D), but are unknown in djadochtatheriids. We consider it unlikely that *Guibaatar* had palatal vacuities in that there is a separate major palatine foramen (Figs. 3, 20B), which is missing from the taxa with vacuities. Among other cimolodontans, palatal vacuities are known in *Ptilodus* (Fig. 22A) and *Stygimys* (Sloan and Van Valen 1965: fig. 4).

Palatine.—A postpalatine torus has been reported for all djadochtatherioids preserving the rear of the palate (Figs. 22D–K); in contrast, in *Ptilodus* (Fig. 22A), *Lambdopsalis* (Fig. 22B), and *Taeniolabis* (Fig. 22C), the rear of the palate does not have a raised prominence. Among djadochtatheriids, the postpalatine torus is more pronounced, projecting ventral to the occlusal plane, and includes a central ridge extending anteriorly in *Guibaatar* (Figs. 3, 18B), *Kryptobaatar* (Fig. 22H; Wible and Rougier 2000), *Tombaatar* (Rougier et al. 1997), and *Mangasbaatar* (Fig. 22J; Rougier et al. 2016). *Catopsbaatar* has a weak torus (Fig. 22I; Kielan-Jaworowska et al. 2005) and the condition in *Djadochtatherium* is unknown. In discussing a possible function for the postpalatine torus, Rougier et al. (2016:236) stated "In extant mammals, such as the aardvark or the hedgehog, this bony feature is located at the attachment for the tensor veli palatini muscle (Barghusen 1986)." Himmelreich (1964) reported the anatomy of the tensor veli palatini in a broad array of placentals (not including the aardvark and hedgehog) and identified three areas of insertion: the soft palate, the pterygoid hamulus, and the sidewall of the nasopharynx; there is no attachment to the palatine. We have not found a specific reference on the hedgehog, but according to Edgeworth (1924), the muscle attaches to the soft palate in *Orycteropus*.

Orbits are generally not well preserved in multituberculates. In the few that have been described (*Lambdopsalis*, Miao 1988; *Kryptobaatar*, Wible and Rougier 2000; *Mangasbaatar*, Rougier et al. 2016), an orbital exposure of the palatine is lacking. Although the orbit is not complete or well delineated by sutures in *Guibaatar* (Figs. 4–5), we suggest that the palatine is also not exposed there. Miao (1988) speculated the absence of a palatine orbital exposure is a synapomorphy for multituberculates. To our knowledge, there are only two instances that might refute that claim: Sloan (1979: fig. 1) dashed in sutures in the orbit of the ptilodontoid *Ectypodus tardus* (YPM VPPU 14724) and included the palatine as an orbital element, and Hurum (1994, 1998) identified the palatine in the orbit in serial sections of *Nemegtbaatar*. For *Ectypodus*, Wible and Rougier (2000) examined YPM VPPU 14724 and reported they were unable to identify any sutures in the orbit. For *Nemegtbaatar*, Rougier et al. (1997) questioned Hurum's (1994) first report of an orbital palatine exposure, noting the illustrated serial sections were ambiguous. Hurum (1998: fig. 16) reiterated the presence of a substantial lamina of palatine in the orbit occurring bilaterally in a second report, but the issue remains unresolved.

Nasal.—The fragile anterior tip of the nasal is seldom well preserved in multituberculates. Nevertheless, some djadochtatherioids show the presence of anterior nasal notches, a possible primitive mammaliaform feature found, for example, in the Late Jurassic docodontid *Haldanodon* (Lillegraven and Krusat 1991). In addition to *Guibaatar* (Figs. 2, 20A), as pointed out by Wible and Rougier (2000), anterior nasal notches are known for *Kryptobaatar* (Fig. 23H), *Catopsbaatar*, and *Kamptobaatar*.

In addition to their wide distribution among Mammaliaformes, nasal foramina are near universally present in multituberculates, the exception reported by Wible and Rougier (2000) being the Late Jurassic *Kuehneodon dryas* (the absence of foramina in *Taeniolabis* in Fig. 23C is because this is unknown although a new well-preserved skull that may resolve this has been recently reported by Lyson et al. 2019: figs. 2K–L). The number of foramina varies

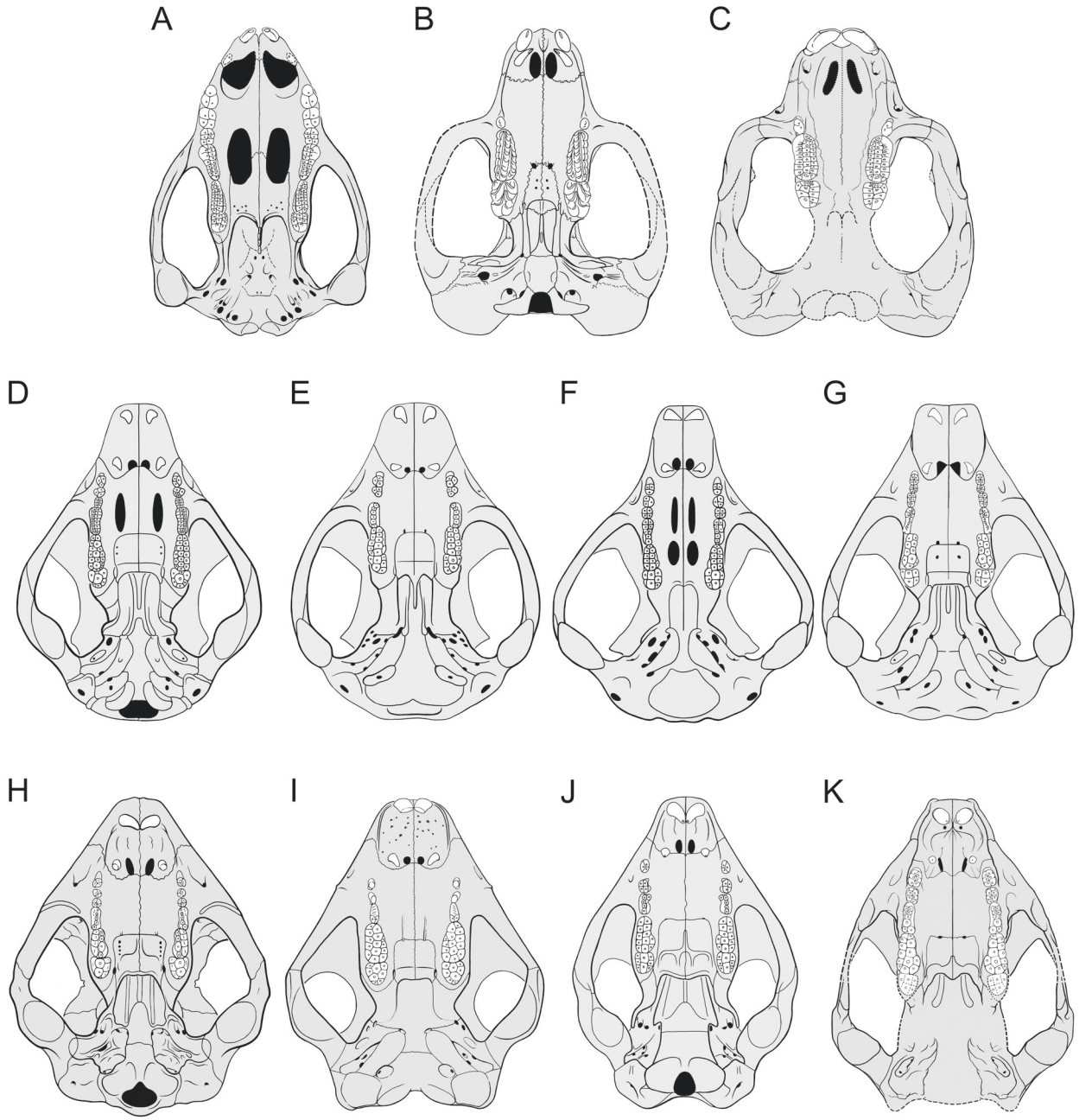

Fig. 22.—Multituberculate skull reconstruction in ventral view, rendered to approximately the same length. **A,** *Ptilodus montanus* (redrawn from Simpson 1937: fig. 6); **B,** *Lambdopsalis bulla* (redrawn from Miao 1988: fig. 18); **C,** *Taeniolabis taoensis* (redrawn from Granger and Simpson 1929: fig. 6); **D,** *Nemegtbaatar gobiensis* (modified from Kielan-Jaworowska et al. 1986: fig. 20c); **E,** *Kamptobaatar kuczynskii* (redrawn from Kielan-Jaworowska 1971: fig. 4); **F,** *Sloanbaatar mirabilis* (redrawn from Kielan-Jaworowska 1971: fig. 9); **G,** *Chulsanbaatar vulgaris* (modified from Kielan-Jaworowska 1974: fig. 5a; Kielan-Jaworowska and Hurum 1997: fig. 11G); **H,** *Kryptobaatar dashzevegi* (redrawn from Wible and Rougier 2000: fig. 34); **I,** *Catopsbaatar catopsaloides* (redrawn from Kielan-Jaworowska et al. 2005: fig. 8); **J,** *Mangasbaatar udanii* (redrawn from Rougier et al. 2016: fig. 20); **K,** *Guibaatar castellanus*.

from a low of a single pair, for example, in Late Jurassic *Pseudobolodon* (Hahn and Hahn 1994) and *Sloanbaatar* (Fig. 23F; Kielan-Jaworowska and Hurum 1997) to seven or eight pairs in *Lambdopsalis* (Fig. 23B; Miao 1988). Among djadochtatheriids, *Guibaatar* (Figs. 2, 20A), *Tombaatar* (Rougier et al. 1997), and *Djadochtatherium* (Kielan-Jaworowska and Hurum 1997) have two pairs per side; *Kryptobaatar* has two or more per side (Fig. 23H; Wible and Rougier 2000); and *Catopsbaatar* has some specimens with two per side and one specimen with four on the right and three on the left (Fig. 23I), suggesting caution in giving too much weight to the number of nasal foramina. For *Mangasbaatar*, not enough is preserved to determine the number of foramina, but there is at least one large one per side (Fig. 23J; Rougier et al. 2016).

Lacrimal.—The facial exposure of the lacrimal in djadochtatherioids is typically depicted as a subrectangular wedge contacting the maxilla laterally, nasal anteriorly, frontal medially, and with its posterior edge free (Figs. 21D–K), and *Guibaatar* exhibits the usual pattern (Figs. 2, 20A). However, although well-developed facial exposures are reconstructed for all djadochtatherioids here, Wible and Rougier (2000) reported that they were unable to identify the lacrimal in specimens of *Sloanbaatar*, *Bulganbaatar*, and *Catopsbaatar* housed in Warsaw. Subsequently, other specimens of *Catopsbaatar* have been reported showing evidence of a typical LCMM lacrimal (Kielan-Jaworowska et al. 2005). This contrasts with the condition in the other multituberculates considered here. In *Lambdopsalis*, the lacrimal is entirely absent (Fig. 21B; Miao 1988); in *Ptilodus*, the maxilla forms the orbital rim where a lacrimal is expected (Fig. 21A; Simpson 1937); and the presence of this bone is uncertain in *Taeniolabis* but it apparently is not exposed on the face (Fig. 21C; Broom 1914: fig. 6; Sloan 1981: fig. 6.14). The lacrimal is also not reconstructed on the face of the kogianoid Barbatodon (Smith and Codrea 2015: fig. 2).

The lacrimal is also an important component of the orbital pocket in *Guibaatar* (Fig. 5), *Kryptobaatar* (Wible and Rougier 2000), and *Mangasbaatar* (Rougier et al. 2016). An orbital pocket is present in other djadochtatherioids, but the bones forming it are not described. Outside of Djadochtatherioidea, an orbital pocket is reported in *Ectypodus* (Sloan 1979), *Taeniolabis* (Sloan 1981), and *Lambdopsalis* in reduced form (Gambaryan and Kielan-Jaworowska 1995).

Frontal.—The frontonasal suture in djadochtatherioids, including *Guibaatar* (Figs. 2, 20A), has a pointed incursion of the frontals between the nasals (Figs. 23D–K). The taxon conforming least to this pattern is *Catopsbaatar*, but there is some variability in the shape of this suture, from a relatively straight suture (Fig. 23I; Kielan-Jaworowska et al. 2005: fig. 2A) to a pointed incursion (Kielan-Jaworowska et al. 2005: fig. 4B). In the outgroups, the ptilodontid *Ptilodus* (Fig. 23A) has a slight sharp incursion of the frontals, whereas the taeniolabidids *Lambdopsalis* (Fig. 23B) and *Taeniolabis* (Fig. 23C) have a broad blunt incusion.

Pterygoid and Vomer.—On the ventral surface of the mesocranium posterior to the choanae, Wible and Rougier (2000) described three longitudinal crests in *Kryptobaatar* (Fig. 22H): a midline one formed by the vomer and lateral to that crests formed by the left and right pterygoids, which they called pterygopalatine ridges, following Barghusen (1986). Among djadochtatherioids, the same arrangement occurs in *Kamptobaatar* (Fig. 22E; Kielan-Jaworowska 1971: fig. 4), *Chulsanbaatar* (Fig. 22G; Kielan-Jaworowska et al. 1986: fig. 6), and *Nemegtbaatar* (Fig. 22D; Kielan-Jaworowska et al. 1986: fig. 20). According to Wible and Rougier (2000), *Ptilodus* shows the same pattern, whereas *Lambdopsalis* has only a low midline crest on the vomer (Fig. 22B; Miao 1988). *Guibaatar* (Figs. 3, 20B) and *Mangasbaatar* (Rougier et al. 2016) differ in that the midline crest on the vomer is lacking but the pterygopalatine ridges are present (the vomer shown on *Mangasbaatar* in Fig. 22J is not raised).

Squamosal.—In *Catopsbaatar*, the zygomatic process of the squamosal extends farther rostrally than in other multituberculates, nearly contacting the lacrimal and so excluding the maxilla from the orbital rim (Fig. 21H). Mangasbaatar also has a rostrally extended squamosal (Fig. 21I; Rougier et al. 2016) but it ends far from the lacrimal. In the other multituberculates preserving sutures in this area, the maxilla has a sizeable contribution to the orbital rim (Figs. 21A–C, G). Kielan-Jaworowska et al. (2005: fig. 11C) showed the *Catopsbaatar* condition in their composite reconstruction of *Djadochtatherium*, which as pointed out above may include specimens that are not of that taxon (see Rougier et al. 2016). Although *Guibaatar* is damaged, the right side preserves enough to show that the maxilla had a large contribution to the orbital rim (Fig. 4).

All djadochtatherioids, including *Guibaatar* (Fig. 6A), have a distinct neck on the zygomatic process that separates the glenoid fossa from the braincase (Figs. 22D–K). Such a neck is widely distributed in multituberculates, including, for example, the Early Cretaceous eobataarid *Sinobaatar* (Hu and Wang 2002: pl. 1), the Late Cretaceous kogaionids *Barbatodon* (Smith and Codrea 2015: figs. 2E–F) and *Litovoi* (Csiki-Sava et al. 2018: fig. 1B), and the ptilodontoids *Ptilodus* (Fig. 20A; Gidley 1909: pl. 70e; Hopson et al. 1989: fig. 2) and *Ectypodus* (Sloan 1979: fig. 1). The exceptions are the taeniolabidids *Lambdopsalis* (Fig. 20B; Miao 1988: fig. 18) and *Taeniolabis* (Fig. 20C; Granger and Simpson 1929: fig. 6).

Jugal.—Following Simpson (1937), the jugal was considered to be absent in multituberculates until Hopson et al. (1989) described a slender splint-like element on the medial side of the zygoma in *Ptilodus*, similarly situated partial jugals in *Nemegtbaatar* and *Chulsanbaatar*, and

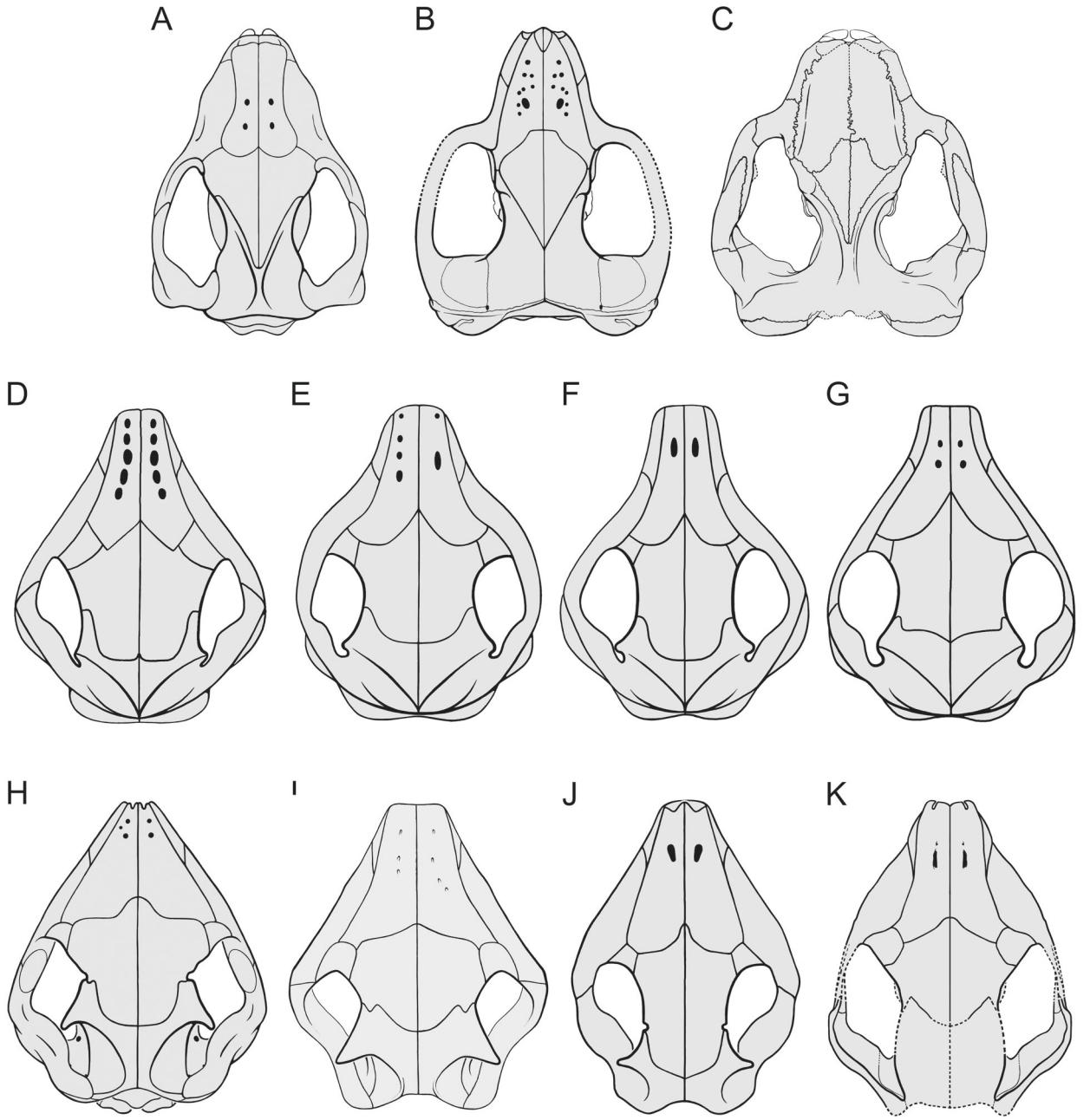

Fig. 23.—Multituberculate skull reconstruction in dorsal view, rendered to approximately the same length. **A,** *Ptilodus montanus* (modified from Simpson 1937: fig. 5); **B,** *Lambdopsalis bulla* (modified from Miao 1988: fig. 12); **C,** *Taeniolabis taoensis* (redrawn from Granger and Simpson 1929: fig. 5A); **D,** *Nemegtbaatar gobiensis* (redrawn from Kielan-Jaworowska et al. 1986: fig. 20a); **E,** *Kamptobaatar kuczynskii* (redrawn from Kielan-Jaworowska 1971: fig. 1); **F,** *Sloanbaatar mirabilis* (redrawn from Kielan-Jaworowska 1971: fig. 6); **G,** *Chulsanbaatar vulgaris* (redrawn from Kielan-Jaworowska and Hurum 1997: fig. 10G); **H,** *Kryptobaatar dashzevegi* (redrawn from Wible and Rougier 2000: fig. 32); **I,** *Catopsbaatar catopsaloides* (redrawn from Kielan-Jaworowska et al. 2005: fig. 6); **J,** *Mangasbaatar udanii* (redrawn from Rougier et al. 2016: fig. 19); **K,** *Guibaatar castellanus*.

similarly situated facets for a jugal in several Late Jurassic paulchoffatiids. A similar jugal was subsequently reported in *Kryptobaatar* (Wible and Rougier 2000) and here for *Guibaatar* (Fig. 7A).

Petrosal.—Multituberculate petrosals have been studied by various techniques, including in situ in the skull (e.g., Hurum et al. 1996; Wible and Rougier 2000), as isolated elements (e.g., Simpson 1937; Kielan-Jaworowska et al. 1986; Luo 1989; Lillegraven and Hahn 1993; Wible and Hopson 1995), by serial grinding and photographing (e.g., Kielan-Jaworowska et al. 1986), by x-rays (Fox and Meng 1997), and by CT scanning (Kik 2002; Ladevèze et al. 2010). Although much has been written about the multituberculate petrosal, there are not many specimens that have been well described and illustrated on multiple surfaces, which is pertinent to tracing neurovascular structures. Among the most thoroughly documented taxa are the djadochtatheriids cf. *Tombaatar*, n. sp. (Ladevèze et al. 2010) and *Kryptobaatar* (Wible and Rougier 2000; Kik 2002), and isolated petrosals from the Hell Creek Formation of Montana that have been assigned to the taeniolabidoid cf. "*Catopsalis*" *joyneri* (= "*Valenopsalis*" *joyneri*, Williamson et al. 2016), the ptilodontoid cf. *Mesodma thompsoni*, and the cimolomyid ?*Meniscoessus* (Kielan-Jaworowska et al. 1986; Luo 1989; Wible and Hopson 1995; Fox and Meng 1997).

Regarding the cavum epiptericum and cavum supracochleare, the confluence of the spaces housing the trigeminal (semilunar) and facial (geniculate) ganglia reported in *Guibaatar* (Fig. 7A) is present in many mammaliaforms outside of Cladotheria (Crompton and Sun 1985; Wible 1990; Crompton and Luo 1993; Wible and Hopson 1993) but not, for example, the gondwanatherian *Vintana* (Krause et al. 2014). All multituberculates with petrosals illustrated in endocranial view show the same pattern (e.g., Paulchoffatiidae, gen. et sp. indet, Lillegraven and Hahn 1993: figs. 1, 6; cf. *Mesodma thompsoni*, Kielan-Jaworowska et al. 1986: fig. 8b; cf. *Tombaatar*, n. sp., Ladevèze et al. 2010: fig. 2B).

The course for the facial nerve reported for *Guibaatar* (Fig. 24A) is essentially the same as in cf. *Tombaatar*, n. sp. (Fig. 24B; Ladevèze et al. 2010: figs. 2A3, B3) with an unenclosed cavum supracochleare leading to a secondary facial foramen anterolateral to the fenestra vestibuli and a hiatus Fallopii on the ventral surface at the anterior pole of the promontorium. In turn, this pattern is essentially the same as in *Morganucodon* (see Kermack et al. 1981: figs. 72C–E; Wible and Hopson 1993: fig. 5.3). *Kryptobaatar* is the only other djadochtatheriid for which the position of the hiatus has been discussed; although Wible and Rougier (2000) were uncertain of the course of the greater petrosal nerve, they reported that there is no visible tympanic aperture for the hiatus Fallopii in *Kryptobaatar* and a possible course was through the cavum supracochleare and cavum epiptericum. In other djadochtatherioids, a hiatus Fallopii visible in ventral view is labeled in various taxa (e.g., *Kamptobaatar*, Kielan-Jaworowska 1971: fig. 4; Hurum 1996: fig. 1; *Sloanbaatar*, Kielan-Jaworowska 1971: fig. 9) but we are not certain that these are equivalent openings.

Among multituberculates, distinct grooves for the internal carotid and stapedial arteries on the promontorium have been reported in only *Kryptobaatar* (Wible and Rougier 2000), cf. *Tombaatar*, n. sp. (Ladevèze et al. 2010), *Mangasbaatar* (Rougier et al. 2016), and the ptilodontoid *Ectypodus* (Sloan 1979). In each, the internal carotid course is positioned anteriorly on the promontorium, requiring a posterolateral direction for the stapedial artery to reach the fenestra vestibuli (Fig. 24B). Other multituberculates, including *Guibaatar*, show faint or no indications for these two arteries. However, given the size of the foramen for the ramus superior of the stapedial artery in these multituberculates, it seems likely that both the stapedial artery and the internal carotid artery were present (Figs. 24C–D).

A petrosal feature distinguishing multituberculates is the medially inflected lateral flange contacting the lateral wall of the promontorium (Kielan-Jaworowska et al. 1986; Rougier et al. 1996a; Wible and Rougier 2000; Rougier and Wible 2006). Usually enclosed by the inflection of the lateral flange is a canal that has been reconstructed as housing the ramus inferior of the stapedial artery and/or the post-trigeminal vein (Figs. 24C–D; Wible and Hopson 1995; Rougier and Wible 2006). A canal for the ramus inferior (post-trigeminal canal or canal for the ?maxillary artery) has been reported in cf. *Mesodma thompsoni* and cf. "*Valenopsalis*" *joyneri* (Kielan-Jaworowska et al. 1986; Wible and Hopson 1985), *Kryptobaatar* (Wible and Rougier 2000; Kik 2002), *Lambdopsalis* (Miao 1988), and ?*Meniscoessus* (Luo 1989). Although a canal for the ramus inferior is absent in *Guibaatar*, we interpret it as having a medially inflected lateral flange in contact with the promontorium (Fig. 6B), and rather than being enclosed in a canal, the ramus inferior and post-trigeminal vein ran endocranially through the cavum supracochleare and cavum epiptericum (Fig. 8). Ladevèze et al. (2010) did not describe a post-trigeminal canal in cf. *Tombaatar*, n. sp., and reconstructed the ramus inferior and post-trigeminal vein on the ventral surface of the petrosal (Fig. 24B). As in other multituberculates, the lateral flange appears to contact the promontorium in cf. *Tombaatar*, n. sp. (Ladevèze et al. 2010: fig. A1). If true, then either the course for the ramus inferior and post-trigeminal vein ventral to the infolded lateral flange in cf. *Tombaatar*, n. sp. (Fig. 24B), is unique among multituberculates or the vascular reconstruction by Ladevèze et al. (2010) for this taxon is not accurate. The incidence of a canal for the ramus inferior in other multituberculates is as yet unreported. Outside of multituberculates, an equivalent canal transmitting only the post-trigeminal vein has only been identified in the echidna *Tachyglossus* (Wible and Hopson 1995).

In the platypus *Ornithorhynchus*, the course of the ramus superior, prootic sinus, and facial nerve through the

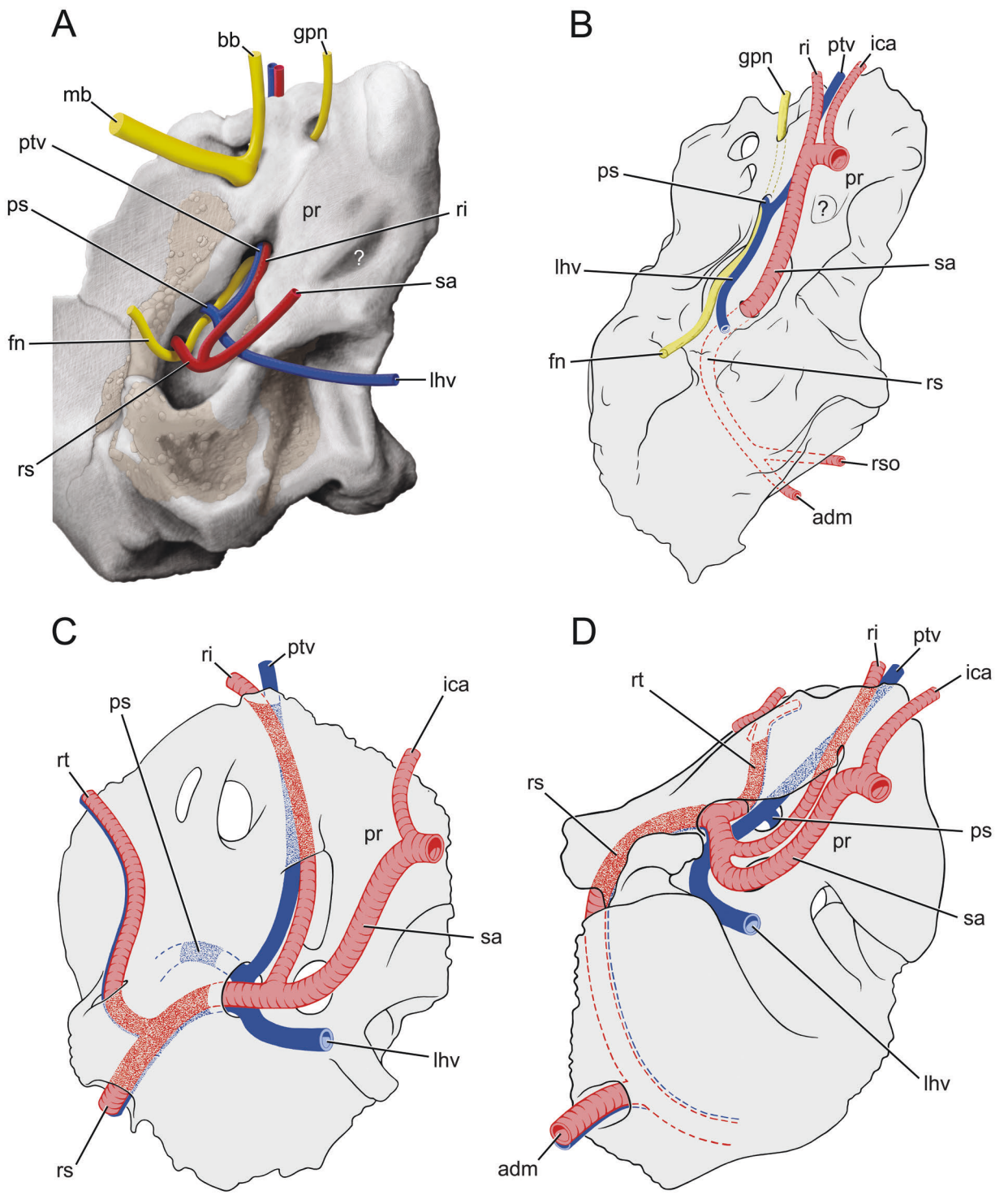

Fig. 24.—Vascular and nervous reconstructions on right petrosals in ventral view. **A,** *Guibaatar castellanus*; **B,** cf. *Tombaatar*, n. sp. (modified from Ladevèze et al. 2010: fig. 2A3); **C,** the ptilodontoid cf. *Mesodma thompsoni* (modified from Wible and Hopson 1995: fig. 8B); **D,** the taeniolabidoid cf. "*Valenopsalis*" *joyneri* (modified from Wible and Hopson 1995: fig. 7B). In B-D, dashed vessels and nerves are hidden by bone and stippled ones are in canals; the course of the facial nerve was not included in the original publications for C and D. "?" in A and B is a pit of uncertain function. Abbreviations: **adm,** arteria diploëtica magna; **bb,** buccinator branch; **fn,** facial nerve; **gpn,** greater petrosal nerve; **ica,** internal carotid artery; **lhv,** lateral head vein; **mb,** masticatory branch; **pr,** promontorium; **ps,** prootic sinus; **ptv,** post-trigeminal vein; **ri,** ramus inferior; **rs,** ramus superior; **rso,** ramus supraorbitalis; **rt,** ramus temporalis; **sa,** stapedial artery.

petrosal is in the area between the promontorium and crista parotica: the first two via a common opening and the last via the secondary facial foramen (Wible and Hopson 1993, 1995). The same three structures have been reconstructed in multituberculates, although the pattern of foramina differs. Most taxa, including *Kryptobaatar* (Wible and Rougier 2000), *Mangasbaatar* (Rougier et al. 2016), cf. *Mesodma thompsoni* (Fig. 24C; Wible and Hopson 1995), and cf. "*Valenopsalis*" *joyneri* (Fig. 22D; Wible and Hopson 1995), have the same arrangement as the platypus, with a common aperture for the ramus superior and prootic sinus. In contrast, *Guibaatar* (Fig. 24A), *Chulsanbaatar* (Wible and Rougier 2000), and ?*Meniscoessus* (Luo 1989) have separate openings for all three structures, as also occurs, for example, in *Morganucodon* (Kermack et al. 1981; Wible and Hopson 1993, 1995). Cf. *Tombaatar*, n. sp., is distinguished from all other multituberculates in that the facial nerve and prootic sinus share a common aperture and the foramen for the ramus superior is not under direct cover of the crista parotica (Fig. 24B).

Kryptobaatar (Wible and Rougier 2000), *Guibaatar* (Fig. 6B), and *Mangasbaatar* (Rougier et al. 2016) have a rostral tympanic process on the anterior pole of the promontorium, which increases in size across the three with the element being exceedingly large in *Mangasbaatar*. In contrast, cf. *Tombaatar*, n. sp., is illustrated with no corresponding prominence (Fig. 24B; Ladèveze et al. 2010: fig. A1). In other djadochtatherioids, stereophotographs of *Chulsanbaatar* (Kielan-Jaworowska et al. 1986: pl. 5, fig. 14A) and *Nemegtbaatar* (Kielan-Jaworowska et al. 1986: pl. 6, figs. 18C, 19A) show a prominence resembling that in *Guibaatar*. This structure may be primitive for multituberculates as Late Jurassic paulchoffatiids have a similar process, identified as the processus promontorii by Hahn (1988) and Lillegraven and Hahn (1993).

The djadochtatheriids *Kryptobaatar* (Wible and Rougier 2000), *Mangasbaatar* (Rougier et al. 2016), *Catopsbaatar* (Kielan-Jaworowska et al. 2005), cf. *Tombaatar*, n. sp. (Fig. 24B; Ladevèze et al. 2010), and *Guibaatar* (Fig. 6) have an irregular outline to the promontorium with incurvatures on both sides, which contrasts with the more regular outline in other multituberculates. This feature is related to the large middle ear space formed by the dorsal excavation of the basicranium in the vicinity of the jugular fossa in djadochtatheriids. Rougier et al. (2016) noted a trend of increasing jugular fossa size with *Kryptobaatar* and *Catopsbaatar* at the smaller end and *Mangasbaatar* and *Tombaatar* (based on an undescribed skull from Ukhaa Tolgod) at the larger end. Based on its petrosal, *Guibaatar* falls at the smaller end of this trend.

Finally, a well-developed tensor tympani fossa on the lateral aspect of the promontorium is widespread in multituberculates (Wible and Rougier 2000), including *Ptilodus* (Simpson 1937: fig. 8A), *Lambdopsalis* (Miao 1988: fig. 30), and *Kryptobaatar* (Wible and Rougier 2000: fig. 21). In contrast, the place occupied by a well-developed fossa in the above taxa is only gently concave in *Guibaatar* (Fig. 6B), *Mangasbaatar* (Rougier et al. 2016: fig. 24), *Catopsbaatar* (Kielan-Jaworowska et al. 2005: fig. 2C), and cf. *Tombaatar*, n. sp. (Ladevèze et al. 2010: fig. 2A1). In the last, Ladevèze et al. (2010: fig. 2A2) identified a fossa on the ventral surface of the promontorium, medial to the course of the stapedial artery, as the tensor tympani fossa ("?" in Fig. 24B), but this position seems too far medial compared to that in other multituberculates. This regular pit in cf. *Tombaatar*, n. sp., is similar in position to a more irregular pit on the promontorium in *Guibaatar* ("?" in Fig. 24A) and likely does not contain the tensor tympani muscle. In discussing the subtle tensor tympani fossa in *Mangasbaatar*, Rougier et al. (2016) suggested the muscle was also relatively small, an arrangement also occurring in the marsupial mole *Notoryctes* (Ladevèze et al. 2008) with the muscle wholly absent in golden moles (Mason 2003) and various other mammals with a subterranean life-style (Mason 2013). The small tensor tympani muscle and enlarged middle ear are suggestive of fossorial habits in djadochtatheriids.

Mandible.— In djadochtatheriids, the coronoid process is higher than the condylar process (Figs. 25I–L), as also found in the ptilodontid *Ptilodus* (Fig. 25A) and the taeniolabidids *Lambdopsalis* (Fig. 25B) and *Taeniolabis* (Fig. 25C). In contrast, in other djadochtatherioids, the coronoid is at the same level or lower than the condylar process (Figs. 25E–H), with the exception of *Nemegtbaatar* (Fig. 25D). This anatomy cannot be assessed in *Guibaatar* as the condylar process is entirely missing. *Guibaatar*, *Mangasbaatar*, and *Catopsbaatar* share a narrow digitiform coronoid process (Figs. 25K–M), which is much broader in the remaining multituberculates sampled here (Figs. 25A–J).

Dentition.—A model of tooth eruption and replacement that occurred in an antero-posterior sequence for the upper incisors and premolars, except the last, in Late Cretaceous and Paleogene multituberculates was proposed by Greenwald (1988) and tentatively accepted by Luo et al. (2004). In this scheme, the P4 and p3–4 are monophyodont, as there are no known specimens showing replacement at these loci. Recently, Xu et al. (2015) described a new multituberculate, *Yubaatar*, the outgroup to Taeniolabidoidea, from the Upper Cretaceous of Henan Province, China that supports Greenwald's model for the upper premolars with one caveat; it has both a deciduous and a replacement tooth at the last upper premolar position, the first multituberculate known to do so. Whereas *Guibaatar* has evidence of replacement at the enlarged incisor in the upper and lower jaws (Figs. 15, 17), there is no evidence of replacement at other tooth positions. Rather than resembling an ontogenetic stage in another multituberculate, *Guibaatar* looks remarkably like the Jurassic euharamiyidan *Arboroharamiya jenkinsi*, which in the lower jaw has an enlarged deciduous incisor, unerupted permanent incisor, p4, m1,

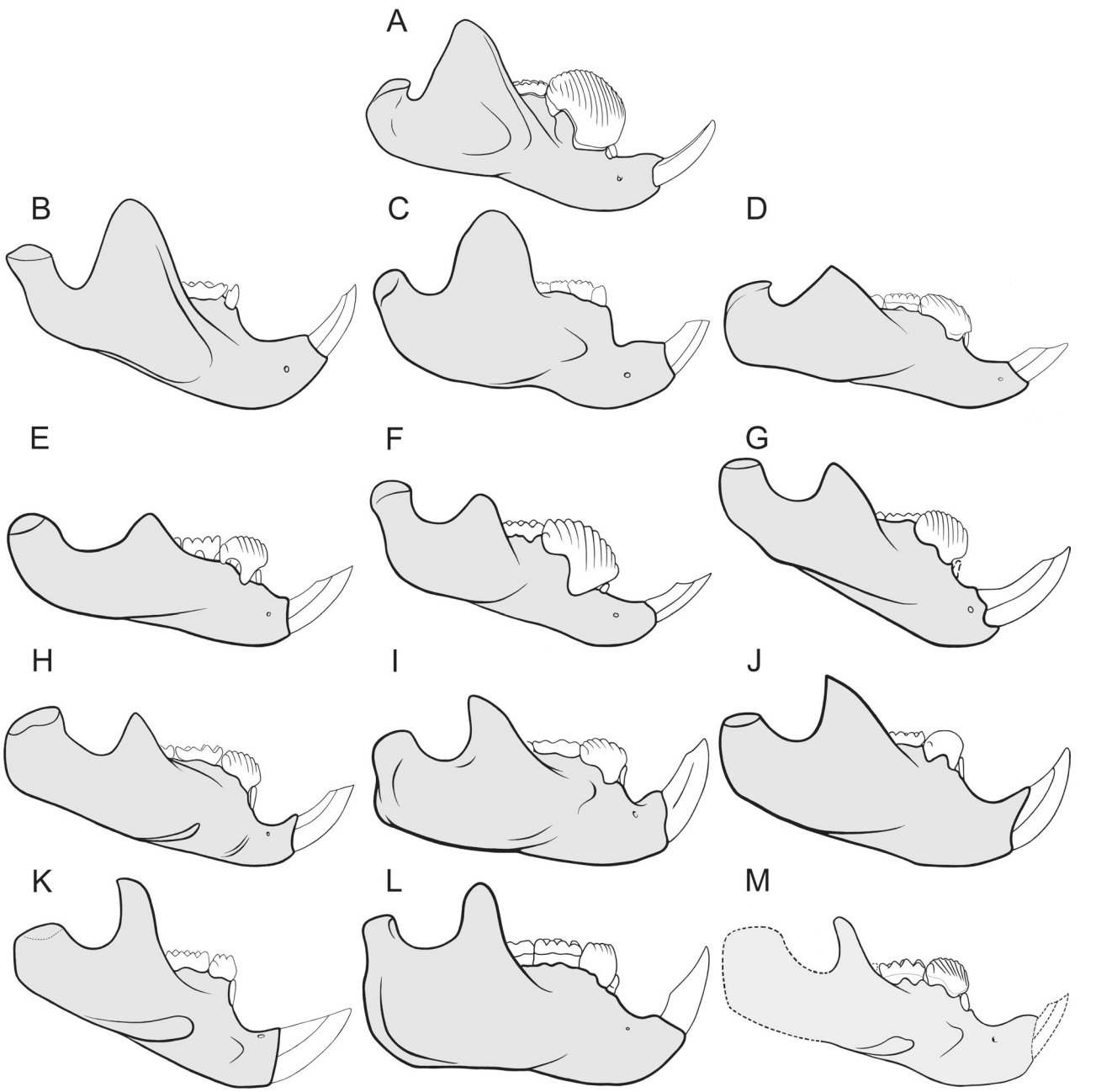

Fig. 25.—Multituberculate mandible reconstructions, in right lateral view, rendered to approximately the same length. **A,** *Ptilodus* (from Krause 1982: fig. 2C); **B,** *Lambdopsalis bulla* (redrawn from Miao 1988: fig. 4); **C,** *Taeniolabis taoensis* (modified from Granger and Simpson 1929: fig. 4); **D,** *Nemegtbaatar gobiensis* (modified from Kielan-Jaworowska and Hurum 1997: fig. 12D); **E,** *Kamptobaatar kuczynskii* (redrawn from Kielan-Jaworowska and Hurum 1997: fig. 12E); **F,** *Nessovbaatar multicostatus* (redrawn from Kielan-Jaworowska and Hurum 1997: fig. 12G); **G,** *Sloanbaatar mirabilis* (redrawn from Kielan-Jaworowska and Hurum 1997: fig. 12F); **H,** *Chulsanbaatar vulgaris* (modified from Kielan-Jaworowska and Hurum 1997: fig. 12H); **I,** *Kryptobaatar dashzevegi* (modified from Wible and Rougier 2000: fig. 33); **J,** *Djadochtatherium matthewi* (redrawn from Kielan-Jaworowska and Hurm 1997: fig. 12J); **K,** *Catopsbaatar catopsaloides* (modified from Kielan-Jaworowska et al. 2005: fig. 7); **L,** *Mangasbaatar udanii* (redrawn from Rougier et al. 2016: fig. 23); **M,** *Guibaatar castellanus*.

and m2 in a crypt (Mao et al. 2019). The resemblance also pertains to the root morphology of the lower deciduous incisor; as in *Guibaatar*, this tooth's root in *A. jenkinsi* is not broadly open but is tapered distally (Mao et al. 2019: fig. 1B). In some recent phylogenetic analyses (e.g., Bi et al. 2014), Euharamiyida and Multituberculata are sister groups.

Guibaatar is the first djadochtatherioid to have the deciduous and permanent enlarged upper and lower incisors illustrated in situ. It shows that the deciduous teeth have uniform, thin enamel, whereas the enamel is thicker mesially and mesiobuccally in the permanent tooth (Fig. 14). We are uncertain if the permanent incisors have a thin layer of enamel or no enamel on the remaining surfaces; all other djadochtatherioids have been reported to have restricted enamel on their enlarged incisors (Kielan-Jaworowska and Hurum 1997; Rougier et al. 2016). To our knowledge, the only similar illustration in a djadochtatherioid is the lower incisors of a *Kryptobaatar* specimen in Kielan-Jaworowska (1980: fig. 2). Unfortunately, the deciduous tooth was damaged and the extent of its enamel was not determined. The only other report documenting the enamel in deciduous and permanent enlarged incisors in multituberculates is that by Mao et al. (2015) on the taeniolabidoid *Lambdopsalis* using SEM images. These authors found that the enamel of the deciduous tooth is not restricted, but is thickest on the mesiobuccal aspect, with the enamel of the upper incisor thinner than the lower; the permanent teeth have enamel restricted buccally, with that of the lower incisor at least twice the thickness of the upper. Moreover, compared to the deciduous teeth, the permanent incisors had "thicker enamel, prismatic covering more area of the tooth, and greater prism density" (Mao et al. 2015:32). Based on these differences, Mao et al. (2015:32) suggested "that *Lambdopsalis* had a soft diet period before the permanent incisors erupted." *Guibaatar* follows a similar pattern with thin uniform enamel in the deciduous incisors and thicker enamel mesially and mesiobuccally in the permanent teeth, with the thickness of the lower twice that of the upper. However, contra Mao et al., we are uncertain how this ontogenetic difference relates to diet. Uniform enamel is the norm, the likely primitive mammaliaform condition, and therefore perhaps merely the starting point in ontogeny. Without a model in extant mammals, we find it premature to link this ontogenetic sequence to a change in diet.

In the upper dentition, in djadochtatheriids, *Kryptobaatar* and *Djadochtatherium* have four premolars, whereas *Tombaatar*, *Catopsbaatar*, *Mangasbaatar*, and *Guibaatar* have three. However, in those with three, a well-developed diastema separates the first two premolars in *Tombaatar* (Rougier et al. 1997), *Catopsbaatar* (Kielan-Jaworowska et al. 2005), and *Mangasbaatar* (Rougier et al. 2016), and following Kielan-Jaworowska (1974), these three premolars have been identified as P1, P3, and P4. In contrast, *Guibaatar* has no diastema between the first two premolars and we identify the three premolars as P2, P3, and P4. We speculate that the diastema posterior to the P1 in *Tombaatar*, *Catopsbaatar*, and *Mangasbaatar* may be created by elongation of the rostrum in the adult, and if so, that the three premolars in these large djadochtatheriids are homologous with those in the juvenile *Guibaatar*. Juveniles of the large djadochtatheriids should supply the evidence to address these homologies, but appropriate stages are not yet known. Regarding the cusp pattern on the P2, all djadochtatherioids have three cusps on that tooth except *Guibaatar*, which doubles that number.

On P4, *Guibaatar* and *Mangasbaatar* differ from the other djadochtatheriids in having a third (buccal) row of cusps with one and two, respectively. We regard *Djadochtatherium* as unknown; a cusp formula for P4 was scored for this taxon in a state that included a range of cusps in three rows of 0–5:1–4:0–5 by Kielan-Jaworowska and Hurum (1997) and Rougier et al. (2016), but we have been unable to find a description of the actual condition in *Djadochtatherium*. The M1 cusp formula of *Guibaatar* of 5:5:2 falls between that of *Mangasbaatar* (5:5:3) and *Tombaatar* (4:5:2); *Kryptobaatar* has 4-5:4-5:ridge, *Catopsbaatar* 5–6:5–6:4, and *Djadochtatherium* is unknown.

In the lower dentition, *Mangasbaatar* and *Catopsbaatar* are distinguished from other djadochtatherioids by the low number of serrations on p4 (five and three, respectively), but the conditions in *Tombaatar* and *Djadochtatherium* are unknown. Additionally, the shape of the p4 is different in *Mangasbaatar* and *Catopsbaatar*, with the tooth less arcuate and almost rectangular. The cusp formula of the m1 is relatively uniform across djadochtatherioids with all taxa having 4:3 except *Catopsbaatar* with 4:4 and *Nemegtbaatar* with 5:4. Regarding m2, *Guibaatar* is unique among LCMM in having only one cusp in the lingual row, with the usual condition being two except for *Catopsbaatar*, which has four.

CONCLUSIONS

Guibaatar castellanus is the second new species of djadochtatheriid multituberculate to be named from the Upper Cretaceous Bayan Mandahu Formation of Inner Mongolia, China, the first being a new species of *Kryptobaatar*. The other djadochtatheriid species are known exclusively from Upper Cretaceous Mongolian localities of the Djadochta and Barun Goyot formations. The only known specimen of *Guibaatar* is that of a juvenile, with the enlarged upper and lower incisors known by deciduous teeth and forming permanent replacements, as well as forming last molars. The deciduous incisors have a covering of thin enamel, whereas the permanent incisors have enamel thicker mesially and mesiobuccally, an ontogenetic pattern resembling that reported already for the taeniolabidoid *Lambdopsalis* from the late Paleocene of Inner Mongolia. Despite its ontogenetic stage, *Guibaatar* is likely closer in size to the large djadochtatheriids, *Djadochtatherium*, *Catopsbaatar*, *Tombaatar*, and *Mangasbaatar*, than the much

smaller *Kryptobaatar*.

Guibaatar has an isolated petrosal that allows for a detailed reconstruction of the associated nervous and vascular structures. Of known djadochtatheriids, its vascular pattern bears general resemblance to *Kryptobaatar* and differs from cf. *Tombaatar*, n. sp., in particular regarding the course of the ramus inferior of the stapedial artery. In the last taxon, the artery runs open on the tympanic surface of the petrosal, whereas in *Guibaatar* and *Kryptobaatar* the artery is enclosed in the petrosal by the infolded lateral flange, a possible synapomorphy of multituberculates.

Phylogenetic analysis supports *Kryptobaatar* as the earliest diverging djadochtatheriid and *Guibaatar* as sister to a clade of *Mangasbaatar* and *Catopsbaatar*. However, at least two djadochtatheriids are very incompletely known: *Tombaatar* is represented by an incomplete rostrum and *Djadochtatherium* by several poorly preserved, incomplete specimens. Reports of more complete specimens of both taxa have already appeared in the literature. Moreover, given the number of multituberculate specimens reported to already have been collected by prior expeditions to the Bayan Mandahu Formation, the known diversity of djadochtatherioids will only increase in the future. We are confident that Djadochtathiidae is natural, but are currently uncertain of the relationships within this clade.

ACKNOWLEDGMENTS

For assistance in the field, we thank Liping Liu and Tao Yu. In the Section of Mammals, Carnegie Museum of Natural History, we thank Paul Bowden for his excellence in illustration. At the Center for Quantitative Imaging at Pennsylvania State University, we thank Odette Mina, Whitney Yetter, and especially Tim Stecko for their assistance with the CT scanning of *Guibaatar*. For their helpful reviews on an earlier version of this paper, we thank Drs. Guillermo Rougier and Thierry Smith, who provided insightful comments that helped us in our interpretation of *Guibaatar*, though mistakes in that interpretation are ours alone. We also thank Ghéreint Devillet and Dr. David Krause for pointing out additional errors. Support for this research is from the Double First-Class joint program of the Science & Technology Department of Yunnan University (2018FY001-005), the National Science Foundation of China (41728003), HKU Faculty of Science RAE Improvement Fund, the National Science Foundation Grant DEB 1654949, and the R.K. Mellon North American Mammal Research Institute.

LITERATURE CITED

ARCHIBALD, J.D. 1982. A study of Mammalia and geology across the Cretaceous-Tertiary boundary in Garfield County, Montana. University of California Publications in Geological Sciences, 122:1–286.

BARGHUSEN, H.R. 1986. On the evolutionary origin of the therian tensor veli palatini and tensor tympani muscles. Pp. 253–262, *in* The Ecology and Biology of Mammal-like Reptiles (N. Hotton III, P.D. MacLean, J.J. Roth, and E.C. Roth, eds.). Smithsonian Institution Press, Washington.

BENTON, M.J. 2000. Conventions in Russian and Mongolian palaeontological literature. Pp. xvi–xxxix, *in* The Age of Dinosaurs in Russia and Mongolia (M.J. Benton, M.A. Shishkin, D.M. Unwin, and E.N. Kurochkin, eds.). Cambridge University Press, Cambridge.

BI, S., Y. WANG, J. GUAN, X. SHENG, AND J. MENG. 2014. Three new Jurassic euharamiyidan species reinforce early divergence of mammals. Nature, 514:579–584.

BROOM, R. 1914. On the structure and affinities of the Multituberculata. Bulletin of the American Museum of Natural History, 33(8):115–134.

CROMPTON, A.W., AND Z. LUO. 1993. Relationships of the Liassic mammals *Sinoconodon*, *Morganucodon oehleri*, and *Dinnetherium*. Pp. 30–44, *in* Mammal Phylogeny: Mesozoic Differentiation, Multituberculates, Monotremes, Early Therians, and Marsupials (F.S. Szalay, M.J. Novacek, and M.C. McKenna, eds.). Springer Verlag, New York.

CROMPTON, A.W., AND A.-L. SUN. 1985. Cranial structure and relationships of the Liassic mammal *Sinoconodon*. Zoological Journal of the Linnean Society, 85:99–119.

CSIKI-SAVA, Z., M. VREMIR, J. MENG, S.L. BRUSATTE, AND M.A. NORELL. 2018. Dome-headed, small-brained island mammal from the Late Cretaceous of Romania. Proceedings of the National Academy of Sciences U.S.A., 115(19):4857–4862.

DASHZEVEG, D., L. DINGUS, D.B. LOOPE, C.C. SWISHER III, T. DULAM, AND M.R. SWEENEY. 2005. New stratigraphic subdivision, depositional environment and age estimage for the Upper Cretaceous Djadokhta Formation, southern Ulan Nur Basin, Mongolia. American Museum Novitates, 3498:1–31.

DINGUS, L., D.B. LOOPE, D. DASHZEVEG, C.C. SWISHER III, C. MINJIN, M.J. NOVACEK, AND M.A. NORELL. 2008. The geology of Ukhaa Tolgod (Djadokhta Formation, Upper Cretaceous, Nemegt Basin, Mongolia). American Museum Novitates, 3616:1–40.

DONG, Z.-M. 1993. The field activities of the Sino-Canadian Dinosaur Project in China, 1987–1990. Canadian Journal of Earth Sciences, 30(10):1997–2001.

EDGEWORTH, F.H. 1924. Mandibular and hyoid muscles of *Orycteropus*. Journal of Anatomy, 58:134–139.

EVANS, H.E. 1993. Miller's Anatomy of the Dog. Third Edition. W.B. Saunders Company, Philadelphia. 1113 pp.

FOX, R.C., AND J. MENG. 1997. An X-radiographic and SEM study of the osseous inner ear of multituberculates and monotremes (Mammalia): implications for mammalian phylogeny and evolution of hearing. Zoological Journal of the Linnean Society, 121:249–291.

GAMBARYAN, P.P., AND Z. KIELAN-JAWOROWSKA. 1995. Masticatory musculature of Asian taeniolabidoid multituberculate mammals. Acta Palaeontologica Polonica, 40(1):45–108.

GIDLEY, J.W. 1909. Notes on the fossil mammalian genus *Ptilodus*, with descriptions of new species. Proceedings of the United States National Museum, 36:611–626.

GOLOBOFF, P.A., AND S.A. CATALANO. 2016. TNT version 1.5, including a full implementation of phylogenetic morphometrics. Cladistics, 23:221–238.

GRANGER, W., AND G.G. SIMPSON. 1929. A revision of the Tertiary Multituberculata. Bulletin of the American Museum of Natural History, 56(9):601–676.

GREENWALD, N.S. 1988. Patterns of tooth eruption and replacement in multituberculate mammals. Journal of Vertebrate Paleontology, 8(3):265–277.

GRIFFITHS, M. 1978. The Biology of Monotremes. Academic Press, New York.

HAHN, G. 1969. Beiträge zur Fauna der Grube Guimarota Nr. 3. Die Multituberculata. Palaeontographica Abteilung A, 133:1–100.

———. 1985. Zur Bau des Infraorbital-Foramens bei den Paulchoffatiidae (Multituberculata, Ober-Jura). Berliner geowissenschaftliche Abhandlungen, 60:5–27.

———. 1988. Die Ohr-Region der Paulchoffatiidae (Multituberculata, Ober-Jura). Palaeovertebrata, 18(3):155–185.

HAHN, G., AND R. HAHN. 1994. Nachweis des Septomaxillare bei *Pseudobolodon krebsi* n. sp. (Multituberculata) aus dem Malm Portugals. Berliner geowissenschaftliche Abhandlungen, E13:9–29.

HIIEMAE, K., AND F.A. JENKINS, JR. 1969. The anatomy and internal architecture of the muscles of mastication in *Didelphis marsupialis*. Postilla, 140:1–49.

HILL, J.E. 1935. Cranial foramina in rodents. Journal of Mammalogy, 16(2):121–129.

HIMMELREICH, H.A. 1964. Der M. tensor veli palatini der Säugetiere unter Berücksichtigung seines Aufbaus, seiner Funktion und seiner Enstehungsgeschichte. Anatomischer Anzeiger, 115:1–26.

HOFFMANN, S., P.M. O'CONNOR, E.C. KIRK, J.R. WIBLE, AND D.W. KRAUSE. 2014. Endocranial and inner ear morphology of *Vintana sertichi* (Mammalia, Gondwanatheria) from the Late Cretaceous of Madagascar. *In Vintana sertichi* (Mammalia, Gondwanatheria) from the Late Cretaceous of Madagascar (D.W. Krause, ed.). Society of Vertebrate Paleontology Memoir 14. Journal of Vertebrate Paleontology, 34, Supplement to Number 6:110–137.

HOPSON, J.A., AND G.W. ROUGIER. 1993. Braincase structure in the oldest known skull of a therian mammal: implications for mammalian systematics and cranial evolution. *In* Functional Morphology and Evolution (P. Dodson and P. Gingerich, eds.). American Journal of Science, 293–A:268–299.

HU, Y., AND Y. WANG. 2002. *Sinobaatar* gen. nov.: first multituberculate from the Jehol Biota of Liaoning, northeast China. Chinese Science Bulletin, 46(5):372–386.

HURUM, J.H. 1994. Snout and orbit of Cretaceous Asian multituberculates studied by serial sections. Acta Palaeontologica Polonica, 39(2):181–221.

———. 1998. The braincase of two Late Cretaceous Asian multituberculates studied by serial sections. Acta Palaeontologica Polonica, 43(1):21–52.

HURUM, J.H., R. PRESLEY, AND Z. KIELAN-JAWOROWSKA. 1996. The middle ear in multituberculate mammals. Acta Palaeontologica Polonica, 41(3):253–275.

JEPSEN, G.L. 1930. Stratigraphy and Paleontology of the Paleocene of northeastern Park County, Wyoming. Proceedings of the American Philosophical Society, 69(7):463–528.

———. 1940. Paleocene faunas of the Polecat Bench Formation, Park County, Wyoming. Proceedings of the American Philosophical Society, 83:217–341.

JERZYKIEWICZ, T., P.J. DURRIE, D.A. EBERTH, P.A. JOHNSTON, E.H. KOSTER, AND J.-J. ZHENG. 1993. Djadokhta Formation correlative strata in Chinese Inner Mongolia: an overview of the stratigraphy, sedimentary geology, and paleontology and comparisons with the type locality in the pre-Altai Gobi. Canadian Journal of Earth Sciences, 10:2180–2195.

KERMACK, K.A., AND Z. KIELAN-JAWOROWSKA. 1971. Therian and non-therian mammals. *In* Early Mammals (D.M. Kermack and K.A. Kermack, eds.). Zoological Journal of the Linnean Society, 50 (supplement 1):103–115.

KERMACK, K.A., F. MUSSETT, AND H.W. RIGNEY. 1981. The skull of *Morganucodon*. Zoological Journal of the Linnean Society, 71(1):1–158.

KIELAN-JAWOROWSKA, Z. 1970. New Upper Cretaceous multituberculate genera from Bayn Dzak, Gobi Desert. Palaeontologia Polonica, 21:35–49.

———. 1971. Skull structure and affinities of the Multituberculata. Palaeontologia Polonica, 25:4–41.

———. 1974. Multituberculate succession in the Late Cretaceous of the Gobi Deseart (Mongolia). Palaeontologia Polonica, 30:23–44.

———. 1980. Absence of ptilodontoidean multituberculates from Asia and its palaeogeographic implications. Lethaia, 13:169–173.

———. 1994. A new generic name for the multitbuerculate mammals '*Djadochtatherium*' *catopsaloides*. Acta Palaeontologica Polonica, 39(1):134–136.

KIELAN-JAWOROWSKA, Z., R.L. CIFELLI, AND Z.-X. LUO. 2004. Mammals from the Age of Dinosaurs: Origins, Evolution, and Structure. Columbia University Press, New York. 630 pp.

KIELAN-JAWOROWSKA, Z., AND D. DASHZEVEG. 1978. New Late Cretaceous mammal locality and a description of a new multituberculate. Acta Palaeontologica Polonica, 23(2):115–130.

KIELAN-JAWOROWSKA, Z., AND J.H. HURUM. 1997. Djadochtatheria – a new suborder of multitbuerculate mammals. Acta Palaeontologica Polonica, 42(2):201–242.

———. 2001. Phylogeny and systematics of multituberculate mammals. Palaeontology, 44(3):389–429.

KIELAN-JAWOROWSKA, Z., J.H. HURUM, P.J. CURRIE, AND R. BARSBOLD. 2002. New data on anatomy of the Late Cretaceous multituberculate mammal *Catopsbaatar*. Acta Palaeontologica Polonica, 47(3):557–560.

KIELAN-JAWOROWSKA, Z., J.H. HURUM, AND A.V. LOPATIN. 2005. Skull structure in *Catopsbaatar* and the zygomatic ridges in multituberculate mammals. Acta Palaeontologica Polonica, 50(3):487–512.

KIELAN-JAWOROWSKA, Z., AND T.E. LANCASTER. 2004. A new reconstruction of multituberculate endocranial casts and encephalization quotient of *Kryptobaatar*. Acta Palaeontologica Polonica, 49(2):177–188.

KIELAN-JAWOROWSKA, Z., R. PRESLEY, AND C. POPLIN. 1986. The cranial vascular system in taeniolabidoid multituberculate mammals. Philosphical Transactions of the Royal Society of London, B313:525–602.

KIELAN-JAWOROWSKA, Z., AND A.V. SOCHAVA. 1969. The first multituberculate mammal from the Uppermost Cretaceous of the Gobi Desert (Mongolia). Acta Palaeontologica Polonica, 14(3):355–367.

KIK, P. 2002. Computed tomographic (CT) examination of the craniomandibular morphology of *Kryptobaatar dashzevegi* (Mammalia Multituberculata). Masters Dissertation, University of Louisville. 92 pp.

KRAUSE, D.W. 1982. Jaw movement, dental function, and diet in the Paleocene multituberculate *Ptilodus*. Paleobiology, 8(3):265–281.

KRAUSE, D.W., J.R. WIBLE, S. HOFFMANN, J.R. GROENKE, P.M. O'CONNOR, AND W.L. HOLLOWAY. 2014. Craniofacial morphology of *Vintana sertichi* (Mammalia, Gondwanatheria) from the Late Cretaceous of Madagascar. *In Vintana sertichi* (Mammalia, Gondwanatheria) from the Late Cretaceous of Madagascar (D.W. Krause, ed.). Society of Vertebrate Paleontology Memoir 14. Journal of Vertebrate Paleontology, 34, Supplement to Number 6:14–109.

KUHN, H.-J., AND U. ZELLER. 1987. The cavum epiptericum in monotremes and therian mammals. *In* Morphogenesis of the Mammalian Skull (H.-J. Kuhn and U. Zeller, eds.). Mammalia depicta, 13:51–70.

LADEVÈZE, S., C. DE MUIZON, M. COLBERT, AND T. SMITH. 2010. 3D computation imaging of the petrosal of a new multituberculate mammal from the Late Cretaceous of China and its paleobiologic inferences. Comptes Rendus Palevol, 9:319–330.

LILLEGRAVEN, J.A., AND G. HAHN. 1993. Evolutionary analysis of the middle and inner ear of Late Jurassic multituberculates. Journal of Mammalian Evolution, 1(1):47–74.

LILLEGRAVEN, J.A., AND G. KRUSAT. 1991. Cranio-mandibular anatomy of *Haldanodon exspectatus* (Docodonta; Mammalia) from the Late Jurassic of Portugal and its implications to the evolution of mammalian characters. Contributions to Geology, University of Wyoming, 28:39–138.

LOFGREN, D.L., B.E. SCHERER, C.K. CLARK, AND B. STANDHARDT. 2005. First record of *Stygimys* (Mammalia, Multituberculata, Eucosmodontidae) from the Paleocene (Puercan) part of the North Horn Formation, Utah, and a review of the genus. Journal of Mammalian Evolution, 12(1/2):77–97.

LUO, Z. 1989. Structure of the petrosals of Multituberculata (Mammalia) and morphology of the molars of early arctocyonids (Condylarthra, Mammalia). Ph.D. dissertation, University of California at Berkeley. 426 pp.

LUO, Z.-X., AND Q. JI. 2005. New study on dental and skeletal features of the Cretaceous "symmetrodontan" mammal *Zhangheotherium*. Journal of Mammalian Evolution, 12(3/4):337-357.

LUO, Z.-X., Z. KIELAN-JAWOROWSKA, AND R.L. CIFELLI. 2004. Evolution of dental replacement in mammals. *In* Fanfare for an Uncommon Paleontologist: Papers in Honor of Malcolm C. McKenna (M.R. Dawson and J.A. Lillegraven, eds.). Bulletin of Carnegie Museum of Natural History, 36:159–175.

LYSON, T.R., I.M. MILLER, A.D. BERCOVICI, K. WEISSENBURGER, A.J. FUENTES, W.C. CLYDE, J.W. HAGADORN, M.J. BUTRIM, K.R. JOHNSON, R.F. FLEMING, R.S. BARCLAY, S.A. MACCRACKEN, B. LLOYD, G.P. WILSON, D.W. KRAUSE, AND S.G.B. CHESTER. 2019. Exceptional continental record of biotic recovery after the Cretaceous–Paleogene mass extinction. Science, 366 (6448):977-

983.

MACRINI, T.E. 2006. The evolution of endocranial spaces in mammals and non-mammalian cynodonts. Ph.D. Dissertation, University of Texas, Austin. 278 pp.

MAKOVICKY, P.J. 2008. Telling time from fossils: a phylogeny-based approach to chronological ordering of paleobiotas. Cladistics, 24:350–371.

MAO, F., Y. WANG, AND J. MENG. 2015. A systematic study on tooth enamel microstructures of *Lambdopsalis bulla* (Multituberculata, Mammalia) - Implications for multituberculate biology and phylogeny. PLoS ONE, 10(5):30128243.

MAO, F.-Y., X.-T. ZHENG, X.-L. WANG, Y.-Q. WANG, S.-D. BI, AND J. MENG. 2019. Evidence of diphyodonty and heterochrony for dental development from Jurassic Yanliao Biota. Vertebrata Palasiatica, 57:51–76.

MIAO, D. 1986. Dental anatomy and ontogeny of *Lambdopsalis bulla* (Mammalia, Multituberculata). Contributions to Geology, University of Wyoming, 24(1):65–76.

———. 1988. Skull morphology of *Lambdopsalis bulla* (Mammalia, Multituberculata) and its implications to mammalian evolution. Contributions to Geology, University of Wyoming, Special Paper, 4:1–104.

PRESLEY, R. 1981. Alisphenoid equivalents in placentals, marsupials, monotremes and fossils. Nature, 294:668–670.

ROUGIER, G.W., M.J. NOVACEK, AND D. DASHZEVEG. 1997. A new multituberculate from the Late Cretaceous locality Ukhaa Tolgod, Mongolia. Considerations on multituberculate interrelationships. American Museum Novitates, 3181:1–26.

ROUGIER, G.W., A.S. SHETH, B.K. SPURLIN, M. BOLORTSETSEG, AND M.J. NOVACEK. 2016. Craniodental anatomy of a new Late Cretaceous multituberculate mammal from Udan Sayr, Mongolia. Palaeontologia Polonica, 67:197–248.

ROUGIER, G.W., AND J.R. WIBLE. 2006. Major changes in the mammalian ear region and basicranium. Pp. 269–311, *in* Amniote Paleobiology: Perspectives on the Evolution of Mammals, Birds, and Reptiles (M.T. Carrano, T.J. Gaudin, R.W. Blob, and J.R. Wible, eds.). University of Chicago Press, Chicago and London.

ROUGIER, G.W., J.R. WIBLE, AND J.A. HOPSON. 1992. Reconstruction of the cranial vessels in the Early Cretaceous mammal *Vincelestes neuquenianus*: implications for the evolution of the mammalian cranial vascular system. Journal of Vertebrate Paleontology, 12(2): 188–216.

———. 1996a. Basicranial anatomy of *Priacodon fruitaensis* (Triconodontidae, Mammalia) from the Late Jurassic of Colorado, and a reappraisal of mammaliaform interrelationships. American Museum Novitates, 3183:1–38.

ROUGIER, G.W., J.R. WIBLE, AND M.J. NOVACEK. 1996b. Middle-ear ossicles of *Kryptobaatar dashzevegi* (Mammalia, Multituberculata): implications for mammaliamorph relationships and the evolution of the auditory apparatus. American Museum Novitates, 3187:1–43.

SEGALL, W. 1970. Morphological parallelisms of the bulla and auditory ossicles in some insectivores and marsupials. Fieldiana, Zoology, 51:169–205.

SERENO, P.C. 2006. Shoulder girdle and forelimb in multituberculates: evolution of parasagittal forelimb posture in mammals. Pp. 315–366, *in* Amniote Paleobiology: Perspectives on the Evolution of Mammals, Birds, and Reptiles (M.T. Carrano, T.J. Gaudin, R.W. Blob, and J.R. Wible, eds.). University of Chicago Press, Chicago and London.

SERENO, P.C., AND M.C. MCKENNA. 1995. Cretaceous multituberculate skeleton and the early evolution of the mammalian shoulder girdle. Nature, 377:144–147.

SIMMONS, N.B. 1993. Phylogeny of Multituberculata. Pp. 146–164, *in* Mammal Phylogeny: Placentals (F.S. Szalay, M.J. Novacek, and M.C. McKenna, eds.). Springer Verlag, New York.

SIMPSON, G.G. 1925. A Mesozoic mammal skull from Mongolia. American Museum Novitates, 201:1–12.

———. 1937. Skull structure of the Multituberculata. Bulletin of the American Museum of Natural History, 73:727–763.

SLOAN, R.E. 1979. Multituberculata. Pp. 492–498, *in* The Encyclopedia of Paleontology (R.W. Fairbridge and D. Jablonski, eds.). Encyclopedia of Earth Sciences, Volume VII. Dowden, Hutchinson & Ross, Stroudsberg.

———. 1981. Systematics of Paleocene multituberculates from the San Juan Basin, New Mexico. Pp. 127–160, *in* Advances in San Juan Basin Paleontology (S. Lucas, K. Rigby, Jr., and B. Kues, eds.). University of New Mexico Press, Albuquerque.

SLOAN, R.E., AND L. VAN VALEN. 1965. Cretaceous mammals from Montana. Science, 148(3667):220–227.

SMITH, T., AND V. CODREA. 2015. Red iron-pigmented tooth enamel in a multituberculate mammal from the Late Cretaceous Transylvanian "Haţeg Island." PLoS ONE, 10(7):e0132550.

SMITH, T., D.-Y. GUO, AND Y. SUN. 2001. A new species of *Kryptobaatar* (Multituberculata): the first Late Cretaceous mammals from Inner Mongolia (P.R. China). Bulletin de l'Institut royal des Sciences naturelles de Belgique, Sciences de la Terre, suppliement 71:29–50.

SZALAY, F.S. 1965. First evidence of tooth replacement in the Subclass Allotheria (Mammalia). American Museum Novitates, 2226:1–12.

TROFIMOV, B.A. 1975. New data on *Buginbaatar* Kielan-Jaworowska et Sochava, 1969 (Mammalia, Multituberculata) from Mongolia. Trudy Sovmestnoi Sovetsko-Mongol'skoi Paleontologicheskoi Ekspeditsoi, 2:7–13. [In Russian].

WAHLERT, J.H. 1974. The cranial foramina of protrogomorphous rodents; an anatomical and phylogenetic study. Bulletin of the Museum of Comparative Zoology, 146(8):363–410.

WIBLE, J.R. 1990. Late Cretaceous marsupial petrosal bones from North America and a cladistic analysis of the petrosal in therian mammals. Journal of Vertebrate Paleontology, 10(2):183–205.

WIBLE, J.R., AND J.A. HOPSON. 1993. Basicranial evidence for early mammal phylogeny. Pp. 45–62, *in* Mammal Phylogeny: Mesozoic Differentiation, Multituberculates, Monotremes, Early Therians, and Marsupials (F.S. Szalay, M.J. Novacek, and M.C. McKenna, eds.). Springer Verlag, New York.

———. 1995. Homologies of the prootic canal in mammals and non-mammalian cynodonts. Journal of Vertebrate Paleontology, 15(3): 331–356.

WIBLE, J.R., AND G.W. ROUGIER. 2000. Cranial anatomy of *Kyrptobaatar dashzevegi* (Mammalia, Multituberculata), and its bearing on the evolution of mammalian characters. Bulletin of the American Museum of Natural History, 247:1–124.

WILLIAMSON, T.E., S.L. BRUSATTE, R. SECORD, AND S. SHELLEY. 2016. A new taeniolabidoid multituberculate (Mammalia) from the middle Puercan of the Nacimiento Formation, New Mexico, and a revision of taeniolabidoid systematics and phylogeny. Zoological Journal of the Linnean Society, 177:183–208.

XU, L., X. ZHANG, H. PU, S. JIA, J. ZHANG, J. LÜ, AND J. MENG. 2015. Largest known Mesozoic multituberculate from Eurasia and implications for multituberculate evolution and biology. Scientific Reports, 5:14950.

ZELLER, U. 1989. Die Entwicklung und Morphologie des Schädels von *Ornithorhynchus anatinus* (Mammalia: Prototheria: Monotremata). Abhandlungen der senckenbergischen naturforschenden Gesellschaft, 545:1–188.

APPENDIX 1.
List of morphological characters adapted and modified from Rougier et al. (2016)
with the addition of 26 new characters.
(*continued on next page*)

1. Lower incisor, enamel covering: thickness uniform (0); thicker on labial surface than on lingual surface (1); completely restricted to labial surface (2). [Modified from Rougier et al. (2016), character 1.]
2. Lower p3, presence: present (0); absent (1). [Rougier et al. (2016), character 2.]
3. Lower p4, serrated tooth: present (0); absent (1). [New.]
4. Lower p4, serration count: five or fewer (0); six to ten (1); more than ten (2). [Rougier et al. (2016), character 3.]
5. Lower p4, serrated tooth in lateral view: rectangular (0); arcuate (1); trapezoidal (2). [Modified from Rougier et al. (2016), character 4.]
6. Lower p4, number of roots: one (0); two (1); three (2). [New.]
7. Lower p4, posterobuccal basal cusp or ridge, presence: absent (0); present (1). [New.]
8. Lower m1, labial row, cusp formula: four (0); five (1); six (2); seven (3). [Modified from Rougier et al. (2016), character 5.]
9. Lower m1, lingual row, cusp formula: three (0); four (1); five (2); six (3). [Modified from Rougier et al. (2016), character 5.]
10. Ratio of lower p4–m1 length: less than 0.6 (0); 0.6 to 1.7 (1); greater than 1.7 (2). [Rougier et al. (2016), character 6.]
11. Lower m2, labial row, cusp formula: two (0); three (1); four (2); five (3); six (4). [Modified from Rougier et al. (2016), character 7.]
12. Lower m2, lingual row, cusp formula: two (0); three (1); four (2); five (3); six (4). [Modified from Rougier et al. (2016), character 7.]
13. Upper I2, enamel covering: thickness uniform (0); thicker on labial surface than on lingual surface (1); completely restricted to labial surface (2). [Modified from Rougier et al. (2016), character 1.]
14. Upper I2, cusp number: two (0); one (1). [Rougier et al. (2016), character 8.]
15. Upper I2, position: separated from midline by equal to or greater than the tooth's width (0); separated from midline by less than the tooth's width (1). [New.]
16. Upper I2, orientation: more vertical (0); more medially directed (1). [New.]
17. Upper I3, position: located on margin of palate (0); slightly shifted from labial margin (1); in middle of palatal part of premaxilla (2). [Rougier et al. (2016), character 9.]
18. Upper P1, presence: present (0); absent (1). [New.]
19. Upper P1, cusp number: three (0); four (1). [New.]
20. Upper P1, number of roots: one (0); two (1). [New.]
21. Upper P2, presence: present (0); absent (1). [New.]
22. Upper P2, cusp number: three (0); four (1); five or more (2). [New.]
23. Upper P2, number of roots: two (0); one (1). [New.]
24. Upper P3, presence: present (0); absent (1). [New.]
25. Upper P3, cusp number: two (0); three (1); four (2); five (3); six (4). [New.]
26. Upper P3, root number: two (0); one (1). [Rougier et al. (2016), character 11.]
27. Length of upper premolar tooth row to molar tooth row, ratio: 1.5 to 0.5 (0); less than 0.5 (1). [Modified from Rougier et al. (2016), character 13.]
28. Upper P4, occlusal morphology: multiple rows of cusps (0); one row of cusps (1). [New.]
29. Upper P4, labial row of cusps, presence: present (0); absent (1). [New.]
30. Upper P4, labial row, cusp formula: one (0); two (1); three (2). [Modified from Rougier et al. (2016), character 14.]
31. Upper P4, middle row, cusp formula: four or five (0); six (1); seven or eight (2); nine or more (3). [Modified from Rougier et al. (2016), character 14.]
32. Upper P4, lingual row of cusps, presence: present (0); absent (1). [New.]
33. Upper P4, lingual row, cusp formula: one (0); two (1); three or more (2). [Modified from Rougier et al. (2016), character 14.]
34. Upper P4, root number two (0); one (1); three (2). [Modified from Rougier et al. (2016), character 12.]
35. Upper M1, labial row, cusp formula: four (0); five (1); six (2); seven (3); eight or more (4). [Modified from Rougier et al. (2016), character 15.]
36. Upper M1, middle row, cusp formula: four (0); five (1); six (2); seven (3); eight (4); nine or more (5). [Modified from Rougier et al. (2016), character 15.]
37. Upper M1, lingual row, cusp formula: ridge (0); one (1); two (2); three (3); four (4); five (5); six (6); seven or more (7). [Modified from Rougier et al. (2016), character 15.]
38. Upper M1, inner ridge length to total length of upper M1: less than 0.5 (0); greater than 0.5 (1). [Rougier et al. (2016), character 16.]
39. Width of upper P4–M1, ratio: greater than or equal to 0.9 (0); greater than or equal to 0.6 but less than 0.9 (1); greater than 0.45 but less than 0.60 (2); less than or equal to 0.45 (3). [Rougier et al. (2016), character 17.]
40. Upper M2, labial row, cusp formula: ridge (0); one (1); two or more (2). [Modified from Rougier et al. (2016), character 18.]
41. Upper M2, middle row, cusp formula: two (0); three (1); four or more (2). [Modified from Rougier et al. (2016), character 18.]

APPENDIX 1.
(*continued from previous page*)

42. Upper M2, lingual row, cusp formula: two (0); three (1); four or more (2). [Modified from Rougier et al. (2016), character 18.]
43. Skull width to skull length ratio: equal to or less than 0.79 (0); greater than 0.8 (1). [Rougier et al. (2016), character 43.]
44. Width of snout:skull length ratio: below 0.3 (0); 0.3–0.39 (1); above 0.4 (2). [Rougier et al. (2016), character 42.]
45. Ridge between palate and lateral wall of premaxilla, presence: absent (0); present (1). [Rougier et al. (2016), character 19.]
46. Thickenings in palatal process of premaxilla, presence: absent (0); present (1). [Rougier et al. (2016), character 30.]
47. Incisive foramen, size: subequal to or greater than the length of I2 and I3 (0); subequal to or less than the length of I2 (1). [New.]
48. Palatal vacuities, presence: absent (0); present (1). [Modified from Rougier et al. (2016), character 32.]
49. Postpalatine torus, presence: absent (0); present (1). [Modified from Rougier et al. (2016), character 44.]
50. Postpalatine torus, development: developed laterally and with a ventral projection from the palate forming a distinctive bulge (0); strongly developed forming a raised, ornate, and sharply angled plate (1). [Modified from Rougier et al. (2016), character 44.]
51. Minor palatine foramen, alisphenoid contribution: present (0); absent (1). [New.]
52. Nasal foramina, number per side: one (0); two (1); more than two (2). [Rougier et al. (2016), character 21.]
53. Infraorbital foramen, position in lateral view: dorsal to P1 (0); dorsal to P1–P2 embrasure (1); dorsal to P2 (2); dorsal to P2–P3 embrasure (3); dorsal to P3 or more posterior (4). [Modified from Rougier et al. (2016), character 22.]
54. Infraorbital foramen, visibility in ventral view: absent (0); present (1). [New.]
55. Secondary infraorbital foramen, presence: present (0); absent (1). [New.]
56. Facial surface of lacrimal, size and shape: very small and arcuate (0); large, roughly rectangular (1). [Rougier et al. (2016), character 29.]
57. Base of zygomatic arch as marked by posterior edge: directly dorsal to P4 (0); dorsal or posterior to P4–M1 embrasure (1). [Rougier et al. (2016), character 23.]
58. Zygomatic process of squamosal, anterior extent: posterior to orbit (0); nearly contacting lacrimal and contributing to orbital rim (1). [New.]
59. Frontal-nasal suture, shape: frontal pointed anteriorly and not deeply inserted between the nasals (0); frontal pointed anteriorly and deeply inserted between the nasals (1); frontal with subtransversal anterior margins (2). [Rougier et al. (2016), character 26.]
60. Midline crest on vomer posterior to choanae, presence: present (0); absent (1). [New.]
61. Postorbital process, size: swelling (0); less than half orbit width but more than swelling (1); equal to or more than half orbit width (2). [Modified from Rougier et al. (2016), character 24.]
62. Supraorbital notch, presence: absent (0); present (1). [New.]
63. Frontal-parietal suture, shape: V-shaped (0); U-shaped (1). [Rougier et al. (2016), character 27.]
64. Contact between nasal and parietal, presence: absent (0); present (1). [Rougier et al. (2016), character 28.]
65. Foramen masticatorium, position: on lateral braincase wall (0); on basicranial surface (1). [New.]
66. Anterior part of promontorium, shape: oval (0); irregular with incurvatures on both sides (1). [Rougier et al. (2016), character 35.]
67. Hiatus Fallopii, visible in ventral view: absent (0); present (1). [New.]
68. Tensor tympani fossa on lateral side of promontorium, depth: deep (0); shallow (1). [New.]
69. Jugular fossa, size and depth: small and shallow (0); large and deep (1). [Rougier et al. (2016), character 34.]
70. Posttemporal foramen, size: large (0); small (1). [Rougier et al. (2016), character 39.]
71. Coronoid process, angle relative to tooth row: steep, equal to 45 degrees or greater than 45 degrees (0); low, less than 45 degrees (1). [Rougier et al. (2016), character 37.]
72. Coronoid process, shape: angle between anterior and posterior edges less than or equal to 50 degrees (0); angle between anterior and posterior edges greater than 50 and less than 70 degrees (1); angle between anterior and posterior edges greater than 70 degrees (2). [New.]
73. Angle between the ventral margin of dentary and occlusal plane: equal to or less than 10 degrees (0); greater than 10 and less than 20 degrees (1); greater than or equal to 20 degrees (2). [Modified from Rougier et al. (2016), character 40. With occlusal plane horizontal, measure angle of elevation of ventral margin.]
74. Mandibular condyle, height to coronoid process: mandibular condyle lower (0); mandibular condyle level with or higher (1). [New.]

APPENDIX 2.
Taxa included in phylogenetic analysis and sources of data.

Ptilodus Cope, 1881 – Gidley (1909); Broom (1914); Granger and Simpson (1929); Simpson (1937); Krause (1982); Wible and Rougier (2000)
Buginbaatar transaltaiensis Kielan-Jaworowska and Sochava, 1969 – Kielan-Jaworowska and Sochava (1969); Trofimov (1975)
Lambdopsalis bulla Chow and Qi, 1978 – Miao (1986, 1988)
Taeniolabis taoensis Cope, 1882 – Granger and Simpson (1929); Simpson (1937); Sloan (1981); Williamson et al. (2016)
Eucosmodon gratus Jepsen, 1930 – Jepsen (1930)
Stygimys kuszmauli Sloan and Van Valen, 1965 – Sloan and Van Valen (1965); Lofgren et al. (2005)
Nemegtbaatar gobiensis Kielan-Jaworowska, 1974 – Kielan-Jaworowska (1974); Kielan-Jaworowska et al. (1986); Hurum (1994, 1998)
Kamptobaatar kuczynskii Kielan-Jaworowska, 1970 – Kielan-Jaworowska (1970, 1971); Hurum (1996); Kielan-Jaworowska and Hurum (1997)
Bulganbaatar nemegtbaataroides Kielan-Jaworowska, 1974 – Kielan-Jaworowska (1974)
Nessovbaatar multicostatus Kielan-Jaworowska and Hurum, 1997 – Kielan-Jaworowska and Hurum (1997)
Sloanbaatar mirabilis Kielan-Jaworowska, 1970 – Kielan-Jaworowska (1970, 1971); Kielan-Jaworowska and Hurum (1997)
Chulsanbaatar vulgaris Kielan-Jaworowska, 1974 – Kielan-Jaworowska (1974); Kielan-Jaworowska et al. (1986); Hurum (1994, 1996, 1998)
Kryptobaatar dashzevegi Kielan-Jaworowska, 1970 – Kielan-Jaworowska (1970); Wible and Rougier (2000); Smith et al. (2001); http://digimorph.org/specimens/Kryptobaatar_dashzevegi/
Tombaatar sabuli Rougier et al., 1997 – Rougier et al. (1997)
Djadochtatherium matthewi Simpson, 1925 – Simpson (1925); Kielan-Jaworowska and Hurum (1997); Rougier et al. (1997)
Mangasbaatar udanii Rougier et al., 2016 – Rougier et al. (2016)
Catopsbaatar catopsaloides (Kielan-Jaworowska, 1974) – Kielan-Jaworowska (1974); Kielan-Jaworowska et al. (1986, 2002, 2005)
Guibaatar castellanus Wible et al., 2019 – this report

APPENDIX 3.
Taxon-character matrix. Matrix is available at http://morphobank.org/permalink/?P3260

Ptilodus
0002010212 1001010001 0100200001 1020455102 120100010- ?140100000 000000?000 0120

Buginbaatar
01001?0320 11???????? ???????002 100?346122 10???????? ?????????? ?????????? ??1?

Lambdopsalis
211--00110 (2,3)0210?11-- 1--1--11-- ---1(2,3)(3,4)(5,6,7)131 0(1,2)1110000- 0240101?20 0001010011 0110

Taeniolabis
211--10330 (2,3,4)2210101-- 1--1--11-- ---1457131 2211000?0- ??2110102? 0001?????1 0100

Eucosmodon
21020?1321 20?0???1-- 0010?1?0?? ???0????0? ?????????? ?????????? ?????????? 1221

Stygimys
21020?1321 (1,2)0?0??2000 0010210001 300033(2,3)01(2,1) 11????01?? ??001?0??? ?????????? 1?1?

Nemegtbaatar
20010?1111 1021??2001 0000(0,1)00002 (1,2)(0,1)00(2,3)(2,3)(4,5)121 1001111110 0221110010 1010000010 1210

Kamptobaatar
10010??001 ???1012001 0000200002 (0,1)1-0110121 0101101010 ?(1,2)11110010 1010001010 1201

Bulganbaatar
?????????? ??1???2001 0000200001 01-0113111 00??1111?? ??1?1?0??? ?????????? ????

Nessovbaatar
?0010?1002 10???????? ?????????? ?????????? ?????????? ?????????? ?????????? 1211

Sloanbaatar
10010?1001 00?111200? 00?0200001 01-?000011 011011111? ?0111???1? 1010001??0 0221

Chulsanbaatar
20010?1001 (0,1)0?11?2011 000020000(1,2) (0,1)1-0011021 (0,1)010111010 0(1,2)01110010 1010100010 1111

Kryptobaatar
2001021001 1021112001 000020001- 0010(0,1)(0,1)0011 0(0,1)12111011 0(1,2)11110010 2110110010 1100

Tombaatar
?????????? ??21???2001 1--02000010??0012020 01??111011 1111?10?1? ???0?????? ????

Djadochtatherium
200?0?1001 ??211020?1 0?00?0???? ?????????? ????111??? ?121110?1? 2?10?????0 0?10

Mangasbaatar
2000121000 002??12001 1--0200000 0000113030 0112111011 1?21010011 2?10110110 0010

Catopsbaatar
200012101(0,1) (0,1)0211120?1 1--0?0?01- 0000(2,1)(1,2)4132 (0,1)(0,1)121?1010 1(1,2)(0,4)1(0,1)1(0,1)1(0,1)? 2110?1?110 0020

Guibaatar
(1,2)001021001 00(1,2)1??21-- 0200300001 000011202? ????111?11 1131010011 ???01111?? 001?